ABSTRACT

Title of Thesis:	GEOCHEMICAL INDICATORS OF REDOX AND WEATHERING ACROSS THE EDIACARAN-CAMBRIAN TRANSITION IN SIBERIA
	Andrew Doerrler, Master of Science, 2024
Thesis Directed By:	Distinguished University Professor Alan Jay Kaufman, Geology

The transition between the Ediacaran and Cambrian periods witnessed the fall of the enigmatic Ediacara biota. The cause of their extinction is poorly understood, but the timing broadly coincides with a significant negative $\delta^{13}C$ anomaly, the BAsal Cambrian Carbon isotope Excursion (BACE). These macroscopic organisms were likely tolerant of anoxic conditions, so oceanic oxidation may have been a kill mechanism. This study utilizes uranium isotopes, sulfur isotopes, and cerium anomalies to understand oceanic redox conditions from two BACE sections in Siberia, as well as lithium isotopes to constrain weathering intensity. Reconstruction of seawater $\delta^{238}U$ values from equivalent evaporite and carbonate-dominated successions indicate a notable increase in oxygen during the event supporting the oxidation hypothesis. Global sea level fall and evaporite formation suggest that seawater salinity increased dramatically along continental margins, which may provide an alternative osmotic kill mechanism for the soft-bodied Ediacaran biota. Support for the salinity hypothesis comes from profound $\delta^{7}Li$ and $\delta^{34}S$ compositions of carbonate and pyrite, respectively, which arguably resulted from the distillation of lithium and sulfate from seawater into evaporite-rich lithologies.

GEOCHEMICAL INDICATORS OF REDOX AND WEATHERING ACROSS THE EDIACARAN-CAMBRIAN TRANSITION IN SIBERIA

by

Andrew D. Doerrler

Thesis submitted to the Faculty of the Graduate School of the
University of Maryland, College Park, in partial fulfillment
of the requirements for the degree of
Master of Science
2024

Advisory Committee:
Distinguished University Professor Alan Jay Kaufman, Chair
Distinguished University Professor James Farquhar
Professor Geoffrey Gilleaudeau

Acknowledgements

I would like to thank my advisor, Dr. Alan Jay Kaufman, for his mentorship and support. I would also like to thank Dr. Geoff Gilleaudeau from George Mason University and Dr. Tian Gan from the University of Maryland for their assistance with all aspects of this project. I would like to thank Matthew Pedersen, Jenna Wollney, and Karel Kletetchka for aiding in sample preparation and measurements.

This work could not have been done without our Russian collaborators from the Trofimuk Institute of Petroleum Geology and Geophysics, Dr. Natalia Bykova, Dr. Vasiliy Marusin, and Dr. Boris Kochnev. Finally, I would like to thank Natalia Ivanova from the Siberian Research Institute of Geology, Geophysics and Mineral Raw Resources for the funding awarded from the All-Russian Research Geological Oil Institute, which made sample collection possible.

Table of Contents

List of Tables

List of Figures

Chapter 1: Introduction

1.1: Ediacaran Biota

Earth's first experiment in multicellularity resulted in the rise of macroscopic, motile, and biomineralizing life during the Ediacaran Period (635.2-538.8 Ma) (Narbonne et al., 2012; Xiao et al., 2016; Linnemann et al., 2019). In the fossil record, they can be found preserved primarily as soft-bodied impressions in fine-grained siliciclastic rocks (Narbonne, 2005). Due to their unusual preservation and bizarre morphologies, it is still not known what the metabolic requirements of these organisms were. Their large surface area suggested that diffusion was important for their metabolic intake (Narbonne, 2005), which led to interpretations of feeding strategies that included osmotrophy or chemosymbiosis with sulfur-oxidizing bacteria (Laflamme et al., 2009; Kaufman, 2019; McIlroy et al., 2021).

As puzzling as their lifestyle is, their disappearance is even more mysterious. The ecosystems of the Ediacaran and Cambrian periods are very different, so something must have occurred during that transition to completely reshape the environment (Fig. 1.1). There are two current hypotheses; a "biotic replacement" model and a "mass extinction" model (Laflamme et al., 2013). The biotic replacement model would likely have drawn out over a longer period, but two possible causes are the advent of predation and ecosystem engineering, where in either scenario the Ediacaran biota were outcompeted by new organisms for availability of suitable substrates (Seilacher et al., 2005). The mass extinction model suggests that the organisms were completely wiped out at the end of the Ediacaran, allowing new life to develop new niches and fill empty ones left behind. Support for a mass extinction lies in the geochemical record of the Ediacaran, as the fall of the Ediacaran biota appears to be associated with a strong negative

carbon isotope anomaly (Darroch et al., 2018; Kaufman, 2019). However, the cause of this geochemical perturbation remains a mystery as well.

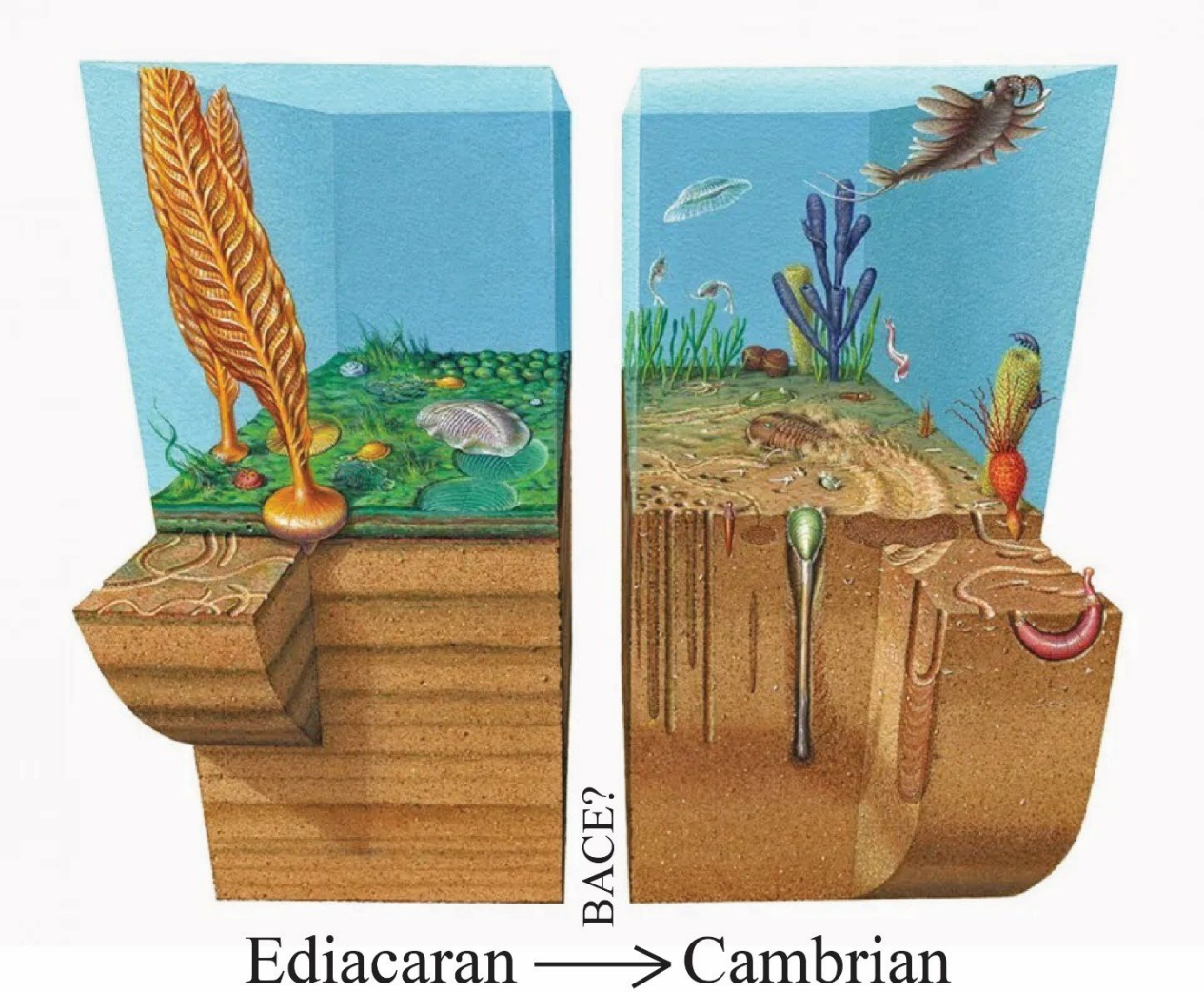

Figure 1.1. Illustration of Ediacaran-style mat grounds vs. Cambrian-style burrowing. Illustration modified from Peter Trusler.

1.2: Carbon Isotope Excursions

The emergence of multicellularity occurred amid profound tectonic reorganization. The Pan-African orogeny coinciding with the evolution of the Ediacaran biota and the subsequent Cambrian Explosion (Squire et al., 2006) could mean a potential connection to the environment and chemical changes in the world ocean. Extreme oscillations in the carbon isotope record

during this time (Fig. 1.2) suggest that their origin occurred in the midst of dramatic environmental changes. Among these excursions (reported as $\delta^{13}C = (^{13}C/^{12}C_{sample}/^{13}C/^{12}C_{std} - 1)*1000$, where the standard is V-PDB and expressed in units of permil (‰)) two of the most studied are the Shuram and BAsal Cambrian carbon isotope Excursion (BACE), which temporally bracket the Ediacaran biota and preserve the lowest carbonate carbon isotope values in the Ediacaran and basal Cambrian periods (Burns and Matter, 1993; Zhu et al., 2006). During and immediately following the Shuram, complex macroscopic organisms of the Ediacaran biota evolved, whereas following the BACE, these enigmatic organisms disappeared. It is still unknown what caused either of these events to occur, but the Shuram appears to be associated with the buildup of oxidants and ventilation of the oceans based on a global stepwise change in the uranium isotope composition of seawater proxies (Zhang et al., 2018). As these events preserve very similar carbon isotope records, it is possible that the BACE was caused by the same oxidation processes, which may have led to the demise of the Ediacaran biota if these organisms thrived in anoxic seawater (Cherry et al., 2022). Negative excursions in the carbon isotope record can be caused by several different factors. One factor that could have implications for the evolution of life is variations in atmospheric and oceanic redox conditions. An increase in molecular oxygen or of oxidants, like sulfate and nitrate, could have driven the remineralization of a ^{12}C-rich dissolved organic carbon (DOC) pool to form ^{12}C-rich dissolved inorganic carbon (DIC) that is preserved in marine carbonates. (Rothman et al., 2003).

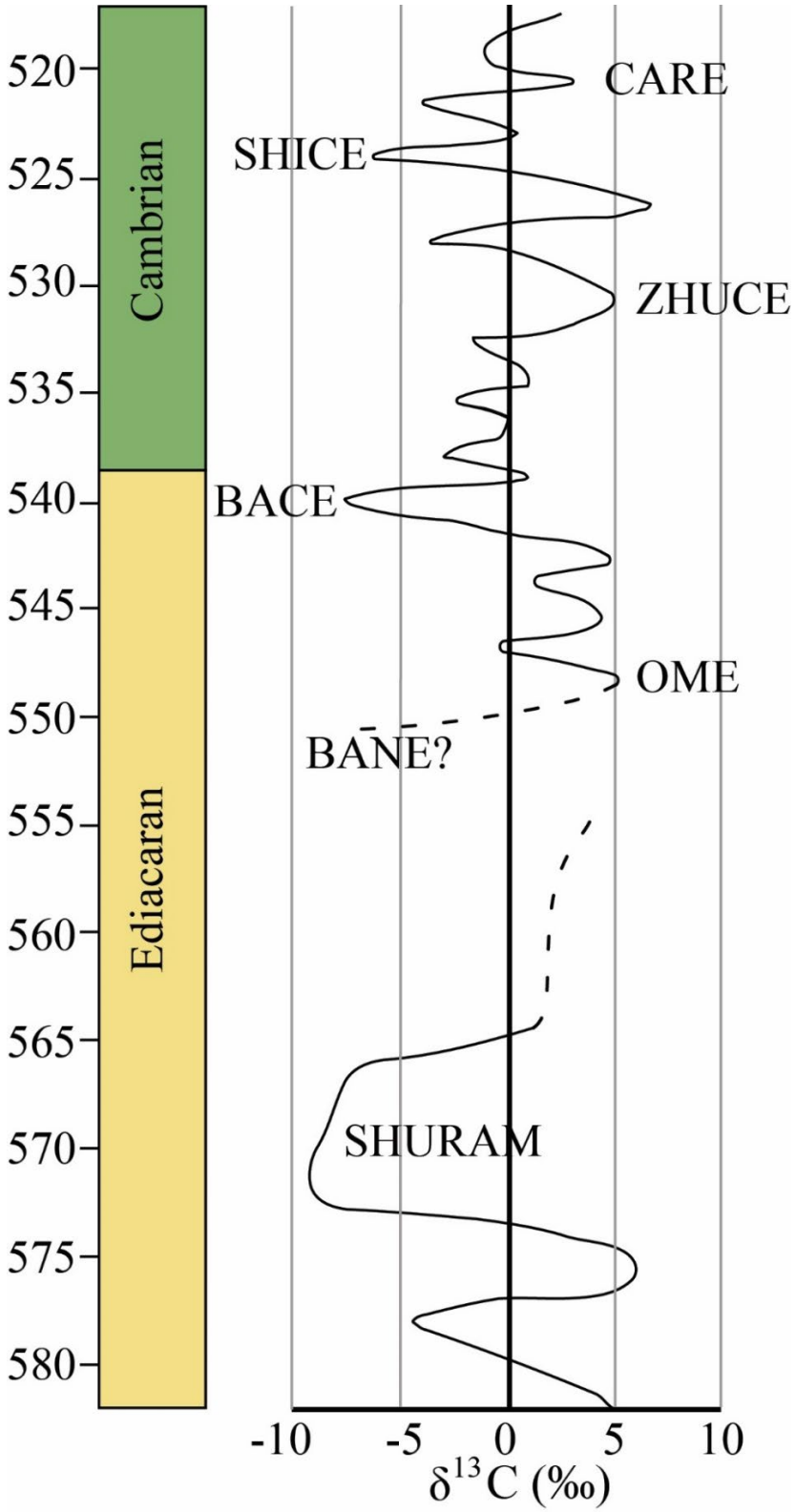

Figure 1.2. Generalized $\delta^{13}C$ curve of the late Ediacaran and early Cambrian (after Bowyer et al., 2022 and references therein). CARE = Cambrian Arthropod Radiation isotope Excursion. SHICE = SHIyantou Carbon isotope Excursion. ZHUCE = ZHUjiaqing Carbon isotope Excursion. BACE = BAsal Cambrian Carbon isotope Excursion. OME = Omkyk Excursion. BANE = Basal Nama Excursion. SHURAM = Shuram-Wonoka Excursion.

1.3: Redox Hypothesis

Understanding the redox conditions of the BACE may provide insight into the kill mechanism for the Ediacaran biota. As the Shuram has been linked to an increase in oceanic oxygen, it is possible that a similar excursion, like the BACE, may also be linked to seawater ventilation (Zhang et al., 2018). Previous studies have shown that the Ediacaran biota may have survived under low oxygen conditions (Cherry et al., 2022), so the prediction that a rise in oxygen could have been the driver for the extinction. To this end, uranium isotopes and cerium anomalies on BACE sections across Siberia serve as a test of global and local redox conditions, as their fractionation mechanisms are redox dependent. Periods expanded of anoxia/euxinia cause negative uranium isotopes via the reduction of U^{+6} to U^{+4}, which preferential incorporates ^{238}U, leaving the resulting seawater with a progressively lighter isotopic composition (Lau et al., 2017). Therefore, I hypothesize that BACE carbonates from two sections in Siberia will reflect an increase in uranium isotope compositions as a result of increased oxygen.

1.4: Weathering Hypothesis

While redox conditions may point towards a driver for extinction, enhanced terrestrial weathering rates may provide a source of the oxidants (and the nutrients that would stimulate oxygenic photosynthesis) that caused the ventilation of seawater and resulting carbon isotope excursion. Physical and chemical erosion of these uplifted terrains during the Pan-African orogeny delivered thick blankets of sediments, nutrients, oxidants, acid buffer capacity (i.e., alkalinity), and salts to the oceans. The delivery of nutrients and oxidants through continental weathering could drive enhanced primary productivity in the oceans that could drive the expansion of marine euxinia along productive coastlines due to organic carbon respiration, as well as long-term buildup of oxygen globally through enhanced organic carbon burial. Lithium

isotopes have the potential to track weathering intensity based on the production of clay minerals on land and in the ocean that fractionate lithium isotopes that are incorporated into marine carbonates. It is plausible that increased congruent weathering on land and rapid formation of clays in the ocean (I.e., reverse weathering) would drive the lithium isotopic composition of marine carbonates to lower values, as has been recently noted for the Shuram Excursion (Gan et al., 2024). Therefore, I hypothesize that lithium isotope values from BACE carbonates will similarly reflect trends toward crustal values associated with intense continental weathering.

1.5: The BACE

1.5.1: Global Record

Worldwide, the BACE is expressed by a negative stratigraphic shift in the carbonate carbon isotope ($\delta^{13}C_{carb}$) compositions of marine carbonates to a nadir of -6‰ or lower (Fig. 1.3). In many successions across Asia and the Middle East, which were equatorial at the time of deposition (Scotese, 2016), the BACE carbonates are interbedded with thick marine evaporites. The biogeochemical event has been broadly recognized in carbonates of Northwest Territories of Canada (Narbonne et al., 1994; Kaufman et al., 1997), the western United States (Corsetti and Kaufman, 1994; Smith et al., 2016), Mexico (Sour-Tovar et al., 2007; Loyd et al., 2012; Hodgin et al. 2021), Morocco (Maloof et al., 2005; Maloof et al., 2010b) Oman (Amthor et al., 2003; Bowring et al., 2007), Iran (Kimura et al., 1997), China (Li and Xiao, 2004; Ishikawa et al., 2008; Li et al., 2009; 2013; Jiang et al., 2012; Steiner et al., 2020), Mongolia (Smith et al., 2015; Bold et al., 2016; Topper et al., 2022), India (Kaufman et al., 2006) and Siberia (Knoll et al., 1995a, b; Kaufman et al., 1996; Bartley et al., 1998; Kouchinsky et al., 2007; Pelechaty et al., 1996). Ichnofossils (i.e., *Trepichtnus pedum*) preserved in siliciclastic sedimentary rocks that

mark the Ediacaran-Cambrian boundary are incompletely recorded in the locations in which the BACE is preserved in carbonates, although the last occurrence of worm-like cloudinids with their funnel-in-funnel carbonate shells appear to precede the BACE in most localities (*contra* Zhu et al., 2017 and Topper et al., 2022), and *T. pedum* is generally found in siliciclastics above the carbon cycle anomaly. Radiometric age constraints for the BACE in Mexico, from U-Pb detrital zircon analyses (providing a maximum potential age) suggest that the event is younger than 539.40±0.23 Ma (Hodgin et al., 2021). This is critical as current constraints on the Ediacaran-Cambrian boundary indicate an age of ca. 538.8 Ma (Linnemann et al., 2019). In Oman, a negative carbon excursion above the Last Appearance Datum (LAD) of cloudinids is constrained by a volcanic U-Pb zircon lower age of 541.0±0.13 Ma (Bowring et al., 2007). In South China, a volcanic ash above the BACE yielded an age of 535.2±1.7 Ma (Zhu et al., 2009). Lacking dateable lithologies in Siberia BACE successions, the age of the event across the vast craton relies either on detrital zircon U-Pb studies or available biostratigraphic and chemostratigraphic data.

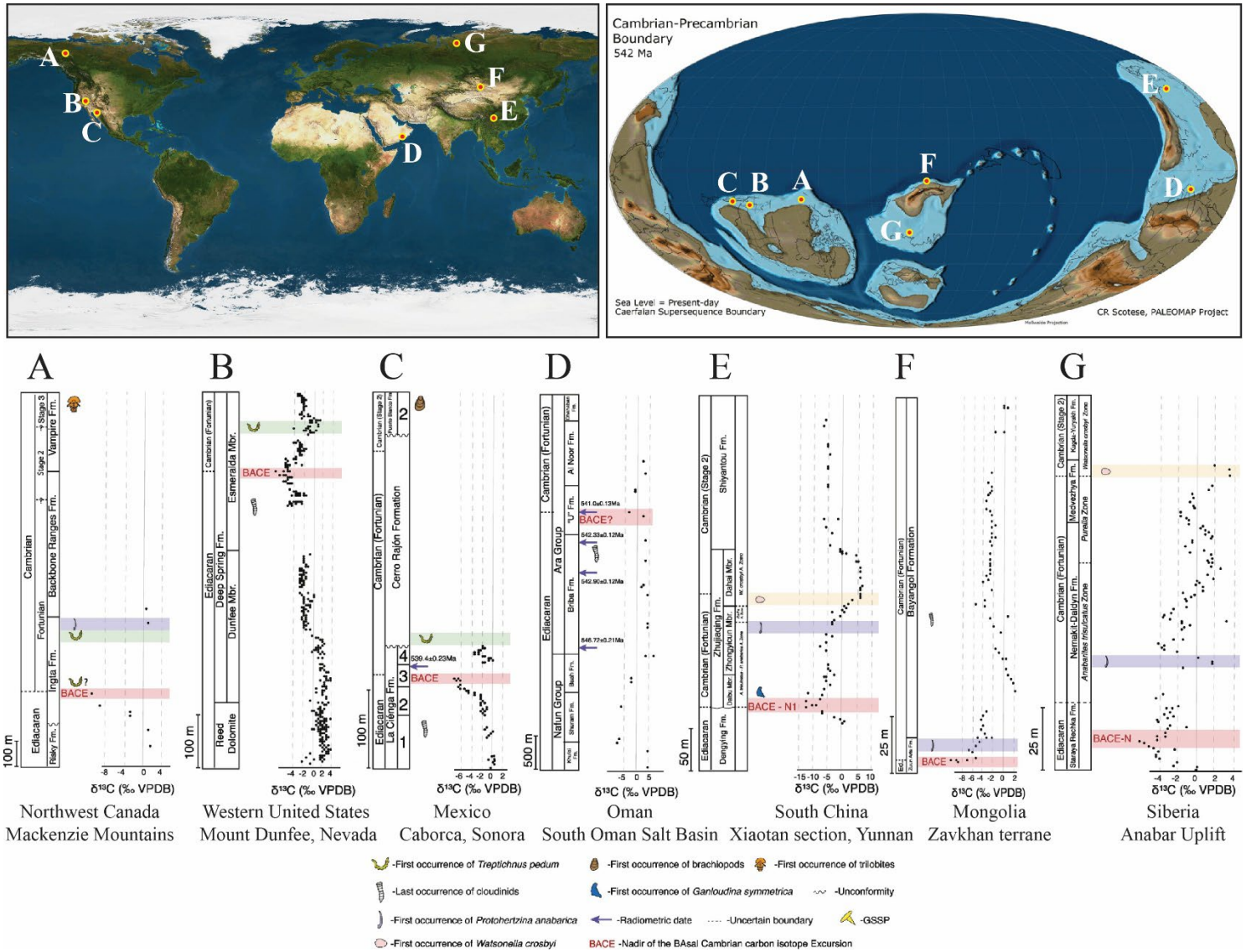

Figure 1.3. Global correlation for the Ediacaran-Cambrian BACE event (modified from Topper et al., 2022 and references therein). Locations shown for both modern and Precambrian-Cambrian continental configurations (paleogeographic base map after Scotese, 2016). (A)Northwest Canada; (B)Western United States; (C)Mexico; (D)Oman; (E)South China; (F)Mongolia; (G)Siberia.

1.5.2: Siberian Record

In northern Siberia, several localities preserve the BACE (Fig. 1.4). The negative excursion has been recognized in the lower and middle members of the Platonovskaya Formation in the Turukhansk region of western Siberia (Bartley et al., 1998), which contain evaporite casts and molds, as well as collapse breccias. The BACE is preserved there with the lowest point at -10‰ (Bartley et al., 1998; Marusin et al., 2019). Roughly 250 km to the north is another BACE section along the Sukharikha River. The Sukharika Formation contains several notable oscillations within the carbon isotope record that have been used at the archetype for the Fortunian Stage, with the lower BACE interval recording the nadir values of -8‰ (Kouchinsky et al., 2007; Maloof et al., 2010a; Marusin et al., 2023). Further to the east in the Anabar Uplift region, along the Kotuy and Kotuikan rivers is another BACE section first recognized by Knoll et al. (1995b) and Kaufman et al. (1996). The units sampled in these studies include the Staraya Rechka and Manykai formations, with the BACE preserved in the former, which is ~40 m thick in the region. The Staraya Rechka Formation is the focus of the current study, based on outcrops 65km to the south that preserve ~130 m of mixed carbonates and evaporites. The thickness difference has been attributed to gradual reduction of evaporite beds (Khomentovsky, 1990) moving from south to north, and possible due to greater erosion of the upper Staraya Rechka lithologies in the north (Marusin et al., 2022).

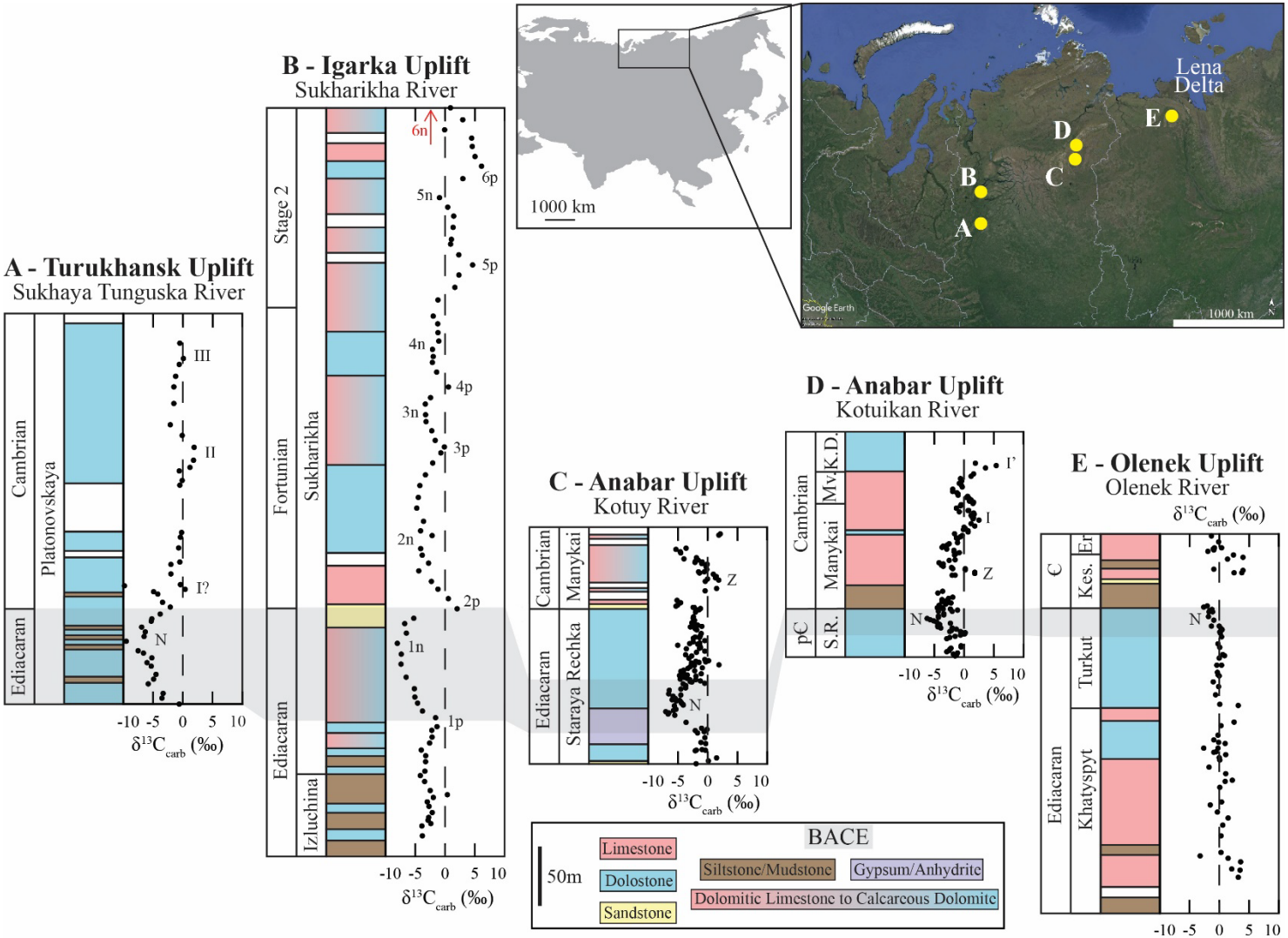

Figure 1.4. Regional correlation for the Ediacaran-Cambrian transition across the Northern Siberian Platform. (A) Turukhansk Uplift, Sukhaya Tunguska River (Bartley et al., 1998; Marusin et al., 2019); (B) Igarka Uplift, Sukharikha River (Kouchinsky et al., 2007; Marusin et al., 2023); (C) Anabar Uplift, Kotuy river (this study); (D) Anabar Uplift, Kotuikan River (Knoll et al., 1995b; Kaufman et al., 1996); (E) Olenek Uplift, Olenek River (Knoll et al., 1995a; Pelechaty et al., 1996). S.R. = Staraya Rechka Formation; Mv = Medvezhya Formation; K.D. = Kyndyn Dolostone; Kes. = Kessyua Group; Er. = Erkeket Formation; pЄ = Precambrian; Є = Cambrian.

Moving 750 km to the west, the onset of the BACE is likely preserved in the upper part of the evaporitic Turkut Formation in the Olenek Uplift along the Olenek and Khorbusuonka rivers of arctic Siberia (Knoll et al., 1995a; Pelechaty et al., 1996). This chemostratigraphic event, however, is variably truncated by a regional unconformity of potential glacial origin (i.e., Baykonurian; Chumakov, 2009). A U-Pb zircon date of 543.9±0.24 Ma from a volcanic breccia at the base of the Syhargalakh Formation (overlying the Turkut; see Grazhdankin et al., 2020) was for some time the best radiometric estimate for the Ediacaran-Cambrian boundary (Bowring et al., 1993), but the current constraint from Namibia (Linneman et al., 2019) is some 5 million years younger (although no BACE event is recorded in the Namibian succession). To date, cloudinids have not been discovered in Turkut carbonates (which do preserve evidence for evaporite-related collapse breccias), but *T. pedum*, as well as Rusophycus (an arthropod resting trace), are noted in a transgressive shale above a thick volcaniclactic diamictite of the uppermost Syhargalakh Formation (Grazhdankin et al., 2020). Higher in the Mattaia Formation the body fossil of the sabelliditid *Paleolina evenkiana* has been reported (Sokolov, 1995), and the same fossils are known from the middle Platonovskaya Formation. (Bartley et al., 1998; Marusin et al., 2019).

It is notable that across Siberia and the Middle East, the BACE is preserved and appears to be related to sea-level regression, evaporites preserved in these sections indicate that there were high rates of evaporation, which could have been further enhanced by sea-level regression. Sea level fall, basinal restriction, and an increase in seawater salinity may thus have been an additional factor in the extinction of the Ediacaran biota. The high surface area of these organisms suggests that diffusion was an important part of their lifestyles (Dufour and McIlroy, 2016). If the sea level were to drop, an increase in salinity could have been detrimental to their

survival. The salty water would draw the fresh water out of their bodies through osmosis, dehydrating and killing them.

1.5.3: Age Constraints

Chemostratigraphic correlations alone are insufficient to identify the BACE, as there are multiple negative carbon isotope excursions throughout the terminal Ediacaran and basal Cambrian intervals. Biostratigraphic information may help pinpoint the BACE, but the incomplete rock record of the Ediacaran-Cambrian boundary across the globe (i.e., the Great Unconformity; Peters et al., 2012; Shahkarami et al., 2020) complicates efforts to use trace and body fossils as stratigraphic markers. Constraining the age of the BACE through U-Pb zircon analyses from volcaniclastic rocks in arctic Siberia (Olenek Uplift) above the anomaly yielded an age of 543.9±0.24 Ma (Bowring et al., 1993), but a recent reinvestigation of detrital zircons from the Syhargalakh Formation suggest that the carbon isotope event is older than 537.20±0.50 Ma (D.V. Grazhdankin, pers. comm. 2023). In Mexico, the BACE has been dated to be older than 539.40±0.23 Ma (Hodgin et al., 2021). In Oman, the BACE has been constrained to be younger than 541.0±0.13 Ma (Bowring et al., 2007), while in South China the event is older than 535.2±1.7 Ma (Zhu et al., 2009). Coupling these ages with the current constraints on the Ediacaran-Cambrian boundary places the BACE in the very latest Ediacaran. (Linnemann et al., 2019); it is unfortunate that the BACE is not preserved in Namibian carbonates where the current radiometric constraint for the boundary is located. The Ediacaran-Cambrian transition encompasses one of the most important evolutionary events in Earth history and the associated BACE is global in distribution, so a better understanding of the redox conditions in this transitional interval would provide insight into the potential environmental cause(s) for the extinction of the Ediacaran biota.

1.6: The Staraya Rechka Formation

The Staraya Rechka Formation is composed of three members, the Kharyyalakh, Chimuka, and Kochokon (Fig. 1.5; Fig. 1.6). The Staraya Rechka Formation overlies the much older Yusmastakh Formation, separated by an angular unconformity, and is disconformably overlain by the Manykai Formation. The Staraya Rechka Formation at this locality contains ~131 m of carbonates inter-leaved with shale or gypsum. Evaporite minerals are abundant in many of the carbonate hand samples and thin sections. The Kharyyalakh (lowermost interval ~16 m thick) contains stromatolitic dolostone and laminated rippled dolosiltite and dololutite with minor evaporite levels. The Chimuka Member (middle interval ~64 m thick) contains three intervals dominated by gypsum, with four intervals of interbedded green shale and shaley dololutite, rippled dolosiltite, stromatolitic dolostone, and a small amount of quartz sandstone. The Kochokon Member (upper interval ~51 m thick) contains a thick unit of evaporite-free dolostones with hummocky and microbial bedding as well as a hydrogen sulfide odor.

The Staraya Rechka Formation is interpreted to represent a shallow marine peritidal environment, supported by abundant evidence for episodic desiccation and development of ubiquitous sulfate evaporites, especially in the Chimuka Member. A disconformity of unknown duration separates the Staraya Rechka Formation from the Manykai Formation around 130 m above the base of the measured section (Fig. 1.7), which contains up to one meter of conglomerate overlain ~10 m of shale and siltstones. Above that there is ~20 m of covered outcrop (likely fine-grained siliciclastics), followed by ~40 m of stromatolitic carbonates. This likely represents the development of a subtidal carbonate platform during sea level transgression (Kaufman et al., 1996).

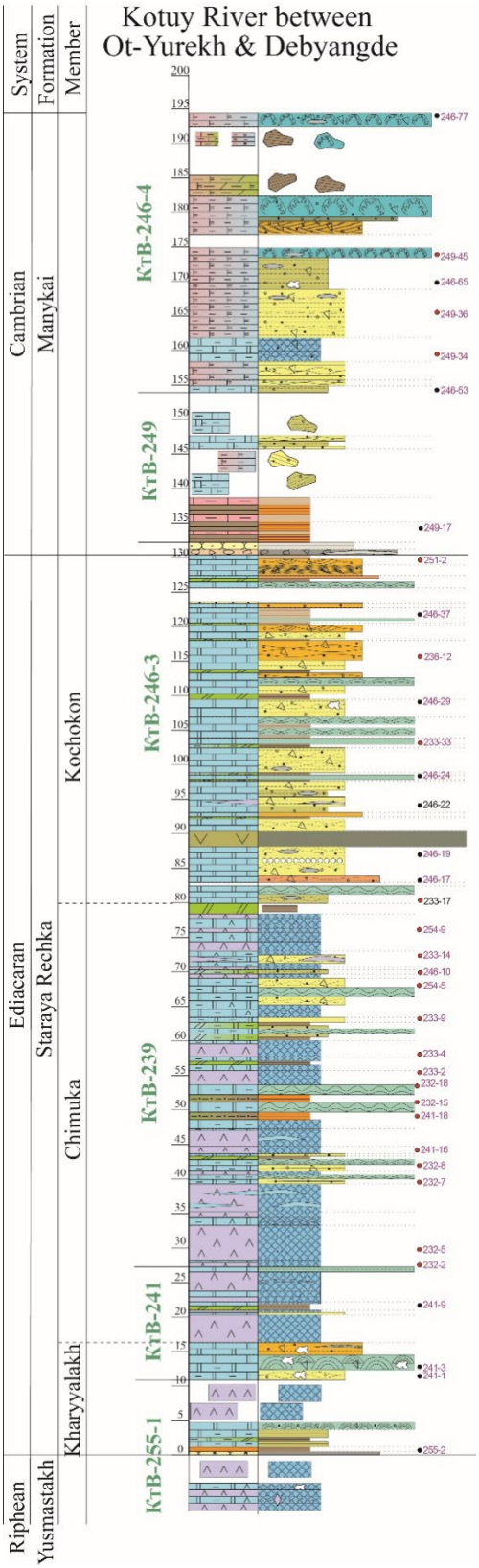

Figure 1.5. Stratigraphic column of the Staraya Rechka and Manykai formations. The height of the samples is shown to the right of the column (courtesy of N. Bykova and V. Marusin).

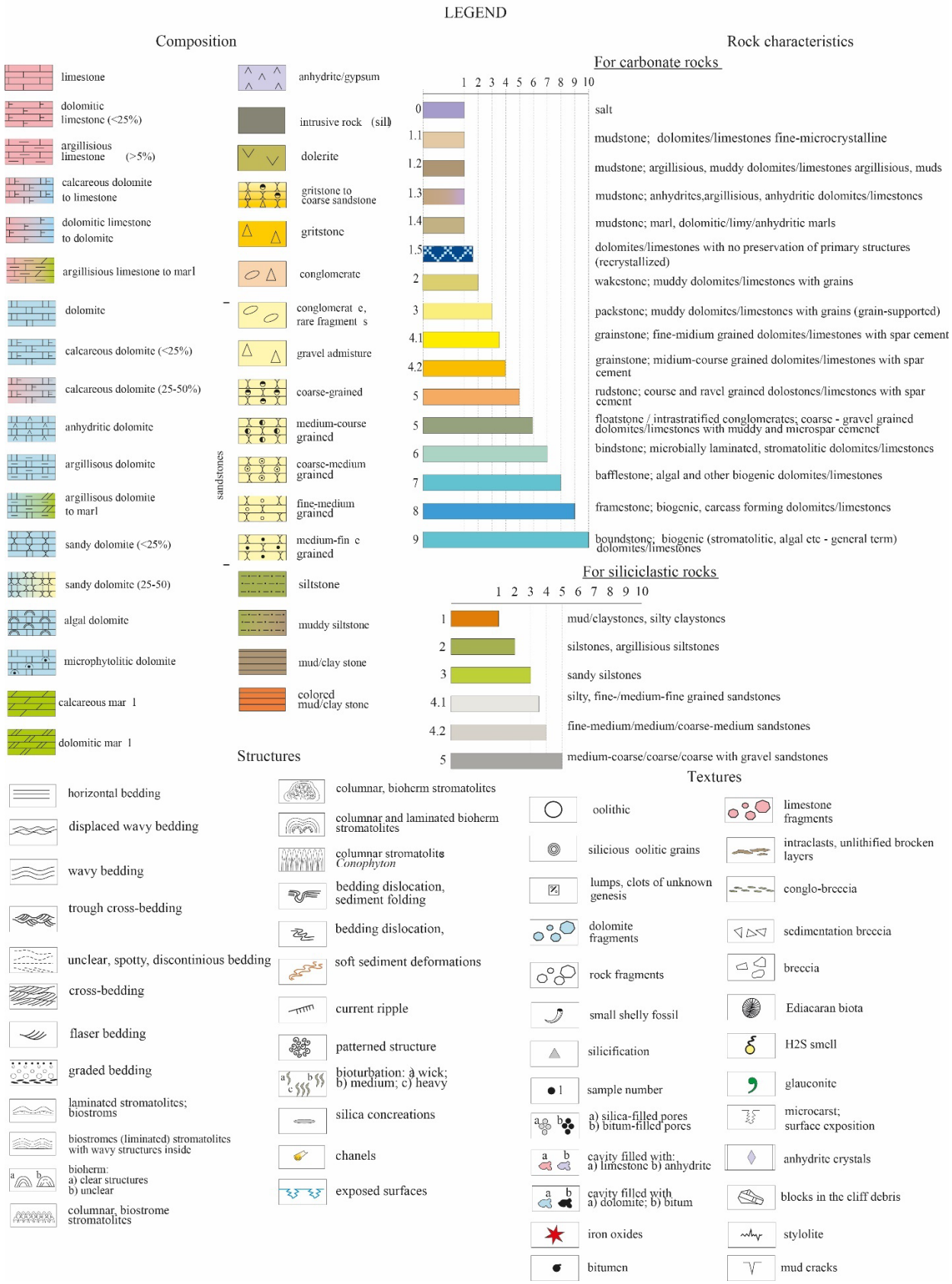

Figure 1.6. Legend associated with the stratigraphic column in Fig. 1.5 (courtesy of N. Bykova and V. Marusin).

Figure 1.7. Disconformity between the dolomites of the Staraya Rechka and the conglomerate of the Manykai (courtesy of N. Bykova and V. Marusin).

Member I of the Manykai Formation contains elements of the early Fortunian *Anabarites trisulcatus* Zone small shelly fossils (SSFs) (Knoll et al., 1995b; Kaufman et al., 1996). None of these are known within the Staraya Rechka carbonates, although the carbonates do contain the remains of the green algae known as *Renalcis,* which is also found in other boundary sections (Adachi et al., 2021). A small population of detrital zircon U-Pb ages from the upper reaches of the Staraya Rechka Formation constrain it to maximally be around 547±6 Ma, but more convincingly, a large population of zircons from the lower Manykai Formation constrains the BACE in the Anabar region of Siberia to be older than 537±3 Ma (Marusin et al., 2022).

1.7: The Sukharikha Formation

The sampled outcrop along the Sukharikha River contains the uppermost Izluchina, Sukharikha, and Krasny Porog formations (Fig. 1.8). The Izluchina Formation is an 800-850 m thick sedimentary succession generally composed of red-colored planar-laminated siltstones and mudstones with interbeds of planar-laminated and cross-bedded sandstones. The studied section contains the uppermost interval (83.5 m), where dolostone interbeds become more abundant. The Izluchina Formation is interpreted to have accumulated in terrestrial alluvial and shallow marine deltaic environments (Kochnev et al., 2022).

The Sukharikha Formation in the studied section is 556 m thick mixed limestone-dolostone and conformably overlies the Izluchina Formation with a gradual transition. Thin interbeds and lenses of reddish-gray siltstones and fine-grained sandstones occur in the lowermost 20 m of the Sukharikha Formation. The rest of the Sukharikha Formation is more or less monotonous in composition and lacks conspicuous sequence boundaries. In the lower part (124 m above the base), there is a 20 m thick interval composed of interbedding coarse- to medium-grained sandstones with dolomitic cement, trough cross-bedding, and wave-rippled to planar-laminated sandy dolostones. In the middle part of the Sukharikha Formation (200-240 m above the base), hummocky cross-stratified dolostones and dolomitic limestone are abundant, ranging from 1-9 m thick separated by intervals of planar-bedded limestones and planar-laminated silty limestones. The upper half of this interval contains the vertical burrows of *Skolithos and Arenicolites* (Korovnikov et al., 2019). The uppermost 150 m of the formation contains isolated calcimicrobial bioherms up to 0.5 m in diameter. The contact with the overlying Krasny Porog Formation is a 1.5 m thick gradual transition. This interval consists of gray limestones similar to the underlying strata of the Sukharikha Formation, to pinkish-gray and red

parallel-laminated silty limestones typical for the basal Krasny Porog Formation. There is no evidence of a hiatus during this interval. The base of this interval hosts the first appearance of abundant small and macroscopic skeletal fossils and archaeocyaths typical for the base of Cambrian Stage 2 *Nochoroicyathus sunnaginicus* Assemblage Zone (Rowland et al., 1998).

The transition between the Izluchina and Sukharikha formations mirrors a shift from alluvial/deltaic environments to shallow-marine carbonate sedimentation during transgression (Rowland et al., 1998, Kochnev et al., 2022). Accumulation of the succession of the Izluchina and Sukharikha formations marks a progressive fill of an accommodation space developed by the mid-Neoproterozoic rift-related trough. The onset of the accumulation of the Sukharikha Formation indicates the trough was filled and the marine carbonate environments expanded as a part of a vast epicontinental basin covering the Siberian Platform in the early Cambrian (Kochnev et al., 2022).

The Krasny Porog Formation (up to 150 m) is mostly composed of planar-laminated and intensely bioturbated red silty limestones and marlstones. The studied section covers the lowermost 15 m of the formation. It starts with a 10 m thick package of red intensively stylolitic silty limestones and marlstones overlain by a 2 m thick gray massive limestone. The overlying package (over 5 m thick) is composed of red limestones like the one at the base of the Formation. The Krasny Porog Formation was accumulated in the open-shelf environments (Rowland et al., 1998; Kouchinsky et al., 2007). The transition between the Sukharikha and Krasny Porog formations corresponds to a transgression and associated shift from the shallow-water marine to open-shelf environments with carbonate sedimentation (Rowland et al., 1998).

The Staraya Rechka and Sukharikha formations are believed to correlate to the very terminal Ediacaran, so constraining the geochemical signals of these formations is critical to

understanding the demise of the Ediacaran biota. Looking at a combination of both redox and weather proxies may be crucial to unlocking this mass extinction mystery.

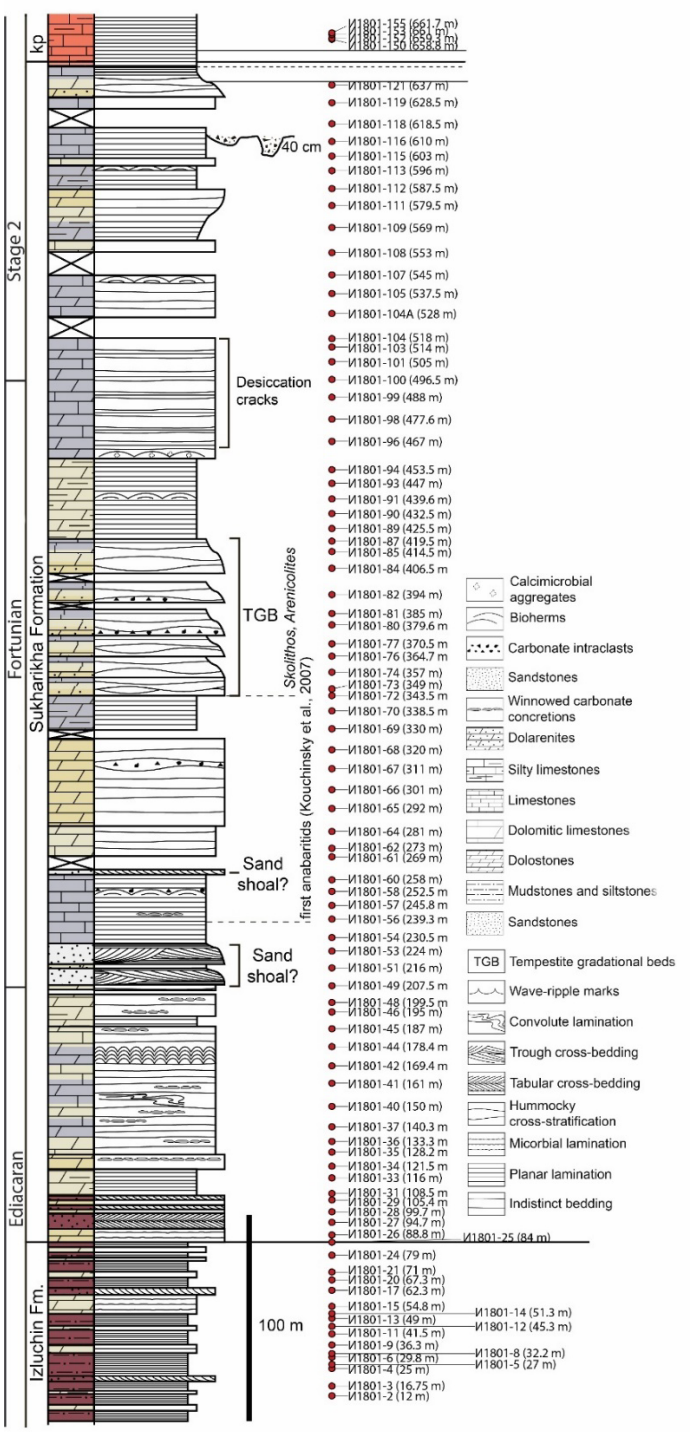

Figure 1.8. Stratigraphic column of the Sukharikha Formation at the Sukharikha River. The height of the samples is shown to the right of the column. Colors of rocks are mirrored in the lithology bars. Kp = Kransy Porog Formation (courtesy of V. Marusin).

1.8: Elemental and Isotopic Systems

1.8.1: Uranium Isotopes

Uranium isotopes have been used extensively over the past decade as a proxy for global seawater redox conditions. In modern oceans, uranium is well mixed throughout the oceans, meaning that local measurements can be representative of global redox states (Lau et al., 2017). The controlling fluxes are riverine inputs and reducing sediments and carbonates as dominant outputs (Andersen et al., 2016). The two most common oxidation states of uranium are the insoluble U^{+4} and soluble U^{+6}. The ability to reduce U^{+6} to U^{+4} depends on the oxygenation state of the oceans. Under oxygenated conditions U^{+6} forms soluble calcium and carbonate complexes. Under anoxic conditions, U^{+6} is reduced to the insoluble U^{+4}, and ^{238}U is preferentially incorporated into sediments, thereby leaving the water column with a greater proportional abundance of the lighter isotope (^{235}U) as compared to the heavier isotope (^{238}U) (Lau et al., 2017). The ratio between ^{238}U to ^{235}U is reported in the delta notation as $\delta^{238}U$. The expansion of ocean anoxia/euxinia will drive the $\delta^{238}U$ composition of global seawater (and carbonate minerals) to lower values (Cherry et al., 2022). The residence time of uranium in the modern ocean is approximately 500,000 years and has an isotopic composition of -0.39‰ (Tissot and Dauphas, 2015). Studies have shown that the $\delta^{238}U$ of modern carbonates (The Bahamas) is slightly offset from the global ocean, which has a value of -0.15‰ (Chen et al., 2018). This study also found that $\delta^{238}U$ signals remain constant regardless of burial depth and mineralogy suggesting that both limestone and dolomite may be used for global redox estimates.

1.8.2: Cerium Anomalies

To assess local water column redox conditions, rare earth element (REE) anomalies have traditionally been employed. Cerium anomalies are most useful as the element is found in both +3 and +4 valence states. Cerium anomalies are reported as Ce/Ce* and are calculated by comparing the cerium abundance relative to neighboring REEs using the following equation: $Ce_{SN}/Ce^*_{SN} = [Ce]_{SN}/([Pr]^2_{SN}/[Nd]_{SN})$. Under oxic conditions Ce^{+3} is oxidized to Ce^{+4}, which binds to the surface of manganese oxides leaving residual seawater depleted in Ce relative to other REEs (Tostevin et al., 2016). Negative anomalies exist in modern oceans, but at varied magnitudes across ocean basins. Anoxic conditions yield Ce/Ce* ratios greater than one, because cerium remains in the Ce^{+3} state and is not removed from the water column (Tostevin et al., 2016). Additional REE abundances and ratios can be used to screen for detrital influence. For example, yttrium to holmium (Y/Ho) ratios greater than 36 indicate authigenic seawater signal (Himmler et al., 2010; Tostevin et al., 2016), while ratios less than 36 may reflect detrital influence. However, Y/Ho ratios of Neoproterozoic carbonates have been found to have consistently lower than modern values, suggesting that the lower values (<36) may be controlled by redox processes rather than detrital contamination (Bau et al., 1997; Wallace et al., 2017).

1.8.3: Lithium Isotopes

While there are several types of redox proxies, lithium isotopes offer insight into the controls on Earth's carbon cycle, specifically continental weathering rates that deliver sediments, alkalinity, and nutrients to seawater. There are two stable isotopes of lithium, ^6Li and ^7Li. The large mass difference between these two isotopes results in large fractionations, making it an excellent tracer of low-temperature processes. The residence time of lithium in the ocean is about 1 Myr and has two input fluxes of continental weathering and hydrothermal activity (Misra and

Froelich, 2012). The sinks of lithium are secondary mineral formation during alteration of oceanic crust and the incorporation of lithium into marine sediments, primarily clay minerals (Stoffyn-Egil and Mackenzie, 1984). The ratio of ^{7}Li to ^{6}Li is reported in the delta notation as $\delta^{7}Li$. In modern oceans, $\delta^{7}Li$ has a value of around +31‰ (Tomascak et al., 1999). The continental crust has an average $\delta^{7}Li$ value of 0±3‰ (Teng et al., 2004), whereas $\delta^{7}Li$ is around 3-5‰ for mid-ocean ridge basalts (Tomascak et al., 1999). During weathering processes, clay minerals are formed that preferentially incorporate the lighter ^{6}Li, leaving the heavier ^{7}Li behind. This results in riverine (and seawater) $\delta^{7}Li$ values that record the combined signal of secondary mineral formation ($\delta^{7}Li$ fractionation and low [Li] in riverine fluxes due to incongruent weathering) and primary silicate dissolution (no $\delta^{7}Li$ fractionation and high [Li] in riverine inputs due to congruent weathering) (Kısakűrek et al., 2005). The delivery of nutrients and oxidants is more efficient when congruent weathering is the dominant mechanism, which led to the hypothesis that enhanced congruent weathering caused the BACE. The $\delta^{7}Li$ of rivers is controlled by the ratio of primary mineral dissolution to secondary mineral formation, which defined as weathering congruency (Pogge von Strandmann et al., 2020). When considering the sinks, reverse weathering (i.e., marine clay formation) can fractionate $\delta^{7}Li$ as well. In oceans of high silica concentration, rapid clay formation occurs. The speed at which this formation occurs does not accommodate high fractionations resulting in $\delta^{7}Li$ that is more reflective of the input. Marine clay formation that occurs slower will allow for large fractionations, driving $\delta^{7}Li$ to higher values (Kalderon-Asael et al., 2021). Marine carbonates represent a relatively small sink for lithium compared to silicates. The incorporation of lithium has a constant isotopic fractionation for inorganically precipitated and biogenically secreted carbonate (~0-5‰). Furthermore, the incorporation of Li into carbonates is negligibly affected by temperature or

salinity (Misra and Froelich, 2012). As a consequence, lithium isotopes in bulk marine carbonates can be used as a proxy for assessing the role of enhanced weathering as both initiator of past ocean anoxic events, via intensified nutrient runoff fueling primary productivity in coastal areas, and terminator of ocean anoxic events via CO_2 sequestration (Lechler et al., 2015).

1.8.4: Organic Carbon Isotopes

Variations in the carbonate carbon isotope record are interpreted to reflect various global changes in the carbon cycle. One approach to establish if these variations reflect changes in the isotopic composition of the inorganic carbon pool is to assess the covariation with the sedimentary organic carbon isotope record ($\delta^{13}C_{org).}$ Traditionally, covariant records of these two carbon reservoirs are interpreted as evidence for simultaneous carbonate and organic matter production in the surface waters of the ocean retaining their original $\delta^{13}C$ composition separated by the kinetic isotope effect associated with photosynthesis, while decoupled records have been interpreted as evidence for diagenetic alteration (e.g., Knoll et al., 1986). The analysis of coeval $\delta^{13}C_{org}$ and $\delta^{13}C_{carb}$ is critical for understanding Earth's history as it is thought to distinguish records of meaningful biogeochemical changes from those altered by diagenesis (Oehlert and Swart, 2014). Freshwater alteration of subaerially exposed shallow marine carbonates is particularly problematic as it has been shown to generate $\delta^{13}C_{carb}$ excursions of similar magnitude to those of early Earth history (Swart and Kennedy, 2012), which is why the assessment between the covariation of $\delta^{13}C_{org}$ and $\delta^{13}C_{carb}$ is essential to understand the preservation quality of a samples geochemical signature. As far as $\delta^{13}C_{org}$ records of the BACE go, very few studies have been conducted. Decoupling between $\delta^{13}C_{org}$ and $\delta^{13}C_{carb}$, as documented in South China (Jiang et al., 2012) was attributed to diagenetically altered signals or overprinting from detrital organic

carbon. However, coupling between the two pools, with shifts of similar magnitude, has been documented as well (Li et al., 2013) and interpreted to represent authigenic seawater signals.

1.8.5: Sulfur Isotopes

The evolution of the sulfur cycle during the Ediacaran provides insight into possible connections between biological evolution, ecosystem engineering, and environmental changes (Wu et al., 2015). Sulfate-bearing minerals (like evaporites) and Carbonate-Associate Sulfate (CAS) are interpreted as records of seawater sulfur isotope composition, whereas sulfides (like pyrite) are interpreted as reflecting local fractionation effects arising from Microbial Sulfate Reduction (MSR) (Canfield and Teske, 1996). During MSR, the lighter ^{32}S in sulfate is preferentially metabolized to form product sulfide, leaving the residual seawater sulfate enriched in ^{34}S. As MSR is carried out by anoxic-dwelling microbes, the biological sulfur cycle is redox-sensitive. During periods of seawater anoxia (like in the Modern Black Sea) MSR will reduce sulfate to sulfide in the water column (eventually depositing as pyrite if ferrous iron is available), resulting in isotopically light pyrite and progressively heavier seawater. In most cases, however, the obligate anaerobes inhabit anoxic sediments rather than the water column. In either case, during an oxygenation event, the distribution of sulfate-reducing microbes would be minimized (Sigalevich et al., 2000), resulting in isotopically lighter seawater sulfate and reduced rates of pyrite burial (He et al., 2019).

Chapter 2: Methods

2.1: Sample Selection

This study was conducted using samples from two locations in remote regions of Siberia, including along the Kotuy River in the Anabar Uplift and along the Sukharikha River in the Igarka Uplift (points C and B respectively in Fig. 1.4), which are over 700 km apart. Samples from the Anabar were collected by Drs. Natalia Bykova and Vasiliy Marusin from the Trofimuk Institute of Petroleum Geology and Geophysics in Novosibirsk, Russia (henceforth Trofimuk) in the summer of 2021. Samples from the Igarka Uplift were collected by Drs. Vasiliy Marusin and Boris Kochnev from Trofimuk in the summer of 2018. A single outcrop section of the stratotype of the Sukharikha Formation and four outcrop sections in the Anabar were measured, evaluated for sedimentary features and depositional environments, and high-resolution stratigraphic samples were collected. All carbonates were analyzed for their carbon and oxygen isotopic compositions at Trofimuk. Of these, 36 carbonate (and four evaporite) samples from the most continuous Anabar section as well as 109 from the Sukharika outcrop were powdered and exported to the University of Maryland (UMD) for the current study. From the Anabar sections, 28 of the samples are from the Staraya Rechka Formation and eight of them are from the Manykai Formation (Knoll et al., 1995b; Kaufman et al., 1996). From the Sukharikha outcrop, 17 samples are from the uppermost Izluchina Formation, 83 are from the Sukharikha Formation, and nine are from the lower Krasny Porog Formation (Kouchinsky at al., 2007; Marusin et al., 2023). In order to assess the redox and weathering history of the samples in this study, petrographic analysis, uranium isotopes, lithium isotopes, organic carbon isotopes, sulfur isotopes, major, minor, trace, and rare earth element (REE) abundances were measured.

Furthermore, the leachates from the uranium, lithium, and REE methods were measured for their elemental abundances to monitor any differences between the extraction techniques.

2.2: Observations and Measurements

2.2.1: Petrography

Prior to any chemical analysis, petrographic observations were conducted to evaluate sedimentary structures and assess the degree of preservation of the samples. Thin section images of the Staraya Rechka and Manykai formations were provided by Dr. Natalia Bykova at Trofimuk and those from the Sukharika Formation were provided by Dr. Vasiliy Marusin. In addition to images, six thin sections were exported by Dr. Bykova for observation at UMD. Of these, petrographic analysis was done using a Nikon LV100POL petrographic microscope connected to a Dell PC along with QCapturePro software for photographic documentation of samples at UMD.

2.2.2: Uranium Isotopes

In order to measure uranium isotopes there is a three-step preparation process of sample acidification followed by sequential dry downs and column chemistry following the procedure in Gilleaudeau et al. (2019) (more details can be found in Weyer et al. (2008) and Brennecka et al. (2011)). Approximately two grams of each sample was weighed out into leached 50% nitric acid (HNO_3) leached 50 mL centrifuge tubes. In each tube, 20 mL of 1M trace-metal grade (TMG) HNO_3 was slowly added followed by 5 mL of concentrated TMG HNO_3, and then 15 mL of 1M TMG HNO_3. The samples were then vortexed and allowed to react overnight. The following morning, the samples were centrifuged in an International Equipment Company Centra-MP4 at 5,000 rpm for 10 minutes. The supernatant was then decanted into separate leached centrifuge

tubes. The residue was washed with 18.2Ω Milli-Q water to remove residual acid, dried at 80°C, and gravimetrically quantified to calculate the percent carbonate in the sample. Aliquots of each sample leachate were taken (~200 μL) and placed into fresh 15 mL centrifuge tubes with ~9.8 mL of 2% TMG HNO_3. The diluted samples from the Staraya Rechka and Manykai formations were then sent to Arizona State University (ASU) to be measured for major, minor, and trace element abundances. Samples from the Sukharikha River were measured at the Carnegie Institution of Washington with the assistance of Dr. Tim Mock (CIW). Both institutes utilized a Thermo Scientific iCAP-Q ICP-MS. Uncertainties were calculated from multiple measurements of a known standard. Once the uranium concentrations were determined from the ASU or CIW data, sample specific amounts of the original 40 mL (to obtain 300 ng of uranium for the isotope analysis) were dried down in Teflon beakers before adding 0.5 mL of $^{233}U/^{236}U$ double-spike to each sample. Following the addition of the double-spike, the samples were capped and placed on a hot plate at 180°C overnight. The following morning samples were removed from the hotplate and allowed to cool completely before adding 6 mL of reverse aqua regia (4.5 mL concentrated TMG HNO_3 and 1.5 mL TMG hydrochloric acid (HCl)) and placed back on the hot plate at 180°C overnight. In the morning samples were uncapped and partially dried until ~1 mL of solution remained. Samples with undissolved particles underwent another round of reverse aqua regia (in some cases samples required several rounds of this step), while samples without undissolved particles moved onto the next step of adding 2 mL of concentrated TMG HNO_3 and 0.2 mL of 30% hydrogen peroxide (H_2O_2). Samples were capped and placed on the hot plate at 180°C overnight. The samples were then uncapped and partially dried down before adding 2 mL of concentrated TMG HNO_3 and set on the hot plate at 180°C overnight. The samples were allowed to partially dry down one final time before receiving 10 mL of 3 M TMG HNO_3. The

samples were capped and set on the hot plate at 180°C for the final time. The following day the samples were allowed to cool completely before being transported to the George Mason University (GMU) for column chemistry.

Two days of ion exchange chromatography were conducted at GMU. Both days of column chemistry utilized element-specific resins in order to purify uranium from the solution. The first day used UTEVA (Uranium and TetraValents Actinides) resin to bind uranium and thorium, while all other elements passed through the column; the target elements were later released and collected, by passing a solution of 5M HCl and 0.05M oxalic acid through the column. The second day of column chemistry uses resin containing Diglycolamine, termed DGA resin, which removes any residual calcium (the major element in carbonates) and sodium that would otherwise suppress uranium ionization during analysis. Additional dry downs are done after each day of column chemistry. Samples were then returned to UMD where several analytical sessions on a Thermo Scientific Neptune Plus MC-ICP-MS with an Aridus II inlet system were conducted to measure the $\delta^{238}U$ compositions of the samples. Two standards, Certified Reference Material (CRM)-145 and CRM-129a were used during the analytical session, which was run at least five times prior to sample analysis. The CRM-145 standard was reanalyzed after every two samples, whereas CRM-129a bracketed by two CRM-145 standards were run every 10 samples. Each sample was analyzed at least twice and the values averaged to determine standard deviations.

2.2.3: Rare Earth Element Leach

A leaching procedure targeting rare earth elements was conducted following the method of Tostevin et al. (2016), which begins with rinsing 25 mg of powered sample with 1 mL of Milli-Q water in microcentrifuge tubes two times, centrifuging with a Thermo Scientific Sorvall

Legend Micro 17 at 5,000 rpm for 10 minutes, decanting, and discarding the supernatant after each treatment. Each sample was then reacted with 312.5 µL of 2% HNO_3, vortexed, and allowed to sit overnight. The solution was centrifuged and the supernatant was decanted and disposed of the following morning, before adding 625 µL of 2% HNO_3 to each sample. The samples were again allowed to react overnight before centrifuging and decanting the entire solution into fresh 15 mL centrifuge tubes. Each solution was then diluted up to 10 mL with 2% HNO_3 before getting sent to ASU for analysis.

2.2.4: Lithium Isotopes

Lithium extractions from carbonate powders were accomplished by performing sequential leaching following the procedure outlined by Cao et al. (2020; 2022; 2023). Two hundred milligrams of each sample are mixed with 10 mL of 1M ammonium acetate (NH_4Ac). This mixture is ultrasonicated in a Seeutek Digital Ultrasonic Cleaner for 30 minutes and then centrifuged in a Model 225 Fisher Scientific Centrific Centrifuge at 6000rpm for 10 minutes. The resulting residue is treated using 10 mL of 1M ammonium carbonate [$(NH_4)_2CO_3$] in an ultrasonic bath for 30 minutes. The resulting supernatant is removed and discarded. The procedure is then repeated, and then the residues are washed with Milli-Q water, centrifuged and decanted. The rinsed sample is dissolved using 10 mL of 0.3M acetic acid (HAc), and the supernatant is filtered with a 0.2 µm syringe filter to remove all remaining solid particles, and the supernatant collected in a Teflon beaker for column chemistry.

Two rounds of column chemistry are performed to isolate lithium in the sample. The first column isolates lithium from the sample while the second column further purifies lithium from residual sodium. Both columns use Bio-Rad ™ AG50W (200-400) mesh resin. Column dimensions are 1.5 cm internal diameter, 10 cm height, and filled with 17 mL of resin for the

first column, and 0.6 cm internal diameter, 20 cm height, and filled with 3.4 mL of resin for the second column. Both columns follow the same procedure but use different types and concentrations of acids to separate lithium from other elements. Prior to each batch, columns are cleaned with 20 mL of 6M HCl followed by 20 mL of Milli-Q water. The conditioning step requires 10 mL of 0.7M HNO_3 or 0.2M HCl for the first and second columns, respectively. After conditioning the samples are carefully loaded onto the column beds. The matrix elution for the first column used 2l mL of 0.7M HNO_3, and the second column used 20 mL of 0.2M HCl. After the matrix elution is complete, three 2 mL pre-cuts (0.7M HNO_3 or 0.2M HCl) are taken. After the pre-cuts the samples are collected in 50 mL of 0.7M HNO_3 for column one, and 32 mL of 0.2M HCl for column two. Once samples have been collected three post-cuts are taken following the same procedure as the pre-cuts. The samples and pre/post-cuts are dried down and diluted for analysis. To ensure 100% lithium collection, the voltage signal of the pre/post-cuts was checked, and any pre/post-cuts with intensities significantly higher than blanks (i.e., samples that went through column chemistry without the introduction of a sample) were added back to the main collection.

Isotopic measurements (as well as pre/post-cut checks) were made on a Thermo Scientific Neptune Plus MC-ICP-MS with an Apex-IR inlet system in the Department of Geology at UMD. Lithium isotopes were measured with a 50 μL/min PFA nebulizer at low resolution using X skimmer and Jet sampler cones. A typical ^{7}Li signal intensity was 2–3V for a 5 ppb Li solution. Samples were measured for their voltage intensity to calculate the amount required for a 5 ppb solution. The international standard LSVEC and samples were diluted to 5 ppb in 2% HNO_3 to match the matrix. The $\delta^{7}Li$ values were analyzed by alternating between standard and samples, bracketing with blanks in between. Each sample was measured three

separate times in order to report sample standard deviation (2SD) values, and each measurement consists of 40 cycles per block with 4.194 second integration time for each cycle. Ultrapure HNO_3 (2%) was measured before each sample and standard for background subtraction. Accuracy and precision were also assessed from repeated measurements of a 2 ppb in-house standard (UMD-1), reporting δ^7Li 55.3‰ ± 0.4‰ (2SD, n = 13), in good agreement with the published values of δ^7Li 54.7‰ ± 1.0‰ (2SD, n = 31) (Penniston-Dorland et al., 2012).

2.2.5: Organic Carbon Isotopes

The organic carbon isotope compositions as well as total organic carbon (TOC) content have been measured by GSMS (gas source mass spectrometry) at UMD following the procedure described by Cui et al. (2015; 2019). This was done through the combustion of the acidified residues to CO_2 with a Eurovector elemental analyzer (EA) in line with an Elementar Isoprime isotope ratio mass spectrometer (IRMS). Acidified residues from the uranium leach were packed into folded tin cups (3x5 mm) for combustion in an 18 mm diameter quartz column packed with chromium oxide and silvered cobaltous/cobaltic oxide heated to 1040°C. The analyte flows from the combustion column in a stream of ultra-high purity helium (Airgas 99.999% purity) to a second reduction column at 650°C packed with elemental copper that converts nitrogen dioxide (NO_2) and nitrous oxide (N_2O) to nitrogen gas (N_2). Excess oxygen gas (O_2) is absorbed in a magnesium perchlorate ($Mg(ClO_4)_2$) water trap. The separation of CO_2 from N_2 occurs in a 3 m stainless steel gas chromatography (GC) column, which is packed with Porapak-Q and heated to 50°C. The analyte was introduced to the IRMS in a flow of helium (80-120 mL/min) through a splitter valve. Reference gas (ultra-high purity helium) was introduced in timed pulses to begin the run using an injector connected to the IRMS. The isotope ratios of reference and sample peaks were determined by monitoring ion beam intensities relative to background values. Results

are expressed in the delta notation as per mil deviations from the Vienna Pee Dee Belemnite (VPDB) standard. Five standard urea aliquots were measured at the start of each analytical session to determine system suitability, and then two standard urea aliquots were measured between each set of 10 samples. Uncertainties for unknowns based on multiple measurements of this known material are typically better than 0.3‰.

2.2.6: Sulfur Isotopes

Pyrite and bulk sulfate sulfur isotope compositions were determined using a similar procedure to organic carbon isotope measurements following the analytical methods from Cui et al. (2015; 2019). The analyses were done using combusted bulk acidified residues or silver sulfide (Ag_2S) precipitates following CRS extractions (modified after Canfield et al., 1986) using equipment and reagents in the Farquhar Laboratory. Sulfur combustions to sulfur dioxide (SO_2) were aided by the addition of 0.1 to 0.3 mg of vanadium pentoxide (V_2O_5) into each 3x5 mm tin cup along with the sample. Sample combustion was done by pulsing the tin cups with O_2 in a catalytic combustion furnace operating at 1030°C. A quartz reaction tube was packed with high purity copper wire for quantitate oxidation and O_2 resorption. The removal of water from the combustion products was done with a 10 cm magnesium perchlorate ($Mg(ClO_4)_2$) column, and the SO_2 was separated from other gases with a 0.8 m GC column packed with Porapak 50-80 mesh heated to 115°C. The analyte was introduced in a flow of helium (80-120 mL/min) through a splitter valve. Similar to the $\delta^{13}C_{org}$ analysis, times pulses of SO_2 reference gas (Air Products 99.9% purity) were introduced at the beginning of the run. Results are expressed in the delta notation as per mil deviations from the Vienna Canyon Diablo Troilite (VCDT) standard. Five NBS-127 barite standards were measured at the start of each analytical session to determine system suitability, and then two of these standards were measured between each set of 10

samples. Based on multiple standard analyses throughout the runs, the sulfur isotope uncertainties are typically better than 0.3‰.

2.3: Seafloor Anoxia Model

To better illustrate how variations in uranium isotopes translate to the degree of seafloor anoxia, a two-sink mass balance model was applied to the $\delta^{238}U$ data produced from this study (Fig. 2.1). This model by Kipp and Tissot (2022) assumes steady state and considers rivers as the sole input into the ocean with two sinks: anoxic sediments and other sediments. The model uses $\delta^{238}U_{seawater}$ as the input, so the $\delta^{238}U_{carb}$ values from this study must be corrected for the offset between carbonates and seawater. An offset of -0.27‰ (from Chen et al., 2018) was used for this calculation. To account for the isotopic fractionation associated with U burial in anoxic sediments (Δ_{anox}) an estimate of 0.7‰ was used (Kipp and Tissot, 2022). This offset what was chosen to reflect the most conservative value, which is, to say the least amount of seafloor anoxia that could be present based on the inputs.

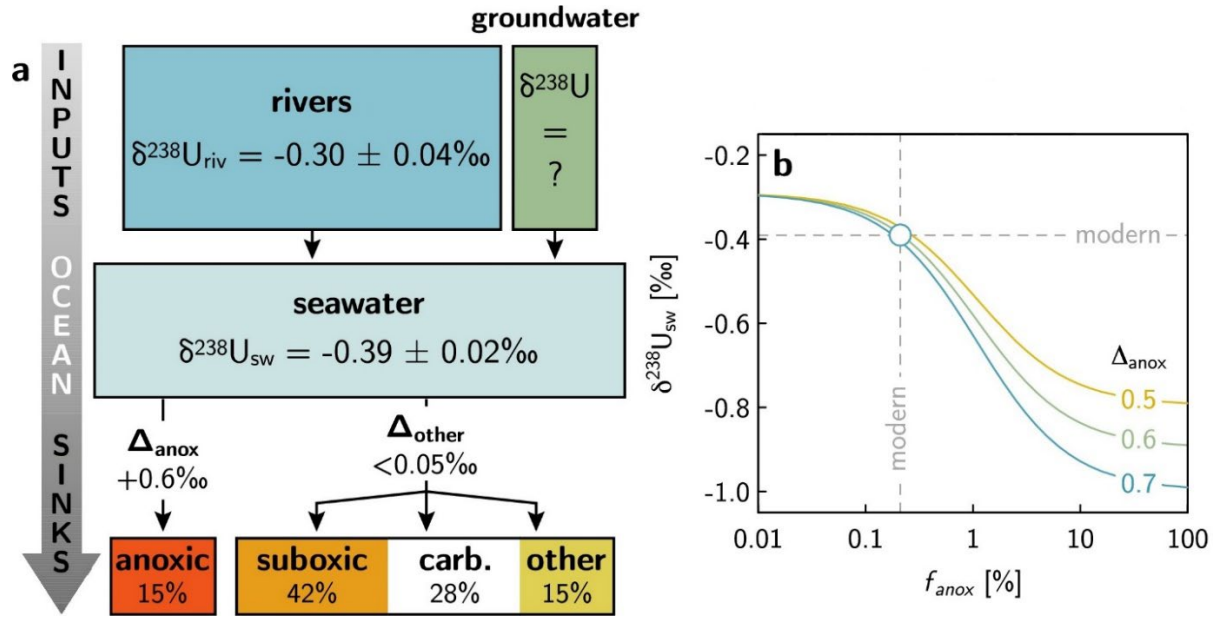

Figure 2.1. (a) Simplified U isotope mass balance model. (b) Steady-state $\delta^{238}U_{sw}$ as a function of ocean anoxia (expressed as the seafloor area covered by anoxic sediments, f_{anox}) (Modified from Kipp and Tissot, 2022).

Chapter 3: Results

3.1: Anabar Uplift

Thin section observations from six samples in the Staraya Rechka Formation show a dominant carbonate matrix, with very few (if any) features or distinct grains. The dolomicrite comprising the majority of the Staraya Rechka samples is fine to very fine-grained preserving original fabrics, although many are simply massive or finely laminated. Sample 233/17 (81 m from the base of the section) preserved a complex chambered structure interpreted as *Renalcis*, the remains of blue-green algae (Fig. 3.1A)(Pratt, 1984). Additional features seen in other samples are rounded to euhedral grains and/or voids left behind evaporite dissolution (233/17, Fig. 3.1B), or pyrite veins (255/2, Fig. 3.1C).

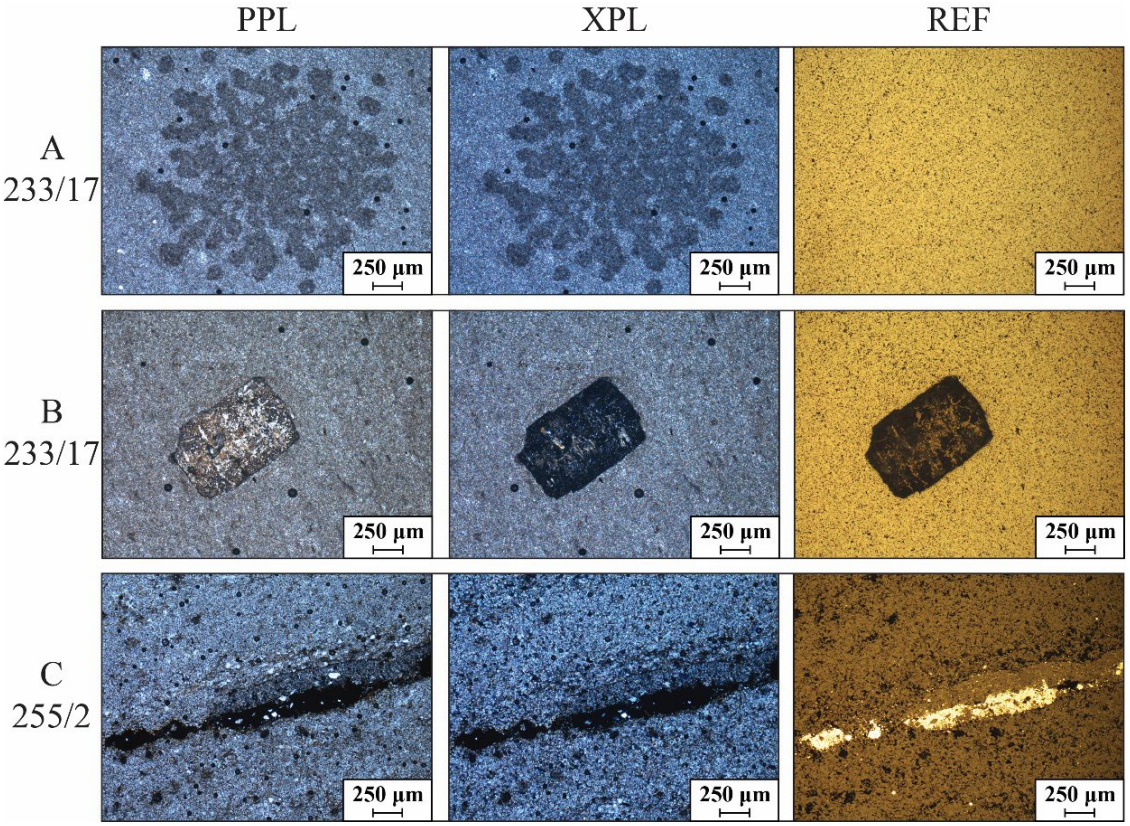

Figure 3.1. Thin section images from the Staraya Rechka Formation. Images were taken using 5x magnification. Images were taken with plane-polarized light (PPL), cross-polarized light (XPL), and reflected light (REF). (A; B) Sample 233/17. (C) Sample 255/2.

The geochemistry of the Anabar Uplift from this study is separated into three categories: diagenesis, redox, and weathering. To assess the extent of diagenesis in the samples, the samples are screened for signs of contamination or alteration. The percentage of carbonate is similar across all the samples, with all of them greater than 85%, except for one sample in the basal Manykai Formation that contains 71% (Fig. 3.2A). The $\delta^{13}C_{carb}$ values show a decrease from values around 0 to -2‰ at the base of the section in the Kharyyalakh Member, and then drop rapidly in the evaporitic Chimuka Member to a minimum of -6.5‰ around 30 m and return to baseline values between 65 and 80 m. This excursion, labeled "N" is what is described as the BACE (Kaufman et al., 1996). Above 80 m the $\delta^{13}C_{carb}$ values hold steady around -2‰ in the Kochokon Member for another 40 m before a slight decrease to around -5‰ across the disconformity separating the Staraya Rechka Formation from the Manykai Formation. Limestone in this formation rises to values as high as +2‰ (Fig. 3.2B), just above 150 m which then falls to about -6‰ at 180 m and then rises back to +2‰ near the top of the sampled interval. The $\delta^{18}O_{carb}$ values start around -2‰ at the base of the measured section and remain there for much of the Staraya Rechka Formation, with the most ^{18}O-enriched samples in the Chimuka Member. However, towards the top of the Staraya Rechka Formation and into the Manykai Formation, there is a notable decrease in the $\delta^{18}O_{carb}$ values, ending around -8‰ (Fig. 3.2C), which broadly corresponds with the transition from dolomite to limestone lithologies.

The leachates produced for the uranium, REE, and lithium leaches were measured for elemental abundances for comparison between leaching techniques. The lithium leaching method shows higher Mg/Ca ratios in the dolomitized samples (Fig. 3.2D). Limestone samples showed little difference between the leaching techniques. The Mn/Sr ratios are less than 10 for all samples, except for the lowest three samples which have elevated values (Fig. 3.2E). The three

leaching methods produced similar Mn/Sr ratios, although the greatest difference was seen in the lowest three samples where the Mn/Sr ratios were greater than 10. The petrographic analysis and elemental ratios indicate the samples are well preserved, and may retain original seawater signals.

Uranium isotopes and cerium anomalies were measured to understand the redox state of the Staraya Rechka Formation. The $\delta^{238}U$ values remain constant averaging at -0.67‰ in the Staraya Rechka Formation, with a slight increase to an average of -0.56‰ in the Manykai Formation (Fig. 3.3B). The Staraya Rechka Formation has Ce/Ce* values slightly above one, while in the Manykai Formation, the values are around 1.5 (Fig. 3.3C). The Y/Ho ratios show a very similar trend to the Ce/Ce* data. The Staraya Rechka Formation has a very tight range, all of them slightly less than 36. In the Manykai Formation, the Y/Ho ratios are slightly higher, but with more variability (Fig. 3.3D). Cross-plots show the relationship between Y/Ho and detrital element concentrations (including Al, Zr, Ti, and Rb), where the high Y/Ho values only occur with low concentrations of these detrital elements (Fig. A1 in Appendix)

Lithium isotopes serve as a proxy for assessing the extent and type of weathering. In the Staraya Rechka Formation, $\delta^{7}L$ compositions reveal a startling rise in values through the 130 m thick interval. Values at the base of the formation begin around 10‰, but steadily increase into the uppermost section of the formation, with a peak of almost 32‰ (Fig. 3.4B). The $\delta^{7}L$ values then fall to ~2‰ in the Manykai Formation before rising back to 15‰. Plots of Al/(Mg + Ca) (used to track detrital influence) do not show any trends that match those of the $\delta^{7}L$ compositions (Fig. 3.4C). The same can be said for plots of Li/(Mg + Ca), where there is no correlation (Fig. 3.4D). It should be noted that the largest range of values for both these plots occurs within the Staraya Rechka Formation, with the range of values decreasing moving up the stratigraphy.

Additional assessments of diagenesis come from the $\delta^{13}C_{corg}$ record. The values range from around -28‰ to around -32‰ (Fig. 3.5B), but within the Staraya Rechka Formation, there is a very slight negative anomaly around 70 m in the Chimuka Member. The Manykai Formation has broadly consistent values, except for one point that is lower than the rest by about 5‰. Looking at the $\Delta\delta^{13}C$, there is a slight negative shift to values around 20‰, corresponding to the BACE (Fig. 3.5C). There is one point in the Kochokon member of the Staraya Rechka Formation that has a value much lower than the neighboring points. The TOC is very low for both the Staraya Rechka and Manykai formations. Only seven samples are greater than 0.1 wt.% TOC, with the greatest (0.33 wt.%) occurring with the lowest $\delta^{13}C_{corg}$ value.

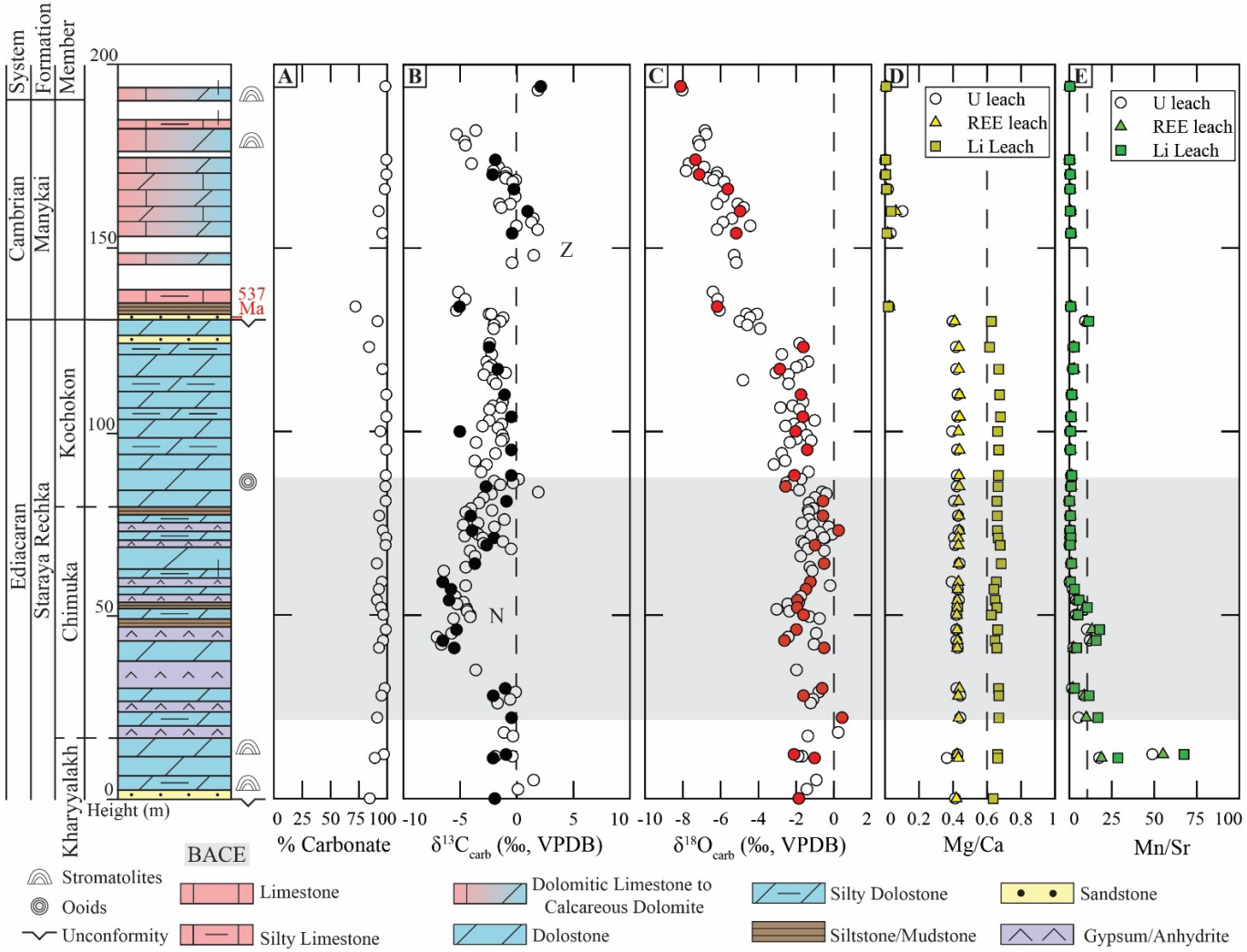

Figure 3.2. Stratigraphy and chemostratigraphy of the Staraya Rechka Formation at the Kotuy River. The gray band represents the BACE interval. (A) Percent carbonate. (B) $\delta^{13}C_{carb}$ referenced to V-PDB. Closed circles represent samples provided for this study. Uncertainties were calculated from averages across multiple measurements (±0.3‰ 2SD $\delta^{13}C$). (C) $\delta^{18}O_{carb}$ referenced to V-PDB. Closed circles represent samples provided for this study. Uncertainties were calculated from averages across multiple measurements (±0.1‰ 2SD $\delta^{18}O$). (D) Mg/Ca from three different leaching techniques. The dashed line at 0.6 represents the division between limestone and dolomite. (E) Mn/Sr from three different leaching techniques. The dashed line at 10 represents the division between unaltered and altered samples.

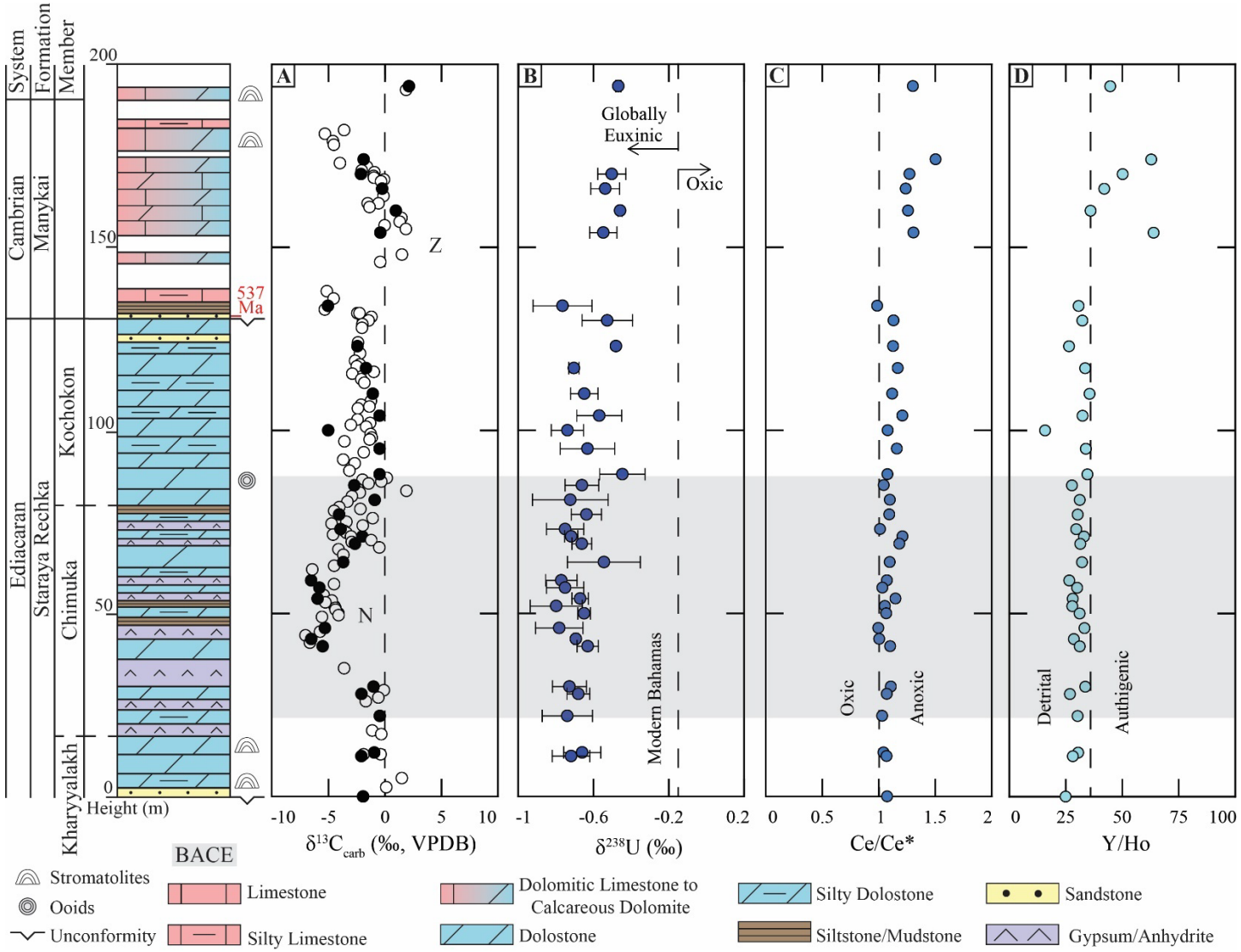

Figure 3.3. Stratigraphy and chemostratigraphy of the Staraya Rechka Formation at the Kotuy River. The gray band represents the BACE interval. (A) $\delta^{13}C_{carb}$ from Fig. 3.2. (B) $\delta^{238}U$ values. The dashed line represents $\delta^{238}U$ of modern carbonate (-0.15‰, Chen et al., 2018). Uncertainties are calculated from duplicate analyses. (C) Ce/Ce*. The dashed line at 1 represents the boundary between oxic and anoxic. (D) Y/Ho. The dashed line at 36 represents the boundary between detrital and authigenic ratios.

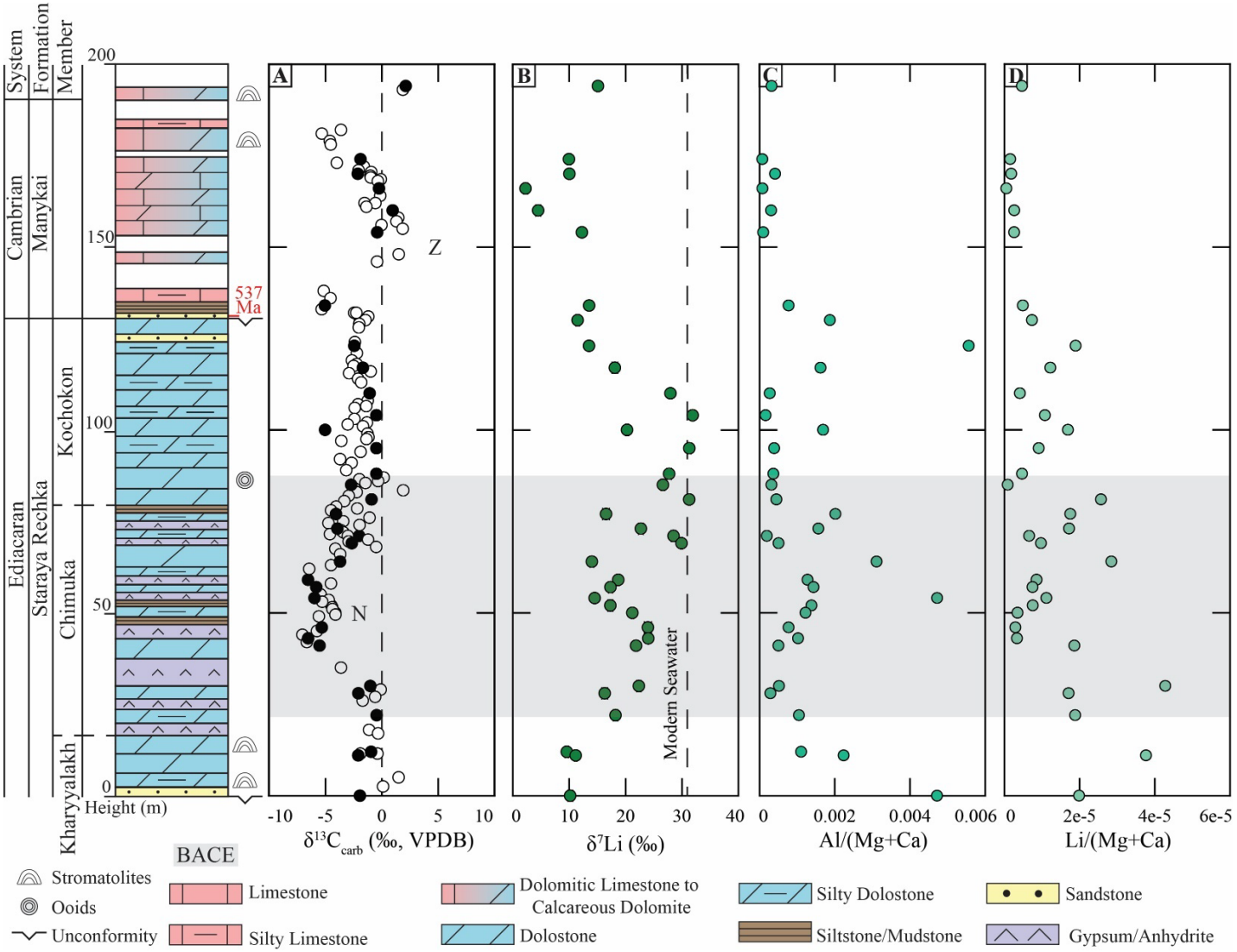

Figure 3.4. Stratigraphy and chemostratigraphy of the Staraya Rechka Formation at the Kotuy River. The gray band represents the BACE interval. (A) $\delta^{13}C_{carb}$ from Fig. 3.2. (B) $\delta^{7}Li$ values. Uncertainties are calculated from duplicate analysis (most uncertainties are around ±0.4‰ 2SD, which is smaller than the plotted point size). The dashed line at +31‰ represents the $\delta^{7}Li$ of modern seawater. (C) Al/(Mg+Ca). (D) Li/(Mg+Ca).

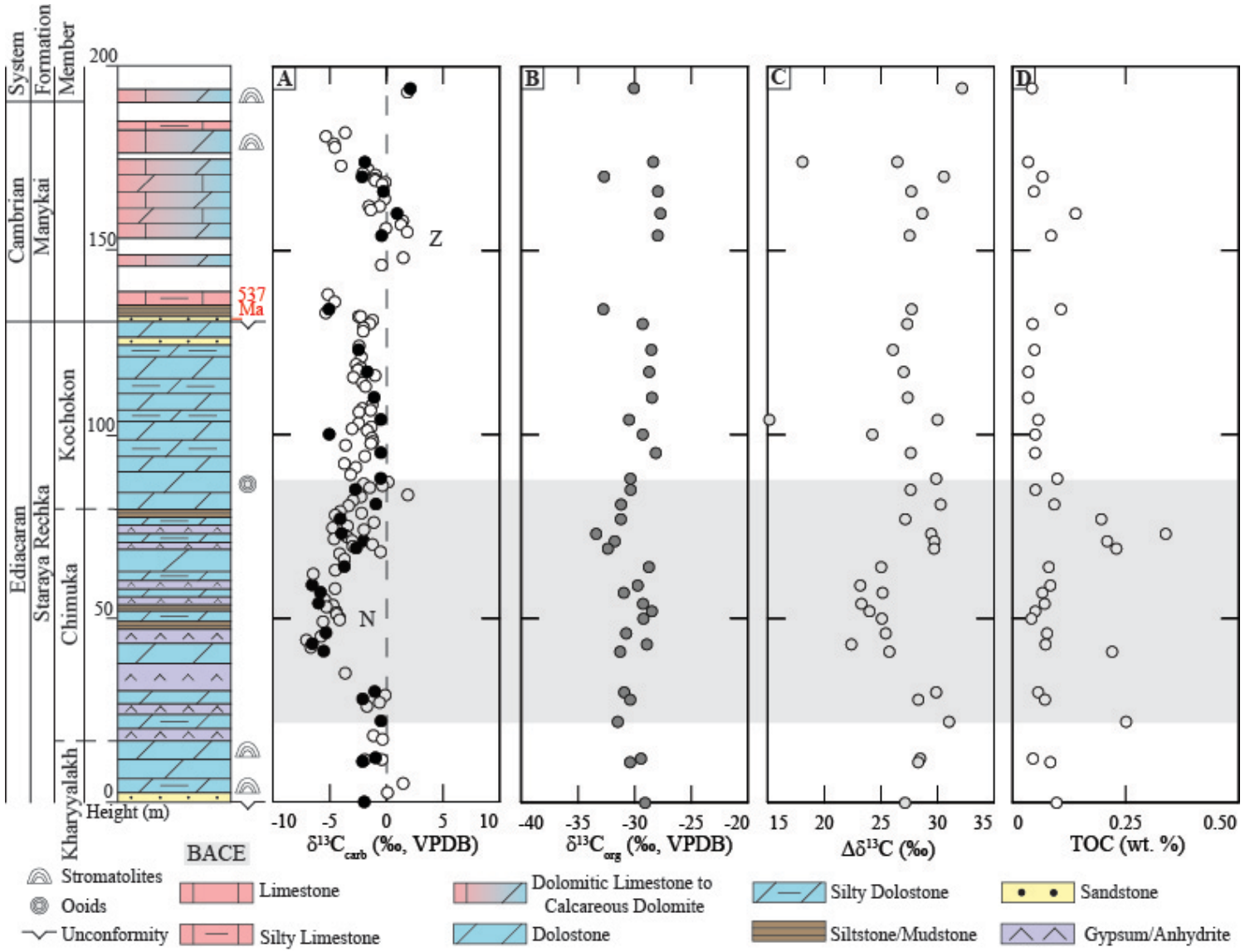

Figure 3.5. Stratigraphy and chemostratigraphy of the Staraya Rechka Formation at the Kotuy River. The gray band represents the BACE interval. (A) $\delta^{13}C_{carb}$ from Fig. 3.2. (B) $\delta^{13}C_{org}$ referenced to VPDB. Uncertainties are calculated from repeated measurements of a known urea standard (±0.33‰ 2SD). (C) $\Delta\delta^{13}C$ values calculated from $\delta^{13}C_{carb}$ - $\delta^{13}C_{org}$. (D) Total organic carbon (TOC) in weight percent (wt. %)

3.2: Igarka Uplift

The majority of the samples from the Sukharikha River section, including the Izluchina, Sukharikha, and Kransy Porog formations show percent carbonate values greater than 70%, however in the lowermost portion, the values have significant ranges, going as low as 35% (Fig. 3.6A). The $\delta^{13}C_{carb}$ values show several negative and positive oscillations that characterize the Fortunian Stage of the basal Cambrian Period (Fig. 3.6B). The first peak, labeled "1n", has a nadir of -8.0‰, and is interpreted to be the BACE (Kouchinsky et al., 2007; Maloof et al., 2010a). There is an overall trend towards more positive values, with each negative perturbation getting smaller in magnitude while the positive ones get larger. The $\delta^{18}O_{carb}$ values show a downward trend at the base of the Sukharikha Formation, going from -4‰ to around -8‰, remaining constant for the duration of the 1n excursion (Fig. 3.6C). After the 1n excursion, the $\delta^{18}O_{carb}$ values show a higher degree of variability, followed by a slight increase at the top of the Sukharikha Formation. While there is limited Mg/Ca data, all points are less than 0.6 (calculated from the uranium leach)(Fig. 3.6D). The Mn/Sr ratios are all below 10 except for the lowest two points, however, given the few data points, it is difficult to say if the other samples would show a similar trend (Fig. 3.6E).

Assessing redox on a global scale, the $\delta^{238}U$ values in the base of the Sukharikha Formation during the 1n perturbation show a minor trend toward positive values, with the highest at -0.17‰ (Fig. 3.7B). The average value during the 1n interval is -0.38‰. The rest of the Sukharikha Formation shows a wider range of values. Three points are within the oxic realm, which occurs during perturbations 2n and at 3p. After the 3p perturbation, the $\delta^{238}U$ values shift towards more negative values but remain rather spread. Looking at a local scale proxy, the Ce/Ce* data shows the majority of points being greater than 1 (Fig. 3.7C). There are a few points

that dip below that mark in the Izluchina Formation and mid to upper Sukharikha Formation. The Y/Ho ratio has the majority of data plotting below 36, indicating detrital influence (Fig. 3.7D). The Ce/Ce* anomaly data shown is only the points that have Y/Ho ratios greater than 36.

Further insight into the redox conditions can be gleaned from assessing $\delta^{34}S$ compositions. The $\delta^{34}S$ values show a negative trend exiting the 1n perturbation, starting around 20‰ and dropping to just below 0‰ (Fig. 3.8B). Then there is a positive trend going from just below 0‰ to ~15‰ and then a drop to ~5‰. that seems to inversely mirror the 2n perturbation. Following this, there is another strong negative trend, with values ranging from ~30‰ to close to 0‰. These observations reveal complex temporal variations, which require deeper exploration into the processes that may be at play.

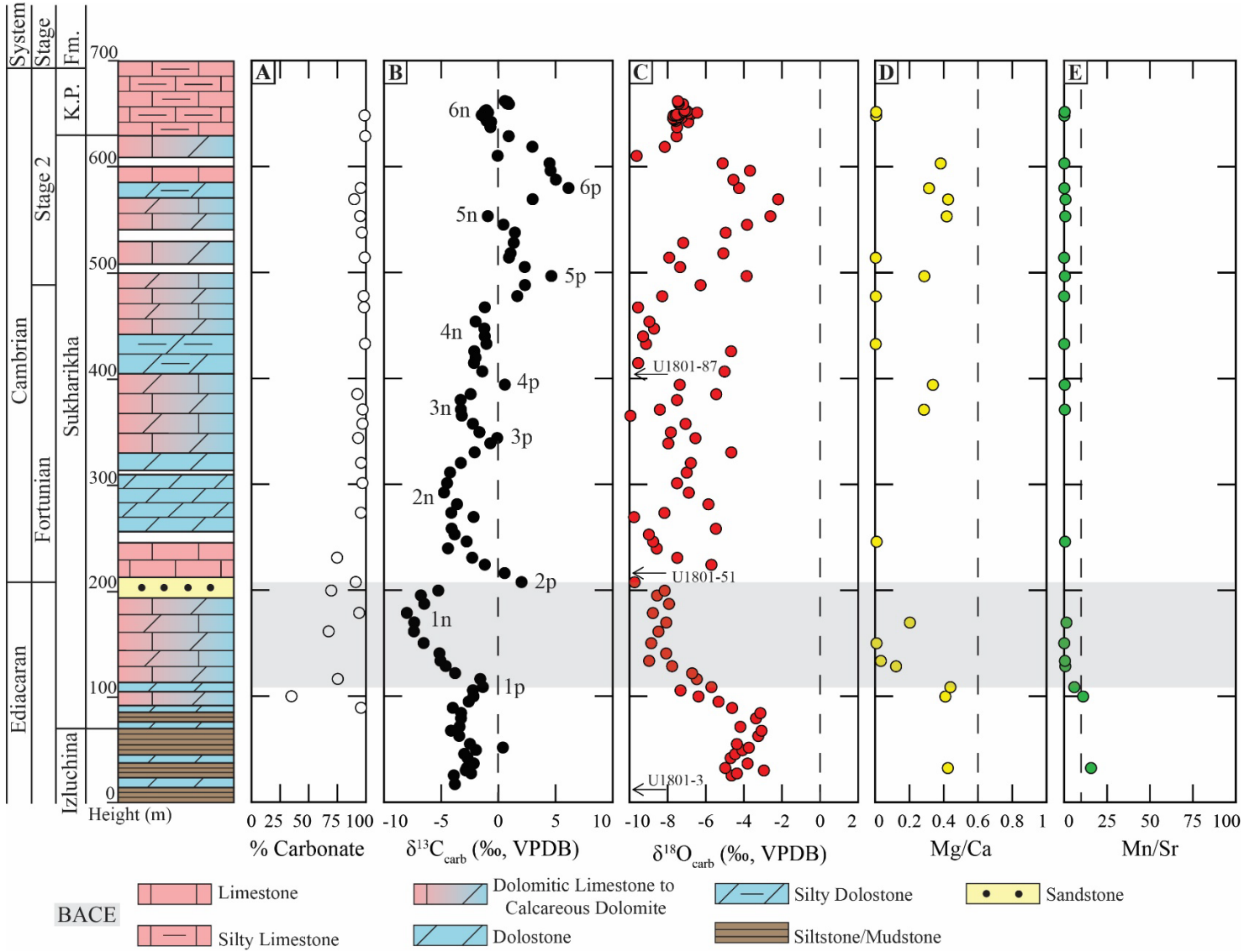

Figure 3.6. Stratigraphy and chemostratigraphy of the Sukharikha Formation at the Sukharikha River. The gray band represents the 1n interval. (A) percent carbonate values. (B) $\delta^{13}C_{carb}$ referenced to V-PDB. (C) $\delta^{18}O_{carb}$ referenced to V-PDB. (D) Mg/Ca. The dashed line at 0.6 represents the division between limestone and dolomite. (E) Mn/Sr. The dashed line at 10 represents the division between unaltered and altered samples.

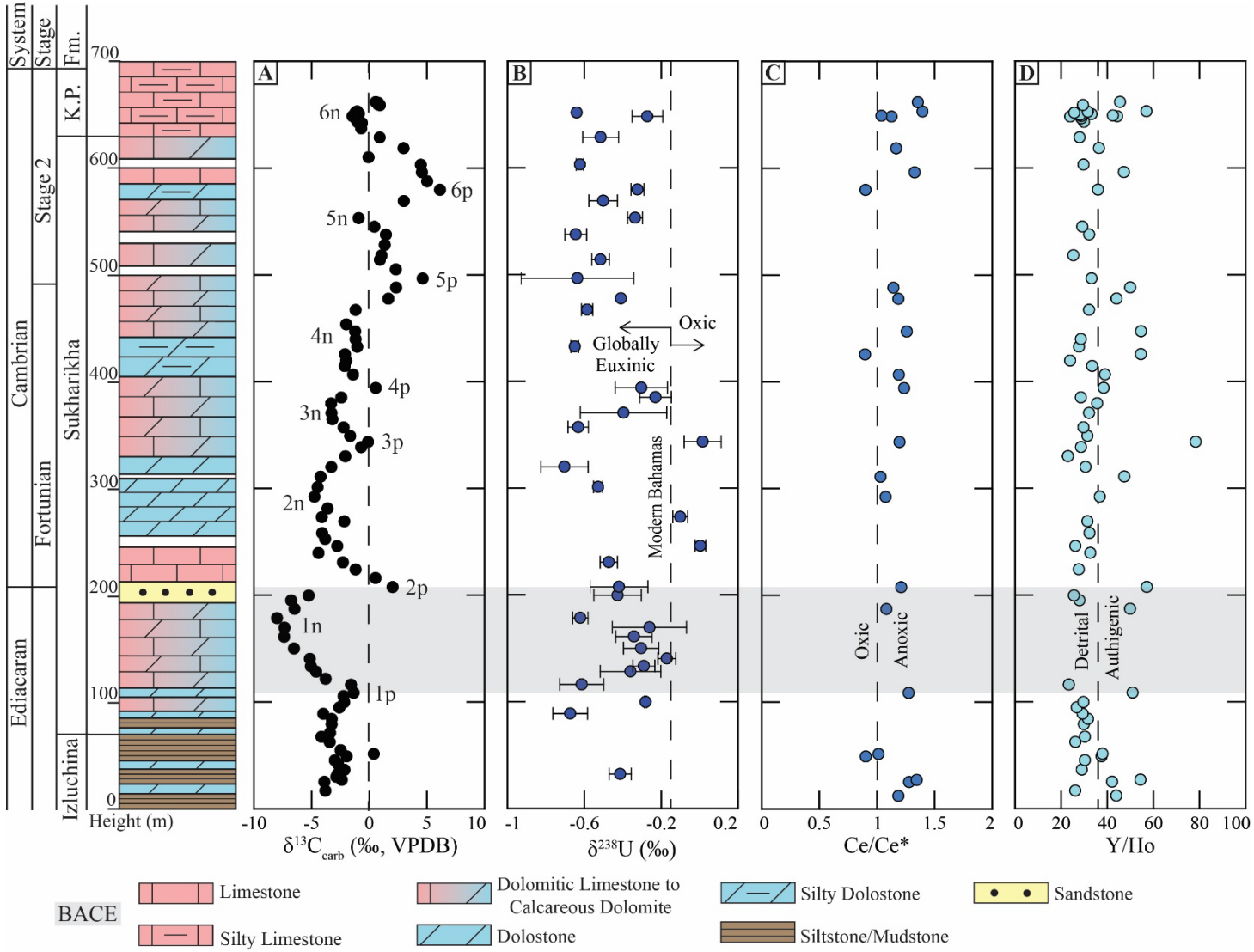

Figure 3.7. Stratigraphy and chemostratigraphy of the Sukharikha Formation at the Sukharikha River. The gray band represents the 1n interval. (A) $\delta^{13}C_{carb}$ from Fig. 3.6. (B) $\delta^{238}U$ values. The dashed line represents $\delta^{238}U$ of modern carbonate (-0.15‰, Chen et al., 2018). Uncertainties are calculated from duplicate analyses. (C) Ce/Ce*. The dashed line at 1 represents the boundary between oxic and anoxic. (D) Y/Ho. The dashed line at 36 represents the boundary between detrital and authigenic ratios.

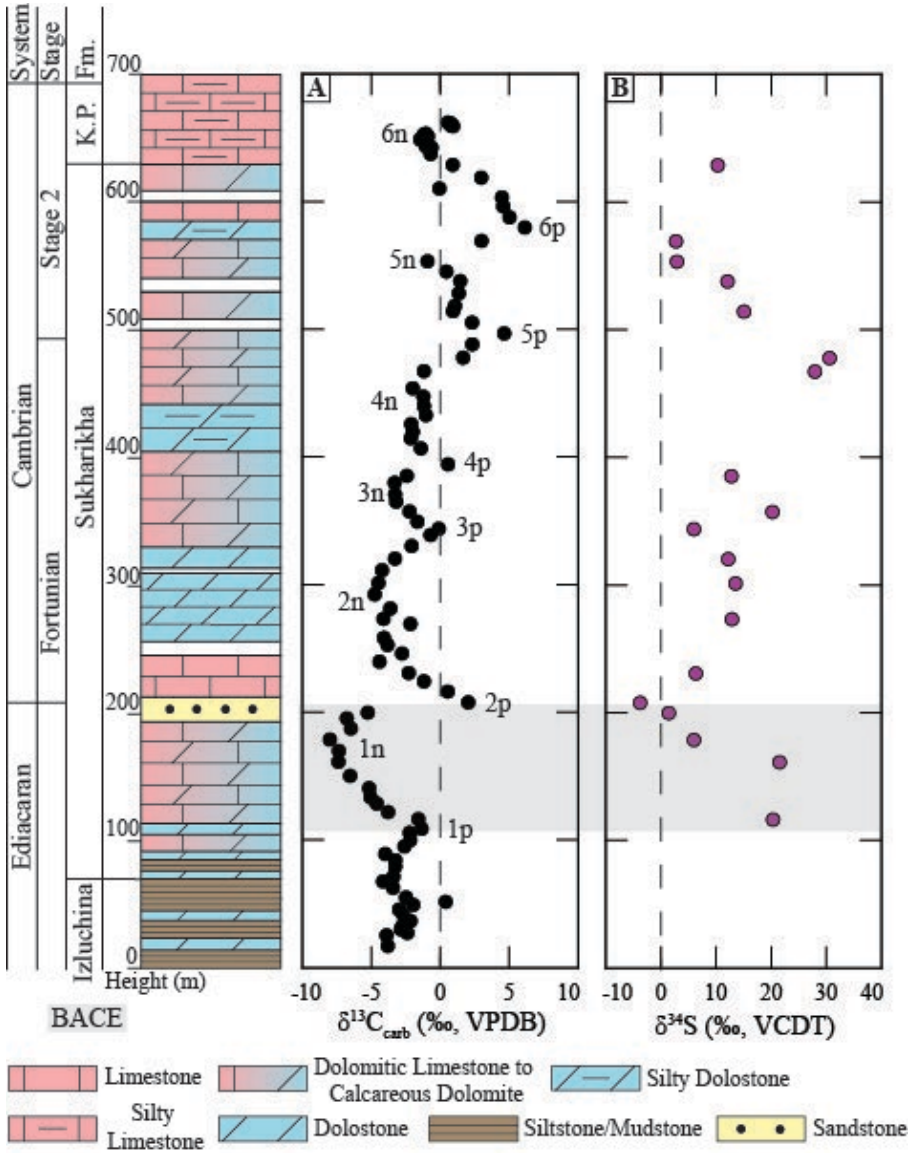

Figure 3.8. Stratigraphy and chemostratigraphy of the Sukharikha Formation at the Sukharikha River. The gray band represents the 1n interval. (A) $\delta^{13}C_{carb}$ from Fig. 3.6. (B) $\delta^{34}S$ referenced to V-CDT. Uncertainties are calculated from repeated measurements of a known NBS-127 standard (±0.66‰ 2SD).

Chapter 4: Discussion

4.1: Diagenesis

4.1.1: Anabar Uplift

Despite being more than 500 million years old, the carbonates of the Staraya Rechka and Manykai formations appear to be well preserved supporting the view that their elemental and isotopic signatures reflect aspects of depositional and diagenetic conditions. Petrographic analysis confirms that the Staraya Rechka dolomite samples are extremely fine-grained, fabric-retentive, and mostly pure carbonate. The low Mn/Sr ratios indicate that all but the lowest three samples were little affected by diagenesis (Kaufman et al., 1992; 1995). The Mg/Ca ratios indicate different mineralogy between the Staraya Rechka and Manykai formations, that being the partial dolomitization of the Staraya Rechka carbonates, which is consistent with the peritidal environment. The interpretation is consistent with all three leaching techniques, although the lithium leach shows Mg/Ca ratios ~0.2 higher than the uranium and REE leaches. Differences seen in the leaches could come from the lithium leach preferentially extracting magnesium from the sample. This has not been previously documented, however, so is it difficult to discount any analytical issue on the measurement. The difference in mineralogy between the Staraya Rechka and Manykai formations has an impact on $\delta^{18}O_{carb}$ values, such that dolomite has a +2‰ shift compared to calcite if co-precipitated from the same solution (Kaufman et al., 1992). However, this data shows a 6‰ difference between the Staraya Rechka (average -2‰) and Manykai (average -8‰) formations, so that mineralogy alone is insufficient to account for the isotopic differences. High rates of evaporation, however, can result in more positive $\delta^{18}O_{carb}$ values (Magaritz and Stemmerik, 1989), which is also consistent with the Staraya Rechka Formation as

inferred by its peritidal depositional environment. The ^{18}O enrichment is consistent with the ubiquitous presence of evaporites and mud cracks as well as the absence of evidence for bioturbation, especially in the Chimuka Member. The $\delta^{18}O_{carb}$ compositions of the Manykai Formation samples are consistent with the average global Cambrian seawater, which is described to be from -6.5‰ to -8‰ (Hearing et al., 2018).

Further assessment of an authigenic signal can be done by evaluating the covariance between $\delta^{13}C_{carb}$ and $\delta^{13}C_{org}$. The $\delta^{13}C_{org}$ record does not show clear coupling with the carbonate record that might be expected with authigenic signals. The values remain very consistent around -30‰, and do not show any significant coupling with the carbonate record. The most negative $\delta^{13}C_{org}$ points have the highest TOC so it is possible that $\delta^{13}C_{org}$ is overprinted from a minor degree of detrital organic contamination. Looking at the difference between $\delta^{13}C_{carb}$ and $\delta^{13}C_{org}$ ($\Delta\delta^{13}C$) there is a slight negative anomaly to lower magnitude of fractionation (~20‰) that corresponds to the BACE interval. Notably the $\Delta\delta^{13}C$ differences in this study smaller than those previously published from BACE sections in South China (Jiang et al., 2013). The previous publication attributed the disparity to diagenetic alteration or detrital organic carbon contamination. It is possible that those factors are also at play here.

4.1.2: Igarka Uplift

Thin section images show that the Igarka Uplift carbonates are very fine-grained and fabric-retentive. The geochemical data from the Sukharikha River section also shows signs of samples being well-preserved. The percent carbonate is above 90% except for those that fall within the 1p, 1n, and 2p perturbations, where four points are below 70%, and thus potentially impacted by detrital contamination. Low $\delta^{18}O_{carb}$ values (below -10‰) can result from diagenetic resetting by meteoric waters and hydrothermal fluids (Kaufman and Knoll, 1995). Even though

$\delta^{13}C_{carb}$ is less prone to alteration, very low $\delta^{18}O_{carb}$ values suggest possible alteration of $\delta^{13}C_{carb}$. In the Sukharikha Formation, only two values are less than -10‰, so the majority of the $\delta^{13}C_{carb}$ record has likely not been influenced by diagenetic alteration using this metric, even though the data is more variable above 200 m in the studied section. The Mg/Ca ratios are all less than 0.6, indicating a dominant limestone mineralogy that has been variably dolomitized. There is only one Mn/Sr data point from the Izluchina Formation, which shows a value higher than 10. This indicates a degree of meteoric alteration, which is likely applicable to the Izluchina Formation based on Mn/Sr data from Kouchinsky et al., (2007). The Sukharikha Formation has one value greater than 10, at the bottom of the formation, so the lowermost Sukharikha Formation (before 1n) may have been similarly altered. Higher than this point, the rest of the Sukharikha Formation has values less than 10, indicating good to excellent preservation. The evidence for good preservation of these carbonates supports their use for environmental interpretations, as they would be reflective of their original depositional condition.

4.2: Redox

Carbonates have widely been used to reconstruct ancient seawater chemistry, including redox proxies that monitor both global and local environmental conditions. Uranium isotopes serve as a global scale proxy while cerium anomalies represent local scale redox conditions. Additionally, sulfur isotopes may provide insight into the activity of redox-sensitive microbial communities and the size of the oceanic sulfate reservoir during the BACE event.

4.2.1: Anabar Uplift

The sulfate-rich peritidal environment of the Staraya Rechka Formation has very consistent uranium concentrations, and ranges between 0.10 and 1ppm, with the average at

0.53ppm, so any variations seen in $\delta^{238}U$ data would not result from changes in uranium concentration (Table A3 in Appendix). When considering $\delta^{238}U$ values, the difference in mineralogy between calcite and dolomite does not impact the $\delta^{238}U$ values, as concluded by Chen et al. (2018) based on a study of modern Bahamian carbonates. This is further supported by the consistent nature of the $\delta^{238}U$ values, especially between the transition between the Staraya Rechka and Manykai formations. The lack of correlation between $\delta^{238}U$ and $\delta^{18}O$, Mn/Sr, and Mg/Ca suggests diagenetic processes and dolomitization did not overprint primary signals in these samples. This places strong confidence in the reliability of the data, which reveals no change in the global oxygenation state during the BACE relative to earlier in the Ediacaran and later in the Fortunian (Cherry et al., 2022). That values remain constant and strongly negative throughout the BACE, is contrary to expectations as previous studies of negative carbon isotope anomalies (like the Shuram) have revealed more enriched and near modern values, suggesting ventilation of global seawater (Zhang et al., 2018; Gong et al., 2023). The $\delta^{238}U$ values are relatively constant between -0.45 and -0.77‰, indicating that the BACE interval was a time of expansive global anoxia. Based on the two-sink uranium isotope mass balance model, $\delta^{238}U_{seawater}$ values from the BACE interval (reconstructed from the carbonates and corrected by -0.27‰) might reflect at least 20% seafloor anoxia, and given that in today's oxygenated oceans, the euxinic environments occupy only about 0.05% of the global ocean (Meyer and Kump, 2008), this degree of anoxia would have a significant impact on global ocean chemistry and extant life. Cherry et al. (2022) found that the Ediacaran biota lived under low oxygen conditions, leading to the hypothesis of this thesis, that a rise in oxygen would have sparked the extinction of these enigmatic organisms. This hypothesis is notably not supported by the $\delta^{238}U$ data from the Anabar Uplift.

More evidence for a lack of oxygen comes from an outcrop of the Staraya Rechka Formation, 65 km to the north. This outcrop contains ~40 m of the Staraya Rechka Formation, which records a rise in $\delta^{34}S$ values from around -15‰ to ~30‰ (Fig. 4.1). This dramatic shift might be explained by a lack of seawater oxygen that would support MSR and pyrite formation in the water column. Over the depositional interval, progressive distillation of ^{32}S into pyrite would result in ^{34}S enrichment of seawater. Alternatively, ^{34}S enrichment could have been the result of a shrinking sulfate reservoir – which would limit the availability of sulfate for MSR (either in the water column or sediments) and thereby decrease apparent fractionation between reactant sulfate and product sulfide – due to the widespread deposition of sulfate evaporites.

Locally, the Ce/Ce* ratios determined for the Staraya Rechka Formation support the lack of water column oxygenation within the BACE, but the strong correlation with Y/Ho puts the validity of the Ce/Ce* data into question, as Y/Ho ratios indicate a detrital component within the leached samples. There is a clear shift in Y/Ho ratios between 135 and 150 m, however, which roughly corresponds with the transition between the Staraya Rechka and Manykai formations. Yttrium/holmium ratios below 36 have been shown in Neoproterozoic carbonates as a result of anoxia (Bau et al., 1997; Wallace et al., 2017), but that does not seem to be the case for these samples. There is a slight correlation of Y/Ho plotted against [Al], [Zr], [Ti], and [Rb], especially with Al and Rb (Fig. A1A, A1D in Appendix). High Y/Ho values occurring in the Manykai Formation correspond to low concentrations of detrital elements, indicating that these samples are predominantly authigenic in origin. In the Staraya Rechka Formation, the highest Y/Ho values correlate with the lowest detrital element concentrations. Given the downward trend in Y/Ho with increasing detrital element concentrations, it is possible that redox conditions (e.g., iron oxides that preferentially release holmium to seawater under anoxic conditions) could still

be driving Y/Ho values to be lower than 36 (Shnyukov et al., 2013). The data from the Staraya Rechka Formation does not support the initial oxidation hypothesis, but the ubiquitous presence of evaporites in Siberia and the Middle East exemplified by this succession may yet provide constraints on the mass extinction of the Ediacaran biota. Comparison with the equivalent BACE succession in the Igarka Uplift might provide more clues to the kill mechanism.

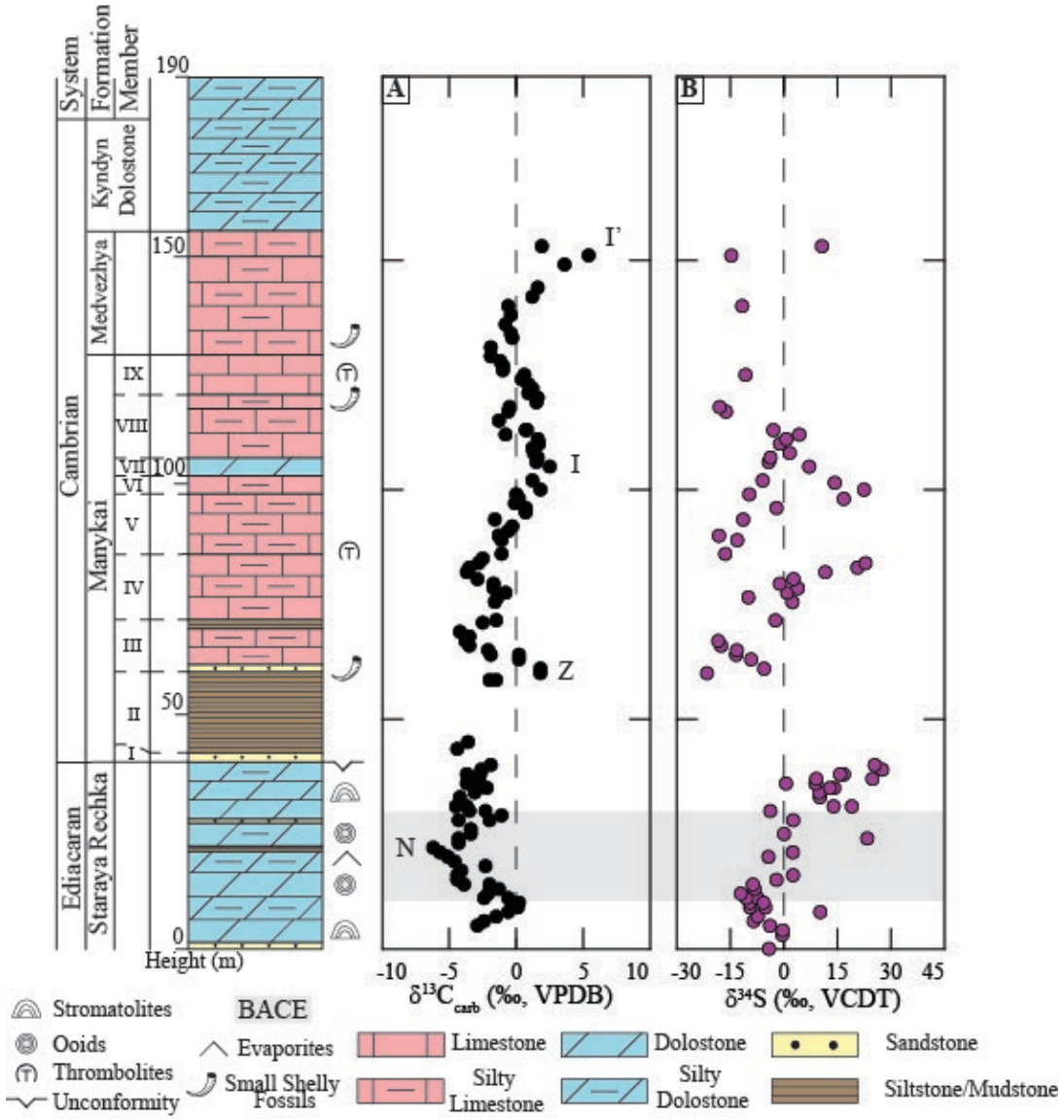

Figure 4.1. Stratigraphy and chemostratigraphy of the Staraya Rechka and Manykai formations at the Kotuikan River. (A) $\delta^{13}C_{carb}$ from Knoll et al., (1995b) and Kaufman et al., (1996). (B) $\delta^{34}S$ referenced to V-CDT. Raw data produced by Alan Jay Kaufman and Karel Kletetchka. Samples with peak heights less than 2nA were excluded from the plotted dataset.

4.2.2: Igarka Uplift

While $\delta^{238}U$ data from the Staraya Rechka Formation in the studied area reveals no change in the degree of seawater oxygenation during the BACE event, the basal Sukharikha Formation associated with the BACE appears to tell a different story. Uranium concentrations from the formation range between 0.1 and 7 ppm, averaging around 0.8 ppm (Tables A4 and A5 in Appendix). The highest concentrations occurred during the 1n interval, which coincided with samples of lower percent carbonate. The average $\delta^{238}U$ values during the BACE interval is around -0.37‰, nearly 0.3‰ heavier than the BACE from the Anabar Uplift with the most ^{238}U enriched sample with a value of -0.17‰, only 0.02‰ away from modern carbonates. According to the two-sink model, the average $\delta^{238}U$ carbonate values from the BACE interval from the Sukharikha Formation, when corrected for a seawater-carbonate fractionation offset, suggest as little as 1% seafloor anoxia. This supports the hypothesis that a ventilation event occurred during the BACE, which is contradictory to what is seen from $\delta^{238}U$ from the Anabar Uplift section only 700 km distant. On the other hand, the C/Ce* data from the Sukharikha Formation reveals a primarily anoxic signal. As Ce/Ce* tracks local redox processes, it is very possible that there was local anoxia present in a globally ventilated ocean. While additional redox conditions could be inferred from $\delta^{34}S$, the very low-resolution sampling makes determining trend very difficult, especially during the 1n interval, where there are only 4 data points. Regardless, based on the $\delta^{238}U$ data from this section, there seems to be a ventilation event. An event like this could be caused by increased nutrient and oxidant input into the ocean from continental weathering.

4.3: Weathering

The Staraya Rechka Formation contains a remarkable stratigraphic rise in δ^7Li from ~10‰ to ~32‰, before falling back to ~2‰ in the Manykai Formation. Indeed, the δ^7Li data from the upper Chimuka and Kochokon members of the Staraya Rechka Formation shows values near modern seawater, which has never before been documented in the Ediacaran or Cambrian periods (Kalderon-Asael et al., 2021). Plots of Al and Li of Mg+Ca (Fig. 3.4C, 3.4D) show that this trend is not a result of detrital contamination. Interpreted straightforwardly, an increase of δ^7Li could result from an increase in clay mineral formation on land (incongruent weathering). This implies that the Ediacaran-Cambrian transition may have experienced the onset of clay mineral formation, as the clays would preferentially take out ^{6}Li, leaving seawater (and marine carbonates) progressively enriched in ^{7}Li assuming minimal change in the degree of reverse weathering (i.e., the formation of marine clays). The onset of incongruent weathering is documented in the early Cambrian from δ^7Li analysis of mudstones (Wei et al., 2024). The δ^7Li from the Staraya Rechka Formation would support this, however, the end of the Staraya Rechka Formation and beginning of the Manykai Formation see δ^7Li values that trend back towards 0‰, suggesting a return to congruent weathering, which is not expressed in δ^7Li analysis from mudstones of the same antiquity (Wei et al., 2024). It is unlikely that the clay mineral factory once switched on, could switch off over such short intervals of geologic time, so interpreting the time-series carbonate data by this process is problematic. Alternatively, if silica concentrations were low during this time, reverse weathering would have happened at a much slower rate, causing greater fractionation (i.e., high δ^7Li values). This, however, is not consistent with the current understanding of the Precambrian oceans (Kalderon-Asael et al., 2021), as they are believed to have high silica concentrations implying that reverse weathering would happen at a

very fast rate, imparting minimal fractionation. This suggests that factors other than the formation of clay minerals on land (incongruent weathering) may be at play in this highly evaporitic environment.

In this regard, the abundant sulfate evaporites within the Staraya Rechka Formation may be the proximal cause for the time-series enrichment of ^{7}Li in these samples. It has recently been demonstrated that lithium concentrations in seawater increase as salts precipitate (Lin et al., 2024). Additionally, ^{6}Li is preferentially incorporated in halite, leaving seawater enriched in ^{7}Li. This process shifts $\delta^{7}Li$ in the same direction as increased incongruent weathering, so the rapid accumulation of marine evaporites on a global scale might serve as an alternative explanation for the positive lithium isotope excursion. The Chimuka Member of the Staraya Rechka Formation is dominated by gypsum, but the Ara Group from Oman contains abundant halite deposits. While the exact effect of these calcium sulfate minerals on $\delta^{7}Li$ requires further experimentation, it is possible that the ^{6}Li was preferentially incorporated, explaining the positive trend through progressive distillation. Additionally, the Staraya Rechka Formation contains occasional euhedral voids seen in thin section, that could indicate the presence of pre-existing halite. Lithium concentrations support this claim, as they are higher in the Chimuka Member compared to the other members of the Staraya Rechka.

4.4: Putting the Pieces Together

The disagreement between $\delta^{238}U$ values from the Staraya Rechka and Sukharikha formations is extremely puzzling. Considering that uranium isotopes are thought to track global scale redox changes, it is odd that two sections, only 700 km apart, show different signals. Two equivalent sections showing differences in a global proxy could be interpreted as one section being restricted and cut off from global ocean circulation. This, however, does not make much

sense given the $\delta^{13}C_{carb}$ data, which records another global ocean process, shows negative perturbations in both sections. If both sections record the same perturbation in one global proxy, but different perturbations in a separate proxy then it is possible that they are not equivalent, therefore recording different geochemical events. Alternatively, it could mean that one of the sections may have experienced some degree of diagenesis or overprinting.

4.4.1: Alternative Event Hypothesis

The current interpretation is that The Staraya Rechka and Sukharikha formations record the same $\delta^{13}C_{carb}$ anomaly. However, the possibility that either of these sections records a $\delta^{13}C_{carb}$ anomaly that is not the BACE should also be considered. The Staraya Rechka Formation lacks any biostratigraphic data, and until recently, that was the case for the Sukharikha Formation as well. There has been one study on detrital zircons from the Staraya Rechka that could provide an alternative explanation. The study by Marusin et al. (2022) dated three sandstone intervals from the basal Staraya Rechka Formation, upper Staraya Rechka Formation, and basal Manykai Formation. The basal Staraya Rechka was dated to ~600 Ma, based on a population of 46 grains. The upper Staraya Rechka was dated to 547 ± 6 Ma, based on a population of seven grains. Finally, the basal Manykai Formation was dated to 537 ± 3 Ma, which is consistent with the current placement of the BACE event in the basal Cambrian Period. Given the significant difference between the basal and upper Staraya Rechka Formation, and no evidence for a hiatus, the difference was attributed to a change in clastic source. The detrital zircon data from the uppermost Staraya Rechka Formation causes some issues with the interpretation of the $\delta^{13}C_{carb}$ anomaly as the BACE, but still allows for this interpretation. That detrital age constraint comes from a very small population of zircons, so the uncertainties are large enough that the uppermost Staraya Rechka Formation could still be younger, at least up to 541 Ma. This is consistent with

the BACE occurring after 541.0±0.13 Ma, as estimated from Oman (Bowring et al., 2007). While the Staraya Rechka Formation may preserve the BACE, other negative $\delta^{13}C_{carb}$ anomalies could fall within these age ranges.

An alternative interpretation to the negative excursion seen in the Staraya Rechka Formation is the well-known Shuram Excursion, which has a nadir of -12‰ and is dated to 574-567 Ma (Rooney et al., 2020). However, given the present age constraints for the upper Staraya Rechka and basal Manykai (which does contain SSFs of Fortunian affinity: Knoll et al., 1995b; Kaufman et al., 1996) formations, this event is likely much younger than the Shuram. A more viable candidate for the Staraya Rechka excursion would be the BAsal Nama Excursion (BANE) (Bowyer et al., 2022; Sun et al., 2024). This excursion, occurring between the Shuram and BACE around 550 Ma, has a similar nadir to the BACE. However, it is not very well established as a global event. In South China where a second and younger Shuram (around 550 Ma) was first proposed, the data are very sparse and the few Dengying Formation carbonates associated with the supposed negative excursion are interbedded with thick shales and only reveal the climbing limb of an event; furthermore, no single section preserves both the Shuram and this supposed excursion (Yang et al., 2021). The only documented carbon isotope event in the world that might be the right age and reveals a clear and complete negative $\delta^{13}C$ excursion is preserved in the Mara Member of the Nama Group in southern Namibia (Smith et al., 1998; Saylor et al., 1998; Wood et al., 2015; Bowyer et al., 2022). That carbon cycle anomaly has previously been related to the Shuram Excursion based on the shape and depth of the isotope excursion, as well as the presence of quartz-lined methane-derived calcite nodules that match those in the Doushantuo Formation of South China (Cui et al., 2017; 2021). While the presence of the methane-derived nodules is not a temporal constraint, these have thus far only been documented in the Shuram era

succession. There are no radiometric age constraints for the Mara Member, but it lies ~150 m stratigraphically below the 547 Ma age for the Omkyk Member (Macdonald et al., 2014). Given the likelihood of multiple unconformities in the mixed siliciclastic and carbonate successions, and the thickness of the interval between the age constraint and the negative carbon isotope anomaly, a Shuram affinity for the excursion remains permissible. If the anomaly were the BANE, the assignment would conflict with the absence of Ediacaran biota and the ubiquitous presence of Fortunian SSFs in the overlying Manykai Formation.

Unlike the Staraya Rechka Formation, the basal Sukharika Formation associated with the 1n event does contain a SSF record that helps constrain its age. *Cambrotubulus* and *Anabarites* are reported in the upper Izluchina and middle Sukharikha formations (Marusin et al., 2023). Notably, *Cambrotubulus* is also known from the terminal Ediacaran-aged Turkut Formation of the Olenek Uplift (Nagovitsin et al., 2015), so the finding of this taxon below the $\delta^{13}C_{carb}$ anomaly does not challenge the correlation of 1n with the BACE event. The ichnotaxon that defines the Cambrian boundary (*T. pedum*) is lacking, so prior studies have placed the Ediacaran-Cambrian boundary at the base of the Sukharika Formation (Marusin et al., 2023). This is an arbitrary placement, however, especially considering that the transition between the Izluchina and Sukharikha formations is suggested to be gradational. As the Ediacaran-Cambrian boundary lies just above the BACE in several sections across the globe, correlating 1n with the BACE suggests that the 1n anomaly is terminal Ediacaran in age.

4.4.2: Alteration Hypothesis

The $\delta^{238}U$ compositions from samples of the BACE event in the Sukharika Formation are similar to $\delta^{238}U$ measurements (-0.4‰) of BACE carbonates in South China (Wei et al., 2018). This average is close to the Sukharikha Formation average of -0.37‰ during the 1n anomaly. In

contrast, the Staraya Rechka Formation has an average carbonate value of -0.69‰ during the BACE interval. If the Sukharikha and Staraya Rechka formations are indeed equivalent, then one of the sections likely has altered or overprinted $\delta^{238}U$ values. Given that the evaporite-rich environment of the Staraya Rechka Formation must have been restricted from open ocean conditions, it seems most likely that the $\delta^{238}U$ value of the carbonates (which suggest anoxia during the BACE), have been impacted. Chen et al. (2017) reported that with increasing salinity (i.e., ionic strength) the fractionation between seawater and carbonate $\delta^{238}U$ would diminish, to as low as 0.06‰ (as opposed to a fractionation of 0.27‰ under normal marine salinities). If correct, the $\delta^{238}U$ value of the Staraya Rechka carbonates would have been more representative of coeval seawater (not requiring correction), while those of the Sukharikha Formations would need the correction of -0.27‰ to yield seawater compositions. Accepting this view, the Staraya Rechka carbonate values would be closer to actual seawater than the carbonates from more open marine environments in the Sukharikha Formation. Assuming the most extreme case (and lowest fractionation), the seawater $\delta^{238}U$ compositions would be around -0.75‰ (Fig. 4.2) during the Staraya Rechka BACE event, which would suggest ~2% seafloor anoxia based on the model results (compared to the previous estimate of 20% as described above). This estimate is much more consistent with that from the Sukharikha Formation, which with the offset applied to open marine carbonates, would have a $\delta^{238}U$ of seawater around -0.64‰ (~1% seafloor anoxia) (Fig. 4.2). Compared to $\delta^{238}U_{seawater}$ average from pre-BACE Ediacaran carbonates (~-0.88‰) (Cherry et al., 2022), the BACE estimate suggests a decrease in seafloor anoxia by ~4%. Considering that modern oceans contain 0.05% seafloor anoxia (Meyer and Kump, 2008); this difference is significant, so that a change in seawater redox state remains a viable mechanism behind the extinction of the Ediacaran biota. However, given the unusual deposition of marine evaporites

across Siberia and the Middle East, this study provides an alternative kill mechanism associated with the development of high seawater salinity near the Ediacaran-Cambrian boundary.

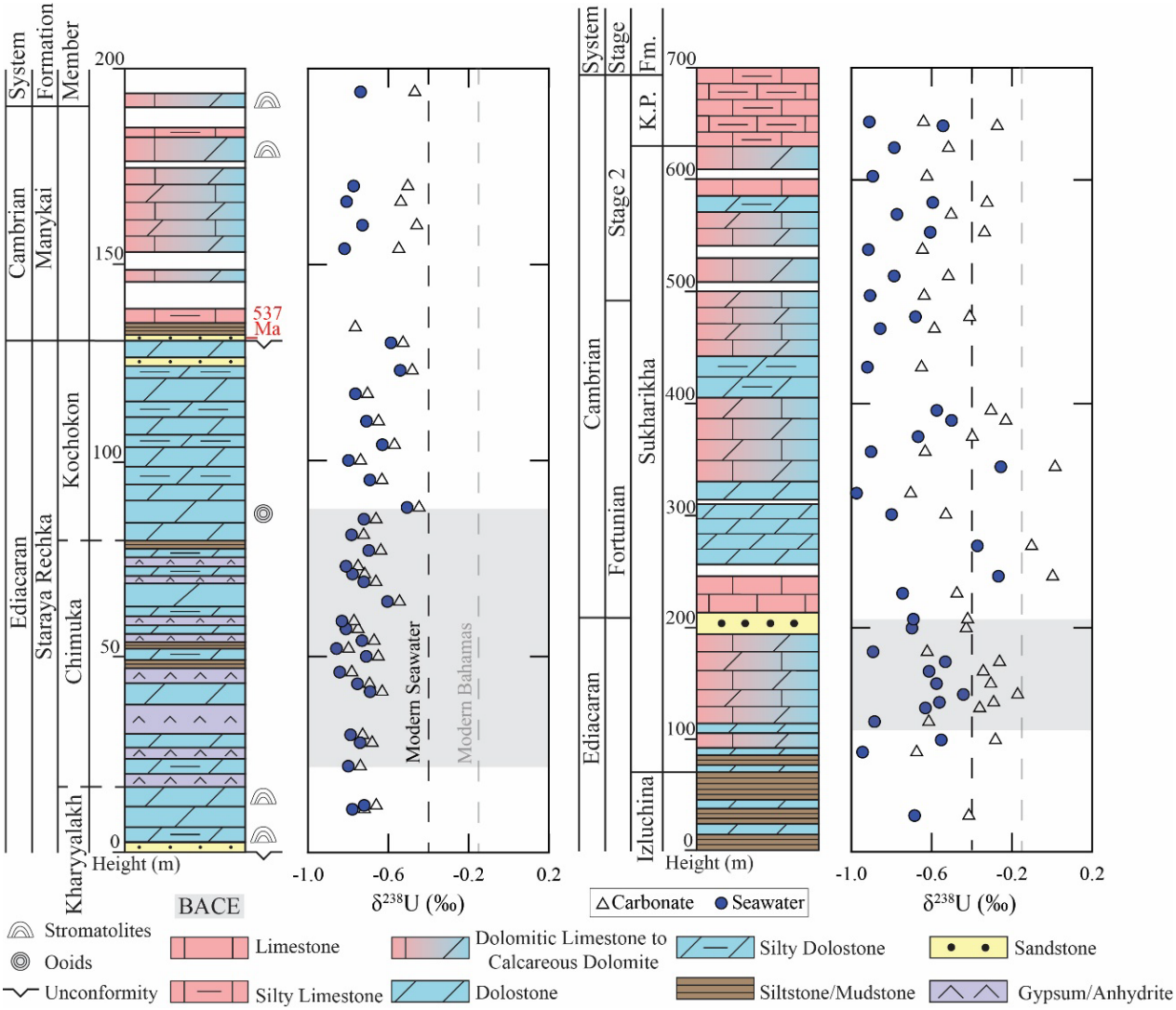

Figure 4.2. Stratigraphy and chemostratigraphy of the Staraya Rechka Formation at the Kotuy River and the Sukharikha Formation at the Sukharikha River. (A) $\delta^{238}U_{seawater}$ from the Staraya Rechka Formation, calculated from $\delta^{238}U_{carb}$ using an offset of 0.06‰ that is expected with saline conditions (Chen et al., 2017). The Manykai Formation was calculated using an offset of -0.27‰ that is expected with carbonates (Chen et al., 2018). (B) $\delta^{238}U_{seawater}$ from the Sukharikha Formation, calculated from $\delta^{238}U_{carb}$ using an offset of 0.27‰. The dark reference line in both plots is -0.39‰ for modern seawater (Tissot and Dauphas, 2015). The gray reference line in both plots is -0.15‰ for modern carbonates (Chen et al., 2018).

High rates of evaporation (a requirement for evaporite formation, that being 85% evaporation of seawater is required for gypsum saturation) are known to fractionate oxygen isotopes (Magaritz and Stemmerik, 1989) resulting in higher $\delta^{18}O$ values of carbonates, and

halite precipitation has been shown to fractionate δ^7Li values by preferentially incorporating ^{6}Li into the mineral lattice (Liu et al., 2024). If the same is true for sulfate evaporites, the profound rise in δ^7Li values through the Staraya Rechka Formation could have resulted from the rapid formation of evaporites that distilled Li from seawater. Such a scenario also explains large ^{34}S enrichment of pyrite in the Staraya Rechka Formation, as the precipitation of evaporite minerals would draw down seawater sulfate concentrations, reducing the reservoir size and the fractionation associated with MSR. Given the distribution of evaporite deposits at this time, a global rise in salinity (perhaps related to sea level drawdown during the Baykonurian ice ace; Chumakov, 2009) seems likely, such that higher global marine salinity could have been the kill mechanism for the Ediacaran biota. As these macroscopic organisms were complex sacs of water, increasing seawater salinity along continental margins would have led to osmosis (pulling water from a reservoir of lower salinity to one of higher salt concentration), essentially dehydrating and killing them.

Chapter 5: Conclusion

The Staraya Rechka Formation contains well-preserved carbonates, based on petrographic analysis and low Mn/Sr ratios. The $\delta^{18}O_{carb}$ values seen in this formation are attributed to high rates of evaporation in the depositional environment. The Sukharikha Formation is well preserved based on Mn/Sr ratios and $\delta^{18}O_{carb}$ values. The $\delta^{13}C_{org}$ record reveals decoupling from $\delta^{13}C_{carb}$, but the smaller magnitude between the two as compares to other studies suggests the impact of alteration or detrital organic matter contamination is limited. Interpreted plainly, the Staraya Rechka $\delta^{238}U$ values suggest global anoxia while $\delta^{238}U$ values from the Sukharikha Formation suggest a more oxygenated ocean, although not to modern values. Cerium anomalies from the Staraya Rechka Formation are likely impacted by detrital contamination, but the Sukharikha Formation shows Ce/Ce* data shows local anoxia was present. Based on this interpretation, the Sukharikha River Formation supports the hypothesis that ventilation killed the Ediacaran biota, whereas the Staraya Rechka Formation does not support this.

The discrepancy between the $\delta^{238}U$ values from the two formations could be explained by one (or both) of the following scenarios: 1) the Staraya Rechka Formation preserves an older $\delta^{13}C_{carb}$ anomaly (likely the BANE) or 2) the Staraya Rechka Formation does preserve the BACE and the $\delta^{238}U$ values have been altered or overprinted. Age constraints from detrital zircons allow for the possibility for the Staraya Rechka Formation to be either the BACE or BANE. However, the BANE is poorly characterized and does not resemble the $\delta^{13}C_{carb}$ recorded in the Staraya Rechka Formation. Alteration due to salinity/evaporite formation seems more likely as those processes have been shown to impact the $\delta^{18}O_{carb}$, $\delta^{7}Li$, and $\delta^{34}S$ data from the section. This salinity could have limited the fractionation between seawater and carbonate, causing the Staraya

Rechka Formation to be more representative of actual seawater. In this scenario, the Staraya Rechka Formation could be interpreted to reflect the actual seawater composition. With this interpretation there would be a limited offset between seawater and carbonate. The Sukharikha Formation would require a larger offset, and the resulting $\delta^{238}U_{seawater}$ values from both formations would be in much more agreement with each other, so that both sections support the rise of oxygen hypothesis.

Lithium isotopes from the Staraya Rechka Formation indicate that one (or a combination) of the following processes occurred: 1) the shift to a dominance of incongruent weathering or 2) $\delta^{7}L$ was driven to more positive values by evaporite formation or 3) assuming an ocean with low silica concentrations, slow rates of reverse weathering caused large degrees of fractionation. None of these scenarios support the hypothesis that the BACE was driven by an increase in congruent weathering, as that would have delivered the nutrients and oxidants necessary to cause ocean oxygenation. However, the very likely scenario that evaporation altered the values is in agreement with the documented $\delta^{18}O_{carb}$, $\delta^{34}S$, and $\delta^{238}U$ trends. This opens the door for an additional kill mechanism of the Ediacaran biota. High salinity along continental margins, as documented by abundant evaporites in the Staraya Rechka Formation, could have killed the organisms such that the dramatic contrast in salinity profiles between the organisms and surrounding seawater causing them to dehydrate and die from osmosis.

Additional research is required to better constrain which processes are causing the signals observed in the data from the Staraya Rechka Formation. First and foremost, additional uranium as well as lithium isotope studies from evaporitic BACE successions, like the Platonovskaya Formation in Siberia, could help determine if the values seen Staraya Rechka Formation are a result of alteration by highly evaporitic conditions and saline water. It could be hypothesized that

BACE successions containing evidence for evaporitic conditions would show values in agreement with the Staraya Rechka Formation, while BACE successions of more open-marine conditions show values similar to the Sukharikha River Formation. Additionally, measuring lithium isotopes from a non-evaporitic interval, like the Sukharikha Formation, could provide insight into the weathering behavior during the BACE. Understanding critical events in Earth's history, like the BACE, requires the combination of multiple proxies to tell a complete story. Applying these proxies to several successions around the world is the key to integrating these stories on a global scale.

Appendices

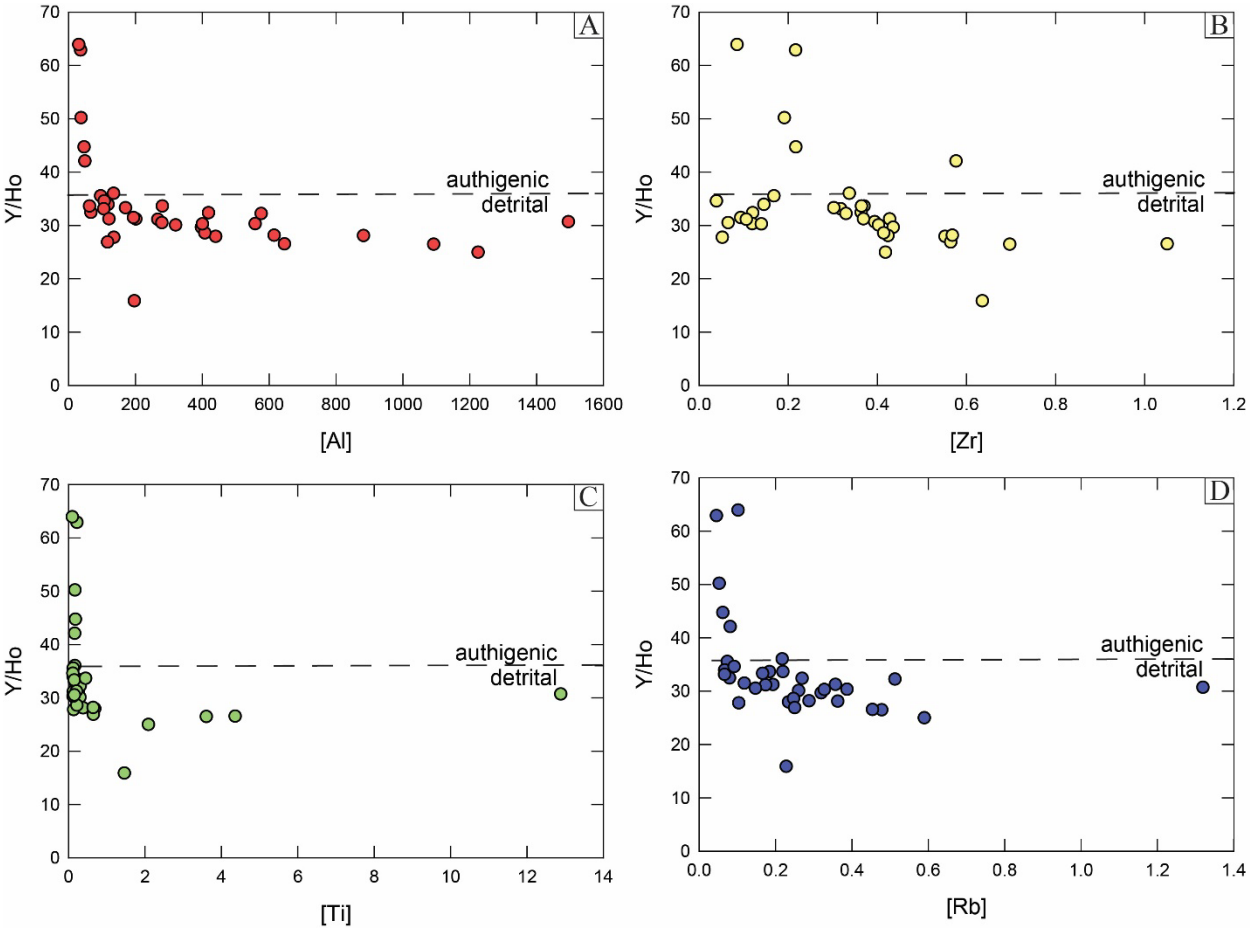

Figure A1. Cross-plots of Y/Ho ratios from the Staraya Rechka and Manykai formations versus detrital element concentrations, (A) [Al], (B) [Zr], (C) [Ti], and (D) [Rb]. The dashed line at 36 represents the boundary between detrital and authigenic Y/Ho ratios.

Locality	Formation	Member	Height Range (m)	$\delta^{13}C_{carb}$ (‰, VPDB)	$\delta^{18}O_{carb}$ (‰, VPDB)	Mg/Ca	Mn/Sr	$\delta^{238}U$ (‰)	Ce/Ce*	Y/Ho	$\delta^{7}Li$ (‰)
Anabar Uplift	Sratava Rechka	Kharyyalakh	0 - 16	-1.66	-1.66	0.40	56.51	-0.69	1.06	27.90	10.3
		Chimuka	16 - 80	-4.02	-1.09	0.42	3.85	-0.70	1.08	30.29	20.5
		Kochokon	80 - 131	-1.73	-2.15	0.42	1.87	-0.61	1.12	30.40	24.0
	Manykai	-	131 - 194	-0.95	-6.36	0.03	0.55	-0.55	1.27	47.22	9.7
Igarka Uplift	Izluchina	-	0 - 83.5	-2.79	-4.48	0.42	15.73	-0.41	1.17	35.27	-
	Sukharikha	-	83.5 - 648	-1.59	-7.14	0.21	1.32	-0.42	1.13	34.94	-
	Kransy Porog	-	648 - 661.7	-0.58	-7.18	0.01	0.37	-0.64	1.20	36.64	-

Table A1. Data table of averages for the Anabar and Igarka uplifts.

Sample	Height (m) From Bottom of Section	Formation	% Carbonate	$\delta^{13}C_{carb}$ (‰, VPDB)	$\delta^{18}O_{carb}$ (‰, VPDB)	Mg/Ca U Leach	Mg/Ca REE Leach	Mg/Ca Li Leach	Mn/Sr U Leach	Mn/Sr REE leach	Mn/Sr Li Leach
KTB-246/77	0	Staraya Rechka	84.54	-1.94	-1.86	0.41	0.42	0.64	103.05	112.56	175.35
KTB-249/45	11	Kharyyalakh Member	89.02	-2.09	-1.02	0.36	0.43	0.66	17.61	18.92	28.65
KTB-246/65	12		97.09	-0.96	-2.11	0.43	0.42	0.66	48.88	55.15	67.47
KTB-249/36	22	Staraya Rechka	91.11	-0.47	0.45	0.44	0.43	0.67	5.50	9.91	16.85
KTB-249/34	28	Chimuka Member	94.92	-2.08	-1.61	0.44	0.43	0.67	8.60	8.81	11.71
KTB-246/53	30		97.72	-1.03	-0.62	0.42	0.44	0.67	1.54	2.15	3.18
KTB-249/17	41		92.72	-5.53	-0.51	0.43	0.42	0.66	2.46	2.53	4.39
KTB-251/2	43		96.36	-6.53	-2.62	0.42	0.43	0.65	12.11	13.29	15.85
KTB-246/37	46		98.73	-5.32	-1.98	0.42	0.42	0.66	10.46	13.35	17.80
KTB-236/12	50		96.54	-4.13	-1.60	0.42	0.42	0.63	3.92	4.44	5.17
KTB-246/29	52		94.62	-4.48	-1.94	0.43	0.42	0.66	8.13	9.24	10.64
KTB-233/33	54		91.06	-5.98	-1.94	0.43	0.43	0.65	4.00	4.16	5.80
KTB-246/24	57		92.63	-5.82	-1.48	0.43	0.43	0.64	1.95	2.66	3.17
KTB-246/22	59		95.29	-6.55	-1.24	0.39	0.43	0.66	0.22	0.63	0.75
KTB-246/19	64		90.88	-3.70	-0.52	0.44	0.43	0.68	1.05	1.26	1.35
KTB-246/17	69		98.55	-2.67	-1.00	0.41	0.43	0.68	0.20	0.53	0.60
KTB-233/17	71		99.05	-2.02	-0.46	0.41	0.43	0.67	0.47	0.86	0.95
KTB-254/9	73		96.17	-3.94	0.25	0.43	0.44	0.66	0.41	0.44	0.55
KTB-233/14	77		92.96	-4.06	-0.58	0.43	0.44	0.66	0.55	0.61	0.78
KTB-246/10	81	Staraya Rechka	98.65	-0.92	-0.57	0.41	0.43	0.66	0.03	0.19	0.21
KTB-254/5	85	Kochokon Member	98.34	-2.72	-2.56	0.42	0.44	0.67	0.93	1.09	1.18
KTB-233/9	88		98.79	-0.49	-2.09	0.42	0.44	0.67	1.04	1.38	1.50
KTB-233/4	95		99.06	-0.49	-1.41	0.42	0.44	0.67	0.52	0.93	0.75
KTB-233/2	100		93.93	-5.03	-2.04	0.40	0.43	0.66	0.50	0.73	0.93
KTB-232/18	104		99.15	-0.48	-1.64	0.43	0.44	0.68	0.90	1.12	1.15
KTB-232/15	110		99.12	-1.09	-1.74	0.43	0.44	0.67	1.26	1.60	1.60
KTB-241/18	117		95.85	-1.69	-2.86	0.42	0.43	0.67	1.99	2.93	2.48
KTB-241/16	123		84.09	-2.45	-1.62	0.42	0.43	0.62	2.27	2.51	2.98
KTB-232/8	130		91.44	-1.95	-4.94	0.40	0.41	0.63	9.27	10.37	11.49
KTB-232/7	134	Manykai	71.95	-5.05	-6.18	0.02	0.03	0.02	0.86	1.04	0.91
KTB-232/5	154		95.75	-0.42	-5.18	0.03	0.02	0.01	0.87	1.05	0.90
KTB-232/2	160		92.43	0.96	-4.97	0.10	0.06	0.04	0.75	0.79	0.55
KTB-241/9	166		97.88	-0.25	-5.62	0.02	0.01	0.01	0.46	0.57	0.49
KTB-241/3	170		99.30	-2.13	-7.13	0.00	0.00	0.00	0.48	0.64	0.63
KTB-241/1	174		99.17	-1.90	-7.33	0.00	0.00	0.00	0.15	0.20	0.18
KTB-255/2	194		98.32	2.12	-8.12	0.01	0.01	0.01	0.30	0.40	0.36

Table A2. Data table containing %carbonate, $\delta^{13}C_{carb}$, $\delta^{18}O_{carb}$, Mg/Ca (U leach), Mg/Ca (REE leach), Mg/Ca (Li leach), Mn/Sr (U leach), Mn/Sr (REE leach), and Mn/Sr (Li leach) from the Staraya Rechka Formation at the Kotuy River.

Sample	Height (m) From Bottom of Section	Formation	[U] (ppm)	$\delta^{238}U$ (‰)	2SD	Ce/Ce*	Y/Ho	$\delta^{7}Li$ (‰)	2SD	Al/(Mg+Ca)	Li/(Mg+Ca)	$\delta^{13}C_{org}$ (‰, VPDB)	$\Delta\delta^{13}C$ (‰, VPDB)	TOC (wt. %)
KTB-246/77	0	Staraya Rechka	0.15	-	-	1.1	25.0	10.2	0.4	4.72E-03	1.99E-05	-29.08	27.14	0.10
KTB-249/45	11	Kharyyalakh Member	0.69	-0.72	0.10	1.1	28.2	11.1	0.2	2.24E-03	3.77E-05	-30.39	28.30	0.08
KTB-246/65	12		0.37	-0.66	0.10	1.0	30.5	9.6	0.3	1.11E-03	-3.83E-06	-29.43	28.47	0.05
KTB-249/36	22	Staraya Rechka	0.61	-0.74	0.13	1.0	30.3	18.2	0.4	1.05E-03	1.88E-05	-31.49	31.02	0.25
KTB-249/34	28	Chimuka Member	0.55	-0.68	0.06	1.1	26.9	16.3	0.5	2.90E-04	1.71E-05	-30.38	28.30	0.07
KTB-246/53	30		0.68	-0.73	0.09	1.1	33.7	22.3	0.4	5.18E-04	4.28E-05	-30.91	29.89	0.06
KTB-249/17	41		1.00	-0.63	0.06	1.1	31.2	21.9	0.1	5.02E-04	1.86E-05	-31.27	25.74	0.22
KTB-251/2	43		0.25	-0.69	0.01	1.0	28.6	24.0	0.0	1.02E-03	3.35E-06	-28.91	22.38	0.07
KTB-246/37	46		0.52	-0.78	0.13	1.0	33.3	23.9	0.6	7.71E-04	2.93E-06	-30.74	25.42	0.08
KTB-236/12	50		0.71	-0.65	0.03	1.1	31.2	21.2	0.2	1.22E-03	3.51E-06	-29.22	25.09	0.04
KTB-246/29	52		0.28	-0.80	0.14	1.1	27.9	17.3	0.4	1.38E-03	7.54E-06	-28.48	24.00	0.05
KTB-233/33	54		0.45	-0.67	0.04	1.1	28.1	14.5	0.1	4.72E-03	1.12E-05	-29.25	23.27	0.07
KTB-246/24	57		0.47	-0.75	0.10	1.0	30.1	17.3	0.3	1.44E-03	7.48E-06	-30.96	25.14	0.07
KTB-246/22	59		0.45	-0.77	0.08	1.1	26.6	18.7	0.2	1.28E-03	8.56E-06	-29.72	23.18	0.08
KTB-246/19	64		0.29	-0.54	0.19	1.1	32.2	14.0	0.3	3.11E-03	2.85E-05	-28.73	25.03	0.08
KTB-246/17	69		0.60	-0.66	0.05	1.2	31.5	29.9	0.2	5.04E-04	9.75E-06	-32.37	29.70	0.23
KTB-233/17	71		0.57	-0.72	0.03	1.2	33.1	28.5	0.4	1.93E-04	6.57E-06	-31.75	29.74	0.21
KTB-254/9	73		0.33	-0.75	0.10	1.0	29.7	22.7	0.4	1.56E-03	1.72E-05	-33.39	29.45	0.34
KTB-233/14	77		0.76	-0.64	0.08	1.1	30.3	16.5	0.6	2.02E-03	1.75E-05	-31.22	27.16	0.20
KTB-246/10	81	Staraya Rechka	0.81	-0.72	0.20	1.1	31.2	31.3	0.2	4.49E-04	2.57E-05	-31.19	30.28	0.09
KTB-254/5	85	Kochokon Member	0.38	-0.66	0.09	1.0	27.8	26.6	0.4	3.18E-04	8.83E-07	-30.35	27.63	0.05
KTB-233/9	88		0.46	-0.45	0.12	1.1	34.6	27.7	0.4	3.66E-04	4.71E-06	-30.37	29.88	0.10
KTB-233/4	95		1.00	-0.63	0.14	1.2	33.9	31.3	0.3	3.88E-04	9.13E-06	-28.13	27.64	0.05
KTB-233/2	100		0.48	-0.74	0.09	1.1	15.9	20.2	0.3	1.69E-03	1.69E-05	-29.28	24.25	0.05
KTB-232/18	104		0.62	-0.57	0.12	1.2	32.5	31.9	0.1	1.62E-04	1.08E-05	-30.49	30.00	0.06
KTB-232/15	110		0.26	-0.65	0.07	1.1	35.6	28.0	0.2	2.73E-04	4.12E-06	-28.47	27.38	0.04
KTB-241/18	117		0.84	-0.70	0.03	1.2	33.6	18.1	0.5	1.62E-03	1.22E-05	-28.71	27.02	0.04
KTB-241/16	123		0.53	-0.48	0.00	1.1	26.5	13.5	0.1	5.56E-03	1.89E-05	-28.51	26.07	0.05
KTB-232/8	130		0.10	-0.53	0.13	1.1	32.4	11.5	0.3	1.87E-03	7.32E-06	-29.28	27.33	0.04
KTB-232/7	134	Manykai	2.14	-0.76	0.16	1.0	30.7	13.5	0.1	7.74E-04	4.89E-06	-32.77	27.72	0.11
KTB-232/5	154		0.21	-0.55	0.07	1.3	63.9	12.3	0.2	9.72E-05	2.60E-06	-27.95	27.53	0.09
KTB-232/2	160		0.39	-0.46	0.01	1.3	36.0	4.5	0.4	3.07E-04	2.62E-06	-27.70	28.66	0.14
KTB-241/9	166		0.41	-0.54	0.08	1.2	42.1	2.3	0.3	7.73E-05	5.18E-07	-27.94	27.68	0.05
KTB-241/3	170		0.18	-0.50	0.07	1.3	50.2	10.0	0.2	4.12E-04	1.83E-06	-32.70	30.56	0.07
KTB-241/1	174		0.09	-	-	1.5	62.9	10.0	0.3	7.25E-05	1.56E-06	-28.35	26.45	0.04
KTB-255/2	194		0.46	-0.47	0.01	1.3	44.7	15.1	0.2	3.19E-04	4.67E-06	-30.06	32.18	0.04

Table A3. Data table containing [U], $\delta^{238}U$ (2SD), Ce/Ce*, Y/Ho, $\delta^{7}Li$ (2SD), Al/(Mg+Ca), Li/(Mg+Ca), $\delta^{13}C_{org}$, $\Delta\delta^{13}C$, and TOC from Staraya Rechka Formation at the Kotuy River.

Sample	Height (m) From Bottom of Section	Formation	% Carbonate	$\delta^{13}C_{carb}$ (‰, VPDB)	$\delta^{18}O_{carb}$ (‰, VPDB)	Mg/Ca	Mn/Sr	[U] (ppm)	$\delta^{238}U$ (‰)	2SD	Ce/Ce*	Y/Ho	$\delta^{34}S$ (‰, VCDT)
И1801-2	12	Izluchina									1.2	44.0	
И1801-3	16.75			-3.81	-11.42						1.2	26.1	
И1801-4	25			-3.90	-4.64						1.3	42.1	
И1801-5	27			-2.39	-4.36						1.3	54.4	
И1801-6	29.8			-2.86	-2.94						1.5		
И1801-8	32.2			-2.75	-4.97	0.42	15.73	0.50	-0.41	0.06	1.0		
И1801-9	36.3			-2.16	-3.80						1.1	29.0	
И1801-11	41.5			-2.70	-4.68						1.2		
И1801-12	45.3			-2.99	-4.45						1.1	30.3	
И1801-13	49			-1.97	-4.07						0.9	37.6	
И1801-14	51.3			0.40	-3.74						1.0	38.0	
И1801-15	54.8			-2.48	-4.35						1.3		
И1801-17	62.3			-3.42	-3.24						1.2	26.2	
И1801-20	67.3			-4.15	-3.07						1.0	30.3	
И1801-21	71			-3.39	-4.18								
И1801-22	75												
И1801-24	79			-3.27	-3.35						1.1	29.9	
И1801-25	84	Sukharikha		-3.25	-3.13						1.1	31.7	
И1801-26	88.8		95.71	-3.99	-4.61				-0.67	0.09	1.1	29.3	
И1801-27	94.7			-2.60	-5.32						1.1	26.8	
И1801-28	99.7		34.97	-2.17	-6.38	0.41	11.07	0.11	-0.28	0.01	1.1	29.7	
И1801-29	105.4			-2.23	-7.32						0.9		
И1801-31	108.5			-1.35	-5.70	0.44	5.93	0.46			1.3	51.0	
И1801-33	116		75.46	-1.59	-6.47				-0.61	0.11	1.0	23.4	20.35
И1801-34	121.5			-3.79	-6.72								
И1801-35	128.2			-4.60	-7.77	0.12	0.69	2.61	-0.36	0.16			
И1801-36	133.3			-5.07	-8.97	0.03	0.48	1.72	-0.29	0.06	1.3		
И1801-37	140.3			-5.16	-8.08				-0.17	0.05	1.0		
И1801-40	150			-6.53	-8.85	0.01	0.10	7.18	-0.30	0.09	1.1		
И1801-41	161		67.48	-7.39	-8.48				-0.34	0.10			21.56
И1801-42	169.4			-7.36	-8.07	0.20	1.35	1.56	-0.26	0.19			
И1801-44	178.4		94.16	-8.01	-8.77				-0.62	0.04	0.9		6.01
И1801-45	187			-6.48	-7.92						1.1	49.9	
И1801-46	195			-6.77	-8.55						1.1	28.0	
И1801-48	199.5		69.78	-5.25	-8.16				-0.43	0.12	1.1	25.6	1.46
И1801-49	207.5		91.13	2.02	-9.73				-0.42	0.15	1.2	57.2	-3.73
И1801-51	216			0.54	-10.06								
И1801-53	224			-1.19	-5.70						1.2	27.7	
И1801-54	230.5		74.86	-2.28	-7.50				-0.47	0.05			6.37
И1801-56	239.3			-4.40	-8.57						1.1	32.7	
И1801-57	245.8			-2.78	-8.76	0.01	0.57	1.78	0.00	0.03	1.1	26.2	
И1801-58	252.5			-3.82	-8.99						0.9		
И1801-60	258			-4.08	-5.46						1.2	32.3	
И1801-61	269			-2.17	-9.76						1.1	31.4	
И1801-62	273		95.66	-4.11	-8.17				-0.10	0.04	1.2		12.91
И1801-64	281			-3.62	-5.86						1.1		
И1801-65	292			-4.76	-6.89						1.1	36.8	
И1801-66	301		96.95	-4.48	-7.50				-0.53	0.02	1.6		13.55
И1801-67	311			-4.23	-7.00						1.0	47.4	
И1801-68	320		95.90	-3.28	-6.78				-0.70	0.12	1.2	30.6	12.24
И1801-69	330			-2.08	-4.65						1.0	23.0	
И1801-70	338.5			-0.71	-7.96						1.2	28.6	
И1801-72	343.5		93.21	-0.10	-6.54				0.02	0.10	1.2	78.4	6.01
И1801-73	349			-1.66	-7.83						1.3	31.4	
И1801-74	357		97.02	-2.22	-7.06				-0.63	0.05	1.2	29.7	20.25
И1801-76	364.7			-3.19	-9.95						1.3		
И1801-77	370.5		97.12	-3.27	-8.41	0.29	0.44	0.13	-0.40	0.22	1.2	32.1	
И1801-80	379.6			-3.31	-7.51						1.1	35.7	
И1801-81	385		92.53	-2.43	-5.44				-0.23	0.08	1.1	28.6	12.81
И1801-82	394			0.56	-7.36	0.34	0.37	0.14	-0.30	0.14	1.2	38.5	
И1801-84	406.5			-1.41	-5.01						1.2	39.0	
И1801-85	414.5			-2.14	-9.55						1.2	33.5	
И1801-87	419.5			-1.99	-11.19						1.1	23.9	
И1801-89	425.5			-2.11	-4.67						0.9	54.6	
И1801-90	432.5		99.21	-1.05	-9.13	0.00	0.09	0.07	-0.65	0.02	1.1	27.8	

Table A4. Data table containing %carbonate, $\delta^{13}C_{carb}$, $\delta^{18}O_{carb}$, Mg/Ca, Mn/Sr, [U], $\delta^{238}U$ (2SD), Ce/Ce*, Y/Ho, and $\delta^{34}S$ from the Sukharikha Formation at the Sukharikha River. Samples 2-90.

Sample	Height (m) From Bottom of Section	Formation	% Carbonate	$\delta^{13}C_{carb}$ (‰, VPDB)	$\delta^{18}O_{carb}$ (‰, VPDB)	Mg/Ca	Mn/Sr	[U] (ppm)	$\delta^{238}U$ (‰)	2SD	Ce/Ce*	Y/Ho	$\delta^{34}S$ (‰, VCDT)
И1801-91	439.6	Sukharikha		-1.19	-9.29						1.2	28.6	
И1801-93	447			-1.22	-8.71						1.3	54.7	
И1801-94	453.5			-1.99	-8.96						1.5		
И1801-96	467		98.39	-1.19	-9.55				-0.59	0.03	1.1	32.1	27.95
И1801-98	477.6		98.03	1.66	-8.28	0.01	0.04	0.21	-0.41	n.d.	1.2	44.1	30.61
И1801-99	488			2.33	-6.27						1.1	50.0	
И1801-100	496.5			4.63	-3.84	0.29	0.49	0.10	-0.64	0.29	1.0	33.2	
И1801-101	505			2.30	-7.34								
И1801-103	514		99.00	0.92	-7.92	0.00	0.02	0.18	-0.52	0.05			15.09
И1801-104	518			1.07	-5.07						1.1	25.3	
И1801-104 A	528			1.34	-7.18						1.2		
И1801-105	537.5		96.45	1.44	-4.94				-0.64	0.06	1.1	32.2	12.11
И1801-107	545			0.44	-3.82						1.1	29.2	
И1801-108	553		95.06	-0.93	-2.60	0.42	0.71	0.13	-0.34	0.04			2.93
И1801-109	569		89.90	3.00	-2.19	0.43	0.81	0.17	-0.50	0.07			2.77
И1801-111	579.5		95.44	6.13	-4.24	0.32	0.19	0.34	-0.32	0.03	0.9	36.0	
И1801-112	587.5			5.03	-4.54						0.9		
И1801-113	596			4.57	-3.67						1.3	47.2	
И1801-115	603			4.47	-5.11	0.38	0.20	0.18	-0.62	0.02	1.2	29.7	
И1801-116	610			-0.06	-9.62			0.24			1.2		
И1801-118	618.5			2.98	-8.15			0.06			1.2	36.4	
И1801-119	628.5		99.41	0.90	-7.53				-0.52	0.09	1.1	28.0	10.33
И1801-121	637			-0.70	-7.51								
И1801-123	642			-0.64	-6.92						1.1		
И1801-125	643			-1.03	-7.57						1.1	29.9	
И1801-126	644			-1.03	-7.65						1.0		
И1801-127	645			-1.09	-7.60								
И1801-129	645.6			-1.13	-7.71								
И1801-130	646.35			-1.12	-7.25						1.0	28.8	
И1801-132	647			-1.19	-7.41						1.0		
И1801-133	648		98.85	-1.07	-7.69	0.01	0.14	0.24	-0.27	0.08	1.1	24.0	
И1801-135	648.45	Sukharikha -		-1.46	-7.44			0.06			1.2	28.7	
И1801-136	648.3	Kransy Porog		-1.36	-7.59						1.1	44.3	
И1801-137	649	transition		-1.30	-7.51						1.0	42.5	
И1801-139	649.6			-1.10	-6.74						1.1	28.2	
И1801-142	650.3	Kransy Porog		-1.05	-6.88						1.4	33.2	
И1801-143	650.8			-0.90	-6.45						1.3		
И1801-145	651.6			-1.22	-7.13	0.01	0.37	0.06	-0.64	n.d.	1.2	25.7	
И1801-147	652.5			-1.15	-7.00						1.1	31.6	
И1801-149	653			-1.05	-7.10						1.4	57.0	
И1801-150	658.8			0.93	-7.19						1.1	29.5	
И1801-152	659.3			0.77	-7.42								
И1801-153	661			0.78	-7.46						1.1		
И1801-155	661.7			0.56	-7.46						1.4	45.6	

Table A5. Data table containing %carbonate, $\delta^{13}C_{carb}$, $\delta^{18}O_{carb}$, Mg/Ca, Mn/Sr, [U], $\delta^{238}U$ (2SD), Ce/Ce*, Y/Ho, and $\delta^{34}S$ from the Sukharikha Formation at the Sukharikha River. Samples 91-155.

Bibliography

Adachi, N., Ezaki, Y., Liu, J., Watabe, M., Altanshagai, G., Enkhbaatar, B., and Dorjnamjaa, D., 2021, Earliest known Cambrian calcimicrobial reefs occur in the Gobi-Altai, western Mongolia: Intriguing geobiological products immediately after the Ediacaran–Cambrian boundary: Global and Planetary Change, v. 203, p. 103530, doi:10.1016/j.gloplacha.2021.103530.

Amthor, J.E., Grotzinger, J.P., Schröder, S., Bowring, S.A., Ramezani, J., Martin, M.W., and Matter, A., 2003, Extinction of Cloudina and Namacalathus at the Precambrian-Cambrian boundary in Oman: Geology, v. 31, p. 431, doi:10.1130/0091-7613(2003)031<0431:EOCANA>2.0.CO;2.

Andersen, M.B., Vance, D., Morford, J.L., Bura-Nakić, E., Breitenbach, S.F.M., and Och, L., 2016, Closing in on the marine 238 U/ 235 U budget: Chemical Geology, v. 420, p. 11–22, doi:10.1016/j.chemgeo.2015.10.041.

Bartley, J.K., Pope, M., Knoll, A.H., Semikhatov, M.A., and Petrov, P.Yu., 1998, A Vendian–Cambrian boundary succession from the northwestern margin of the Siberian Platform: stratigraphy, palaeontology, chemostratigraphy and correlation: Geological Magazine, v. 135, p. 473–494, doi:10.1017/S0016756898008772.

Bau, M., Möller, P., and Dulski, P., 1997, Yttrium and lanthanides in eastern Mediterranean seawater and their fractionation during redox-cycling: Marine Chemistry, v. 56, p. 123–131, doi:10.1016/S0304-4203(96)00091-6.

Bold, U., Smith, E.F., Rooney, A.D., Bowring, S.A., Buchwaldt, R., Dudas, F.., Ramezani, J., Crowley, J.L., Schrag, D.P., and Macdonald, F.A., 2016, Neoproterozoic stratigraphy of the Zavkhan terrane of Mongolia: The backbone for Cryogenian and early Ediacaran chemostratigraphic records: American Journal of Science, v. 316, p. 1–63, doi:10.2475/01.2016.01.

Bowring, S.A., Grotzinger, J.P., Isachsen, C.E., Knoll, A.H., Pelechaty, S.M., and Kolosov, P., 1993, Calibrating Rates of Early Cambrian Evolution: Science, v. 261, p. 1293–1298, doi:10.1126/science.11539488.

Bowring, S.A., Grotzinger, J.P., Condon, D.J., Ramezani, J., Newall, M.J., and Allen, P.A., 2007, Geochronologic constraints on the chronostratigraphic framework of the Neoproterozoic Huqf Supergroup, Sultanate of Oman: American Journal of Science, v. 307, p. 1097–1145, doi:10.2475/10.2007.01.

Bowyer, F.T., Zhuravlev, A.Y., Wood, R., Shields, G.A., Zhou, Y., Curtis, A., Poulton, S.W., Condon, D.J., Yang, C., and Zhu, M., 2022, Calibrating the temporal and spatial dynamics of the Ediacaran - Cambrian radiation of animals: Earth-Science Reviews, v. 225, p. 103913, doi:10.1016/j.earscirev.2021.103913.

Brennecka, G.A., Herrmann, A.D., Algeo, T.J., and Anbar, A.D., 2011, Rapid expansion of oceanic anoxia immediately before the end-Permian mass extinction: Proceedings of the National Academy of Sciences, v. 108, p. 17631–17634, doi:10.1073/pnas.1106039108.

Burns, S.J., and Matter, A., 1993, Carbon isotopic record of the latest Proterozoic from Oman: Eclogae Geol. Helv., v. 86, p. 595–607, doi:10.5169/SEALS-167254.

Canfield, D.E., Raiswell, R., Westrich, J.T., Reaves, C.M., and Berner, R.A., 1986, The use of chromium reduction in the analysis of reduced inorganic sulfur in sediments and shales: Chemical Geology, v. 54, p. 149–155, doi:10.1016/0009-2541(86)90078-1.

Canfield, D.E., and Teske, A., 1996, Late Proterozoic rise in atmospheric oxygen concentration inferred from phylogenetic and sulphur-isotope studies: Nature, v. 382, p. 127–132, doi:10.1038/382127a0.

Cao, C., Liu, X.-M., Bataille, C.P., and Liu, C., 2020, What do Ce anomalies in marine carbonates really mean? A perspective from leaching experiments: Chemical Geology, v. 532, p. 119413, doi:10.1016/j.chemgeo.2019.119413.

Cao, C., Bataille, C.P., Song, H., Saltzman, M.R., Tierney Cramer, K., Wu, H., Korte, C., Zhang, Z., and Liu, X.-M., 2022, Persistent late Permian to Early Triassic warmth linked to enhanced reverse weathering: Nature Geoscience, v. 15, p. 832–838, doi:10.1038/s41561-022-01009-x.

Cao, C., Liu, X.-M., Wang, X.-K., and Chen, J., 2023, Effective use of limestones to reconstruct seawater Li isotope compositions - A community standard proposal: Chemical Geology, v. 626, p. 121441, doi:10.1016/j.chemgeo.2023.121441.

Chen, X., Romaniello, S.J., and Anbar, A.D., 2017, Uranium isotope fractionation induced by aqueous speciation: Implications for U isotopes in marine CaCO3 as a paleoredox proxy: Geochimica et Cosmochimica Acta, v. 215, p. 162–172, doi:10.1016/j.gca.2017.08.006.

Chen, X., Romaniello, S.J., Herrmann, A.D., Hardisty, D., Gill, B.C., and Anbar, A.D., 2018, Diagenetic effects on uranium isotope fractionation in carbonate sediments from the Bahamas: Geochimica et Cosmochimica Acta, v. 237, p. 294–311, doi:10.1016/j.gca.2018.06.026.

Cherry, L.B., Gilleaudeau, G.J., Grazhdankin, D.V., Romaniello, S.J., Martin, A.J., and Kaufman, A.J., 2022, A diverse Ediacara assemblage survived under low-oxygen conditions: Nature Communications, v. 13, p. 7306, doi:10.1038/s41467-022-35012-y.

Chumakov, N.M., 2009, The Baykonurian glaciohorizon of the Late Vendian: Stratigraphy and Geological Correlation, v. 17, p. 373–381, doi:10.1134/S0869593809040029.

Corsetti, F.A., and Kaufman, A.J., 1994, Chemostratigraphy of Neoproterozoic-Cambrian Units, White-Inyo Region, Eastern California and Western Nevada: Implications for Global Correlation and Faunal Distribution: PALAIOS, v. 9, p. 211, doi:10.2307/3515107.

Cui, H., Kaufman, A.J., Xiao, S., Zhu, M., Zhou, C., and Liu, X.-M., 2015, Redox architecture of an Ediacaran ocean margin: Integrated chemostratigraphic (δ13C–δ34S–87Sr/86Sr–Ce/Ce*) correlation of the Doushantuo Formation, South China: Chemical Geology, v. 405, p. 48–62, doi:10.1016/j.chemgeo.2015.04.009.

Cui, H., Kaufman, A.J., Xiao, S., Zhou, C., and Liu, X.-M., 2017, Was the Ediacaran Shuram Excursion a globally synchronized early diagenetic event? Insights from methane-derived authigenic carbonates in the uppermost Doushantuo Formation, South China: Chemical Geology, v. 450, p. 59–80, doi:10.1016/j.chemgeo.2016.12.010.

Cui, H., Xiao, S., Cai, Y., Peek, S., Plummer, R.E., and Kaufman, A.J., 2019, Sedimentology and chemostratigraphy of the terminal Ediacaran Dengying Formation at the Gaojiashan section, South China: Geological Magazine, v. 156, p. 1924–1948, doi:10.1017/S0016756819000293.

Cui, H. et al., 2021, Deposition or diagenesis? Probing the Ediacaran Shuram excursion in South China by SIMS: Global and Planetary Change, v. 206, p. 103591, doi:10.1016/j.gloplacha.2021.103591.

Darroch, S.A.F., Smith, E.F., Laflamme, M., and Erwin, D.H., 2018, Ediacaran Extinction and Cambrian Explosion: Trends in Ecology & Evolution, v. 33, p. 653–663, doi:10.1016/j.tree.2018.06.003.

Dufour, S.C., and McIlroy, D., 2017, Ediacaran pre-placozoan diploblasts in the Avalonian biota: the role of chemosynthesis in the evolution of early animal life: Geological Society, London, Special Publications, v. 448, p. 211–219, doi:10.1144/SP448.5.

Gan, T., Gilleaudeau, G., Pedersen, M., Doerrler, A., Maximenko, V., Grazhdankin, D., Xiao, s., and Kaufman, A., 2024, Intense Continental Chemical Weathering during the Ediacaran Shuram Excursion, *in* Geological Society of America Abstracts with Programs v. 56, doi:10.1130/abs/2024AM-404983.

Gilleaudeau, G.J. et al., 2019, Uranium isotope evidence for limited euxinia in mid-Proterozoic oceans: Earth and Planetary Science Letters, v. 521, p. 150–157, doi:10.1016/j.epsl.2019.06.012.

Gong, Z., Wei, G., Fakhraee, M., Alcott, L.J., Jiang, L., Zhao, M., and Planavsky, N.J., 2023, Revisiting marine redox conditions during the Ediacaran Shuram carbon isotope excursion: Geobiology, v. 21, p. 407–420, doi:10.1111/gbi.12547.

Grazhdankin, D.V. et al., 2020, Quo vadis, Tommotian? Geological Magazine, v. 157, p. 22–34, doi:10.1017/S0016756819001286.

He, T., Zhu, M., Mills, B.J.W., Wynn, P.M., Zhuravlev, A.Yu., Tostevin, R., Pogge Von Strandmann, P.A.E., Yang, A., Poulton, S.W., and Shields, G.A., 2019, Possible links between extreme oxygen perturbations and the Cambrian radiation of animals: Nature Geoscience, v. 12, p. 468–474, doi:10.1038/s41561-019-0357-z.

Hearing, T.W., Harvey, T.H.P., Williams, M., Leng, M.J., Lamb, A.L., Wilby, P.R., Gabbott, S.E., Pohl, A., and Donnadieu, Y., 2018, An early Cambrian greenhouse climate: Science Advances, v. 4, p. eaar5690, doi:10.1126/sciadv.aar5690.

Himmler, T., Bach, W., Bohrmann, G., and Peckmann, J., 2010, Rare earth elements in authigenic methane-seep carbonates as tracers for fluid composition during early diagenesis: Chemical Geology, v. 277, p. 126–136, doi:10.1016/j.chemgeo.2010.07.015.

Hodgin, E.B., Nelson, L.L., Wall, C.J., Barrón-Díaz, A.J., Webb, L.C., Schmitz, M.D., Fike, D.A., Hagadorn, J.W., and Smith, E.F., 2021, A link between rift-related volcanism and end-Ediacaran extinction? Integrated chemostratigraphy, biostratigraphy, and U-Pb geochronology from Sonora, Mexico: Geology, v. 49, p. 115–119, doi:10.1130/G47972.1.

Ishikawa, T., Ueno, Y., Komiya, T., Sawaki, Y., Han, J., Shu, D., Li, Y., Maruyama, S., and Yoshida, N., 2008, Carbon isotope chemostratigraphy of a Precambrian/Cambrian boundary section in the Three Gorge area, South China: Prominent global-scale isotope excursions just before the Cambrian Explosion: Gondwana Research, v. 14, p. 193–208, doi:10.1016/j.gr.2007.10.008.

Jiang, G., Wang, X., Shi, X., Xiao, S., Zhang, S., and Dong, J., 2012, The origin of decoupled carbonate and organic carbon isotope signatures in the early Cambrian (ca. 542–520 Ma) Yangtze platform: Earth and Planetary Science Letters, v. 317–318, p. 96–110, doi:10.1016/j.epsl.2011.11.018.

Kalderon-Asael, B. et al., 2021, A lithium-isotope perspective on the evolution of carbon and silicon cycles: Nature, v. 595, p. 394–398, doi:10.1038/s41586-021-03612-1.

Kaufman, A.J., Knoll, A.H., and Awramik, S.M., 1992, Biostratigraphic and chemostratigraphic correlation of Neoproterozoic sedimentary successions: Upper Tindir Group, northwestern Canada, as a test case: Geology, v. 20, p. 181, doi:10.1130/0091-7613(1992)020<0181:BACCON>2.3.CO;2.

Kaufman, A., and Knoll, A., 1995, Neoproterozoic variations in the C-isotopic composition of seawater: stratigraphic and biogeochemical implications: Precambrian Research, v. 73, p. 27–49, doi:10.1016/0301-9268(94)00070-8.
Kaufman, A.J., Knoll, A.H., Semikhatov, M.A., Grotzinger, J.P., Jacobsen, S.B., and Adams, W., 1996, Integrated chronostratigraphy of Proterozoic–Cambrian boundary beds in the western Anabar region, northern Siberia: Geological Magazine, v. 133, p. 509–533, doi:10.1017/S0016756800007810.
Kaufman, A.J., Knoll, A.H., and Narbonne, G.M., 1997, Isotopes, ice ages, and terminal Proterozoic earth history: Proceedings of the National Academy of Sciences, v. 94, p. 6600–6605, doi:10.1073/pnas.94.13.6600.
Kaufman, A.J., Jiang, G., Christie-Blick, N., Banerjee, D.M., and Rai, V., 2006, Stable isotope record of the terminal Neoproterozoic Krol platform in the Lesser Himalayas of northern India: Precambrian Research, v. 147, p. 156–185, doi:10.1016/j.precamres.2006.02.007.
Kaufman, A.J., 2019, The Ediacaran-Cambrian Transition: A Resource-Based Hypothesis for the Rise and Fall of the Ediacara Biota, *in* Sial, A.N., Gaucher, C., Ramkumar, M., and Ferreira, V.P. eds., Geophysical Monograph Series, Wiley, p. 115–142, doi:10.1002/9781119382508.ch7.
Khomentovsky, V.V., 1990, Vendian of the Siberian Platform, *in* Sokolov, B.S., Fedonkin, M.A., eds., The Vendian System Volume 2: Regional Geology: Springer-Verlag, Berlin, p. 102-183
Kimura, H., Matsumoto, R., Kakuwa, Y., Hamdi, B., and Zibaseresht, H., 1997, The Vendian-Cambrian δ13C record, North Iran: evidence for overturning of the ocean before the Cambrian Explosion: Earth and Planetary Science Letters, v. 147, p. E1–E7, doi:10.1016/S0012-821X(97)00014-9.
Kipp, M.A., and Tissot, F.L.H., 2022, Inverse methods for consistent quantification of seafloor anoxia using uranium isotope data from marine sediments: Earth and Planetary Science Letters, v. 577, p. 117240, doi:10.1016/j.epsl.2021.117240.
Kısakűrek, B., James, R.H., and Harris, N.B.W., 2005, Li and δ7Li in Himalayan rivers: Proxies for silicate weathering? Earth and Planetary Science Letters, v. 237, p. 387–401, doi:10.1016/j.epsl.2005.07.019.
Knoll, A.H., Hayes, J.M., Kaufman, A.J., Swett, K., and Lambert, I.B., 1986, Secular variation in carbon isotope ratios from Upper Proterozoic successions of Svalbard and East Greenland: Nature, v. 321, p. 832–838, doi:10.1038/321832a0.
Knoll, A.H., Grotzinger, J.P., Kaufman, A., and Kolosov, P., 1995a, Integrated approaches to terminal Proterozoic stratigraphy: an example from the Olenek Uplift, northeastern Siberia: Precambrian Research, v. 73, p. 251–270, doi:10.1016/0301-9268(94)00081-2.
Knoll, A.H., Kaufman, A.J., Semikhatov, M.A., Grotzinger, J.P., and Adams, W., 1995b, Sizing up the sub-Tommotian unconformity in Siberia: Geology, v. 23, p. 1139, doi:10.1130/0091-7613(1995)023<1139:SUTSTU>2.3.CO;2.
Kochnev, B.B., Khudoley, A.K., Priyatkina, N.S., Andrew Dufrane, S., Pokrovsky, B.G., Kuznetsov, A.B., Kaurova, O.K., and Marusin, V.V., 2022, Neoproterozoic evolution of the northwestern margin of the Siberian Platform: Precambrian Research, v. 382, p. 106877, doi:10.1016/j.precamres.2022.106877.
Korovnikov, I.V., Marusin, V.V., Tokarev, D.A., and Obut, O.T., 2019, Trace Fossils from the Vendian-Cambrian Transitional Strata of the Igarka Uplift (Northwestern Siberian Platform): Paleontological Journal, v. 53, p. 566–574, doi:10.1134/S0031030119060030.

Kouchinsky, A., Bengtson, S., Pavlov, V., Runnegar, B., Torssander, P., Young, E., and Ziegler, K., 2007, Carbon isotope stratigraphy of the Precambrian–Cambrian Sukharikha River section, northwestern Siberian platform: Geological Magazine, v. 144, p. 609–618, doi:10.1017/S0016756807003354.

Laflamme, M., Xiao, S., and Kowalewski, M., 2009, Osmotrophy in modular Ediacara organisms: Proceedings of the National Academy of Sciences, v. 106, p. 14438–14443, doi:10.1073/pnas.0904836106.

Laflamme, M., Darroch, S.A.F., Tweedt, S.M., Peterson, K.J., and Erwin, D.H., 2013, The end of the Ediacara biota: Extinction, biotic replacement, or Cheshire Cat? Gondwana Research, v. 23, p. 558–573, doi:10.1016/j.gr.2012.11.004.

Lau, K.V., Macdonald, F.A., Maher, K., and Payne, J.L., 2017, Uranium isotope evidence for temporary ocean oxygenation in the aftermath of the Sturtian Snowball Earth: Earth and Planetary Science Letters, v. 458, p. 282–292, doi:10.1016/j.epsl.2016.10.043.

Lechler, M., Pogge Von Strandmann, P.A.E., Jenkyns, H.C., Prosser, G., and Parente, M., 2015, Lithium-isotope evidence for enhanced silicate weathering during OAE 1a (Early Aptian Selli event): Earth and Planetary Science Letters, v. 432, p. 210–222, doi:10.1016/j.epsl.2015.09.052.

Li, D., Ling, H.-F., Jiang, S.-Y., Pan, J.-Y., Chen, Y.-Q., Cai, Y.-F., and Feng, H.-Z., 2009, New carbon isotope stratigraphy of the Ediacaran–Cambrian boundary interval from SW China: implications for global correlation: Geological Magazine, v. 146, p. 465–484, doi:10.1017/S0016756809006268.

Li, D., Ling, H.-F., Shields-Zhou, G.A., Chen, X., Cremonese, L., Och, L., Thirlwall, M., and Manning, C.J., 2013, Carbon and strontium isotope evolution of seawater across the Ediacaran–Cambrian transition: Evidence from the Xiaotan section, NE Yunnan, South China: Precambrian Research, v. 225, p. 128–147, doi:10.1016/j.precamres.2012.01.002.

Li, G., and Xiao, S., 2004, Tannuolins and Micrina (Tannuolinidae) from the Lower cambrian of Eastern Yunnan, South China, and their Scleritome Reconstruction: Journal of Paleontology, v. 78, p. 900–913, doi:10.1666/0022-3360(2004)078<0900:TAMTFT>2.0.CO;2.

Lin, Y. et al., 2024, Experimental and theoretical constraints on lithium isotope fractionation during brine evaporation and halite precipitation: Geochimica et Cosmochimica Acta, v. 374, p. 250–263, doi:10.1016/j.gca.2024.03.003.

Linnemann, U. et al., 2019, New high-resolution age data from the Ediacaran–Cambrian boundary indicate rapid, ecologically driven onset of the Cambrian explosion: Terra Nova, v. 31, p. 49–58, doi:10.1111/ter.12368.

Loyd, S.J., Marenco, P.J., Hagadorn, J.W., Lyons, T.W., Kaufman, A.J., Sour-Tovar, F., and Corsetti, F.A., 2012, Sustained low marine sulfate concentrations from the Neoproterozoic to the Cambrian: Insights from carbonates of northwestern Mexico and eastern California: Earth and Planetary Science Letters, v. 339–340, p. 79–94, doi:10.1016/j.epsl.2012.05.032.

Macdonald, F.A., Pruss, S.B., and Strauss, J.V., 2014, Trace Fossils with Spreiten from the Late Ediacaran Nama Group, Namibia: Complex Feeding Patterns Five Million Years Before the Precambrian–Cambrian Boundary: Journal of Paleontology, v. 88, p. 299–308, doi:10.1666/13-042.

Magaritz, M., and Stemmerik, L., 1989, Oscillation of carbon and oxygen isotope compositions of carbonate rocks between evaporative and open marine environments, Upper Permian of East Greenland: Earth and Planetary Science Letters, v. 93, p. 233–240, doi:10.1016/0012-821X(89)90071-X.

Maloof, A.C., Schrag, D.P., Crowley, J.L., and Bowring, S.A., 2005, An expanded record of Early Cambrian carbon cycling from the Anti-Atlas Margin, Morocco: Canadian Journal of Earth Sciences, v. 42, p. 2195–2216, doi:10.1139/e05-062.

Maloof, A.C., Porter, S.M., Moore, J.L., Dudas, F.O., Bowring, S.A., Higgins, J.A., Fike, D.A., and Eddy, M.P., 2010a, The earliest Cambrian record of animals and ocean geochemical change: Geological Society of America Bulletin, v. 122, p. 1731–1774, doi:10.1130/B30346.1.

Maloof, A.C., Ramezani, J., Bowring, S.A., Fike, D.A., Porter, S.M., and Mazouad, M., 2010b, Constraints on early Cambrian carbon cycling from the duration of the Nemakit-Daldynian–Tommotian boundary δ13C shift, Morocco: Geology, v. 38, p. 623–626, doi:10.1130/G30726.1.

Marusin, V.V., Kochnev, B.B., Karlova, G.A., and Nagovitsin, K.E., 2019, Resolving Terreneuvian stratigraphy in subtidal–intertidal carbonates: palaeontological and chemostratigraphical evidence from the Turukhansk Uplift, Siberian Platform: Lethaia, v. 52, p. 464–485, doi:10.1111/let.12325.

Marusin, V.V., Kochnev, B.B., Semenova, D.V., Bykova, N.V., Ivanova, N.A., 2022. Composition, age, and provenance of the clastics in the Vendian Staraya Rechka Formation of the Eastern Anabar Uplift, *in* Geodynamic evolution of lithosphere of the Central Asian Fold Belt (from ocean to continent). Proceedings of conference. v. 20, Irkutsk, IEC SB RAS. p. 195-197. [in Russian]

Marusin, V.V., Kochnev, B.B., Karlova, G.A., Izokh, O.P., Sarsembaev, Zh.A., and Ivanova, N.A., 2023, Precambrian–Cambrian Transition at the Igarka Uplift (Northwestern Siberian Platform): Russian Geology and Geophysics, v. 64, p. 682–697, doi:10.2113/RGG20224523.

McIlroy, D., Dufour, S.C., Taylor, R., and Nicholls, R., 2021, The role of symbiosis in the first colonization of the seafloor by macrobiota: Insights from the oldest Ediacaran biota (Newfoundland, Canada): Biosystems, v. 205, p. 104413, doi:10.1016/j.biosystems.2021.104413.

Meyer, K.M., and Kump, L.R., 2008, Oceanic euxinia in earth history: causes and consequences: Annual Review of Earth and Planetary Sciences, v. 36, p. 251–288, doi:10.1146/annurev.earth.36.031207.124256.

Misra, S., and Froelich, P.N., 2012, Lithium Isotope History of Cenozoic Seawater: Changes in Silicate Weathering and Reverse Weathering: Science, v. 335, p. 818–823, doi:10.1126/science.1214697.

Nagovitsin, K.E., Rogov, V.I., Marusin, V.V., Karlova, G.A., Kolesnikov, A.V., Bykova, N.V., and Grazhdankin, D.V., 2015, Revised Neoproterozoic and Terreneuvian stratigraphy of the Lena-Anabar Basin and north-western slope of the Olenek Uplift, Siberian Platform: Precambrian Research, v. 270, p. 226–245, doi:10.1016/j.precamres.2015.09.012.

Narbonne, G.M., Kaufman, A.J., and Knoll, A.H., 1994, Integrated chemostratigraphy and biostratigraphy of the Windermere Supergroup, northwestern Canada: Implications for Neoproterozoic correlations and the early evolution of animals: Geological Society of America Bulletin, v. 106, p. 1281–1292, doi:10.1130/0016-7606(1994)106<1281:ICABOT>2.3.CO;2.

Narbonne, G.M., 2005, The Ediacaran Biota: Neoproterozoic Origin of Animals and Their Ecosystems: Annual Review of Earth and Planetary Sciences, v. 33, p. 421–442, doi:10.1146/annurev.earth.33.092203.122519.

Narbonne, G.M., Xiao, S., Shields, G.A., and Gehling, J.G., 2012, The Ediacaran Period, *in* The Geologic Time Scale, Elsevier, p. 413–435, doi:10.1016/B978-0-444-59425-9.00018-4.

Oehlert, A.M., and Swart, P.K., 2014, Interpreting carbonate and organic carbon isotope covariance in the sedimentary record: Nature Communications, v. 5, p. 4672, doi:10.1038/ncomms5672.

Pelechaty, S.M., Kaufman, A.J., and Grotzinger, J.P., 1996, Evaluation of δ13C chemostratigraphy for intrabasinal correlation: Vendian strata of northeast Siberia: Geological Society of America Bulletin, v. 108, p. 992–1003, doi:10.1130/0016-7606(1996)108<0992:EOCCFI>2.3.CO;2.

Penniston-Dorland, S.C., Bebout, G.E., Pogge Von Strandmann, P.A.E., Elliott, T., and Sorensen, S.S., 2012, Lithium and its isotopes as tracers of subduction zone fluids and metasomatic processes: Evidence from the Catalina Schist, California, USA: Geochimica et Cosmochimica Acta, v. 77, p. 530–545, doi:10.1016/j.gca.2011.10.038.

Peters, S.E., and Gaines, R.R., 2012, Formation of the 'Great Unconformity' as a trigger for the Cambrian explosion: Nature, v. 484, p. 363–366, doi:10.1038/nature10969.

Pogge Von Strandmann, P.A.E., Kasemann, S.A., and Wimpenny, J.B., 2020, Lithium and Lithium Isotopes in Earth's Surface Cycles: Elements, v. 16, p. 253–258, doi:10.2138/gselements.16.4.253.

Pratt, B.R., 1984, Epiphyton and Renalcis--Diagenetic Microfossils from Calcification of Coccoid Blue-Green Algae: SEPM Journal of Sedimentary Research, v. Vol. 54, doi:10.1306/212F853F-2B24-11D7-8648000102C1865D.

Rooney, A.D., Cantine, M.D., Bergmann, K.D., Gómez-Pérez, I., Al Baloushi, B., Boag, T.H., Busch, J.F., Sperling, E.A., and Strauss, J.V., 2020, Calibrating the coevolution of Ediacaran life and environment: Proceedings of the National Academy of Sciences, v. 117, p. 16824–16830, doi:10.1073/pnas.2002918117.

Rothman, D.H., Hayes, J.M., and Summons, R.E., 2003, Dynamics of the Neoproterozoic Carbon Cycle: Proceedings of the National Academy of Sciences of the United States of America, v. 100, p. 8124–8129, https://www.jstor.org/stable/3139891 (accessed July 2024).

Rowland, S.M., Luchinina, V.A., Korovnikov, I.V., Sipin, D.P., Tarletskov, A.I., and Fedoseev, A.V., 1998, Biostratigraphy of the Vendian-Cambrian Sukharikha River section, northwestern Siberian Platform: Canadian Journal of Earth Sciences, v. 35, p. 339–352, doi:10.1139/e98-002.

Saylor, B.Z., Kaufman, A.J., Grotzinger, J.P., and Urban, F., 1998, A composite reference section for terminal Proterozoic strata of southern Namibia: Journal of Sedimentary Research, v. 68, p. 1223–1235, doi:10.2110/jsr.68.1223.

Scotese, C.R., 2016, PALEOMAP PaleoAtlas for GPlates and the PaleoData Plotter Program:, doi:10.13140/RG.2.2.34367.00166.

Seilacher, A., Buatois, L.A., and Gabriela Mángano, M., 2005, Trace fossils in the Ediacaran–Cambrian transition: Behavioral diversification, ecological turnover and environmental shift: Palaeogeography, Palaeoclimatology, Palaeoecology, v. 227, p. 323–356, doi:10.1016/j.palaeo.2005.06.003.

Shahkarami, S., Buatois, L.A., Mángano, M.G., Hagadorn, J.W., and Almond, J., 2020, The Ediacaran–Cambrian boundary: Evaluating stratigraphic completeness and the Great Unconformity: Precambrian Research, v. 345, p. 105721, doi:10.1016/j.precamres.2020.105721.

Shnyukov, E.F., Korzhova, S.A., Sokol, E.V., and Kozmenko, O.A., 2013, Methane-Derived Mg-Calcites and Aragonites From the NE Black Sea: Mineralogical and Geochemical Evidence, *in* Bekker, T.B., Litasov, K.D., Sobolev, N.V., eds., Abstracts of the III International Conference "Crystallogenesis and Mineralogy": Novosibirsk, 27 September – 1 October, 2013: Russian Academy of Sciences Siberian Branch V.S. Sobolev Institute of Geology and Mineralogy - Novosibirsk: Publishing House of SB RAS, p.193–194.

Sigalevich, P., Baev, M.V., Teske, A., and Cohen, Y., 2000, Sulfate Reduction and Possible Aerobic Metabolism of the Sulfate-Reducing Bacterium *Desulfovibrio oxyclinae* in a Chemostat Coculture with *Marinobacter* sp. Strain MB under Exposure to Increasing Oxygen Concentrations: Applied and Environmental Microbiology, v. 66, p. 5013–5018, doi:10.1128/AEM.66.11.5013-5018.2000.

Smith, E.F., Macdonald, F.A., Petach, T.A., Bold, U., and Schrag, D.P., 2015, Integrated stratigraphic, geochemical, and paleontological late Ediacaran to early Cambrian records from southwestern Mongolia: Geological Society of America Bulletin, v. 128, p. 442–468, doi:10.1130/B31248.1.

Smith, E.F., Nelson, L.L., Strange, M.A., Eyster, A.E., Rowland, S.M., Schrag, D.P., and Macdonald, F.A., 2016, The end of the Ediacaran: Two new exceptionally preserved body fossil assemblages from Mount Dunfee, Nevada, USA: Geology, v. 44, p. 911–914, doi:10.1130/G38157.1.

Smith, O., 1998. Terminal Proterozoic Carbonate Platform Development: Stratigraphy and Sedimentology of the Kuibis Subgroup (ca. 550–548 Ma). Massachusetts Institute of Technology, Northern Nama Basin, Namibia.

Sokolov, B.S., 1995, The Vendian System and "Neoproterozoic-III": Stratigraphy and Geological Correlation , v. 3, p. 575–590.

Sour-Tovar, F., Hagadorn, J.W., and Huitrón-Rubio, T., 2007, Ediacaran and Cambrian Index fossils From Sonora, Mexico: Palaeontology, v. 50, p. 169–175, doi:10.1111/j.1475-4983.2006.00619.x.

Squire, R.J., Wilson, C.J.L., Dugdale, L.J., Jupp, B.J., and Kaufman, A.L., 2006, Cambrian backarc-basin basalt in western Victoria related to evolution of a continent-dipping subduction zone: Australian Journal of Earth Sciences, v. 53, p. 707–719, doi:10.1080/08120090600827405.

Steiner, M., Yang, B., Hohl, S., Zhang, L., and Chang, S., 2020, Cambrian small skeletal fossil and carbon isotope records of the southern Huangling Anticline, Hubei (China) and implications for chemostratigraphy of the Yangtze Platform: Palaeogeography, Palaeoclimatology, Palaeoecology, v. 554, p. 109817, doi:10.1016/j.palaeo.2020.109817.

Stoffyn-Egli, P., and Mackenzie, F.T., 1984, Mass balance of dissolved lithium in the oceans: Geochimica et Cosmochimica Acta, v. 48, p. 859–872, doi:10.1016/0016-7037(84)90107-8.

Sun, L. et al., 2024, Cryogenian and Ediacaran integrative stratigraphy, biotas, and paleogeographical evolution of the Qinghai-Tibetan Plateau and its surrounding areas: Science China Earth Sciences, v. 67, p. 919–949, doi:10.1007/s11430-023-1228-x.
Swart, P.K., and Kennedy, M.J., 2012, Does the global stratigraphic reproducibility of δ13C in Neoproterozoic carbonates require a marine origin? A Pliocene–Pleistocene comparison: Geology, v. 40, p. 87–90, doi:10.1130/G32538.1.
Teng, F., McDonough, W.F., Rudnick, R.L., Dalpé, C., Tomascak, P.B., Chappell, B.W., and Gao, S., 2004, Lithium isotopic composition and concentration of the upper continental crust: Geochimica et Cosmochimica Acta, v. 68, p. 4167–4178, doi:10.1016/j.gca.2004.03.031.
Tissot, F.L.H., and Dauphas, N., 2015, Uranium isotopic compositions of the crust and ocean: Age corrections, U budget and global extent of modern anoxia: Geochimica et Cosmochimica Acta, v. 167, p. 113–143, doi:10.1016/j.gca.2015.06.034.
Tomascak, P.B., Carlson, R.W., and Shirey, S.B., 1999, Accurate and precise determination of Li isotopic compositions by multi-collector sector ICP-MS: Chemical Geology, v. 158, p. 145–154, doi:10.1016/S0009-2541(99)00022-4.
Topper, T., Betts, M.J., Dorjnamjaa, D., Li, G., Li, L., Altanshagai, G., Enkhbaatar, B., and Skovsted, C.B., 2022, Locating the BACE of the Cambrian: Bayan Gol in southwestern Mongolia and global correlation of the Ediacaran–Cambrian boundary: Earth-Science Reviews, v. 229, p. 104017, doi:10.1016/j.earscirev.2022.104017.
Tostevin, R., Shields, G.A., Tarbuck, G.M., He, T., Clarkson, M.O., and Wood, R.A., 2016, Effective use of cerium anomalies as a redox proxy in carbonate-dominated marine settings: Chemical Geology, v. 438, p. 146–162, doi:10.1016/j.chemgeo.2016.06.027.
Wallace, M.W., Hood, A. vS., Shuster, A., Greig, A., Planavsky, N.J., and Reed, C.P., 2017, Oxygenation history of the Neoproterozoic to early Phanerozoic and the rise of land plants: Earth and Planetary Science Letters, v. 466, p. 12–19, doi:10.1016/j.epsl.2017.02.046.
Wei, G.-Y., Planavsky, N.J., Tarhan, L.G., Chen, X., Wei, W., Li, D., and Ling, H.-F., 2018, Marine redox fluctuation as a potential trigger for the Cambrian explosion: Geology, v. 46, p. 587–590, doi:10.1130/G40150.1.
Wei, G.-Y. et al., 2024, Lithium isotopic constraints on the evolution of continental clay mineral factory and marine oxygenation in the earliest Paleozoic Era: Science Advances, v. 10, p. eadk2152, doi:10.1126/sciadv.adk2152.
Weyer, S., Anbar, A.D., Gerdes, A., Gordon, G.W., Algeo, T.J., and Boyle, E.A., 2008, Natural fractionation of 238U/235U: Geochimica et Cosmochimica Acta, v. 72, p. 345–359, doi:10.1016/j.gca.2007.11.012.
Wood, R.A. et al., 2015, Dynamic redox conditions control late Ediacaran metazoan ecosystems in the Nama Group, Namibia: Precambrian Research, v. 261, p. 252–271, doi:10.1016/j.precamres.2015.02.004.
Wu, N., Farquhar, J., and Fike, D.A., 2015, Ediacaran sulfur cycle: Insights from sulfur isotope measurements (Δ33S and δ34S) on paired sulfate–pyrite in the Huqf Supergroup of Oman: Geochimica et Cosmochimica Acta, v. 164, p. 352–364, doi:10.1016/j.gca.2015.05.031.
Xiao, S., Narbonne, G.M., Zhou, C., Laflamme, M., Grazhdankin, D.V., Moczydlowska-Vidal, M., and Cui, H., 2016, Towards an Ediacaran Time Scale: Problems, Protocols, and Prospects: Episodes, v. 39, p. 540–555, doi:10.18814/epiiugs/2016/v39i4/103886.

Yang, C., Rooney, A.D., Condon, D.J., Li, X.-H., Grazhdankin, D.V., Bowyer, F.T., Hu, C., Macdonald, F.A., and Zhu, M., 2021, The tempo of Ediacaran evolution: Science Advances, v. 7, p. eabi9643, doi:10.1126/sciadv.abi9643.

Zhang, F., Xiao, S., Kendall, B., Romaniello, S.J., Cui, H., Meyer, M., Gilleaudeau, G.J., Kaufman, A.J., and Anbar, A.D., 2018, Extensive marine anoxia during the terminal Ediacaran Period: Science Advances, v. 4, p. eaan8983, doi:10.1126/sciadv.aan8983.

Zhu, M.-Y., Babcock, L.E., and Peng, S.-C., 2006, Advances in Cambrian stratigraphy and paleontology: Integrating correlation techniques, paleobiology, taphonomy and paleoenvironmental reconstruction: Palaeoworld, v. 15, p. 217–222, doi:10.1016/j.palwor.2006.10.016.

Zhu, M.-Y., Zhuravlev, A.Yu., Wood, R.A., Zhao, F., and Sukhov, S.S., 2017, A deep root for the Cambrian explosion: Implications of new bio- and chemostratigraphy from the Siberian Platform: Geology, v. 45, p. 459–462, doi:10.1130/G38865.1.

Zhu, R., Li, X., Hou, X., Pan, Y., Wang, F., Deng, C., and He, H., 2009, SIMS U-Pb zircon age of a tuff layer in the Meishucun section, Yunnan, southwest China: Constraint on the age of the Precambrian-Cambrian boundary: Science in China Series D: Earth Sciences, v. 52, p. 1385–1392, doi:10.1007/s11430-009-0152-6.